Transcriptional regulation of *MuRF1* in skeletal muscle atrophy

Dissertation

zur Erlangung des akademischen Grades

doctor rerum naturalium (Dr. rer. nat.)

im Fach Biologie

eingereicht an der

Mathematisch-Naturwissenschaftlichen Fakultät I

an der Humboldt-Universität zu Berlin

von

M. Sc. Philipp Du Bois

Präsident der Humboldt-Universität zu Berlin

Prof. Dr. Jan-Hendrik Olbertz

Dekan der Mathematisch-Naturwissenschaftlichen Fakultät I

Prof. Stefan Hecht, Ph.D.

Gutachter/innen

1. Prof. Dr. rer. nat. Thomas Sommer
2. Prof. Dr. Michael Bader
3. PD Dr. med. Jens Fielitz

Datum der Einreichung: 08. März 2014

Datum der mündlichen Prüfung: 20. November 2014

Index of contents

List of Figures and Illustrations

Index of Table

Abbreviations and acronyms

°C	degree Celsius
µ	micro
AA	amino acids
AB	antibody
ACE	angiotensin-converting enzyme
AIDS	acquired immunodeficiency syndrome
AngI	angiotensin I
AngII	angiotensin II
ATP	adenosine tri-phosphate
bHLH	basic helix-loop-helix
BMI	body mass index
bp	base pairs
C1 a and b	cysteine-rich domain
C2C12	mouse skeletal muscle cell line
CA	constitutive active
caFoxO1	constitutive active FoxO1
cDNA	complementary DNA
CDS	coding sequence
CFU	colony-forming unit
CHF	chronic heart failure
ChIP	chromatin immunoprecipitation
CKD	chronic kidney disease
cKO	conditional knockout
CMA	chaperone-mediated autophagy
CMV	cauliflower mosaic virus promoter
Co-IP	co-immunoprecipitation
Co-IP	protein complex immunoprecipitation
COS-7	fibroblast-like cell line derived from monkey kidney tissue
CP	core particle
CSA	cross-sectional area
CtBP	C-terminal-binding protein 1 binding domain
Dexa	dexamethasone
DME Medium	Dulbecco’s modified eagle's medium
DN	dominant negative
DNA	deoxyribonucleic acid
DTT	dithiothreitol
DUB	de-ubiquitinating enzyme
E1	ubiquitin activating enzyme
E2	ubiquitin conjugating enzyme
E3	ubiquitin ligating enzymes
EDTA	ethylene-diamine-tetra-acetic acid
eIF3f	eukaryotic translation initiation factor 3 subunit F

EtOH	ethanol
FBS	fetal bovine serum
Fbxo32 or Atrogin1/MAFbx	F-box protein family member 32
FL	full length
FLAG®	FLAG-tag
FoxO	Forkhead box transcription factor
FoxO1	Forkhead box transcription factor 1
FoxO3a	Forkhead box transcription factor 3a
g	gram
g	gravity
Gapdh	glyceraldehyde 3-phosphate dehydrogenase
GRE	glucocorticoid response element
h	hours
HDAC	histone deacetylase
HDAC4	histone deacetylase 4
HDAC5	histone deacetylase 5
HDAC7	histone deacetylase 7
HDAC9	histone deacetylase 9
HEK293	human embryonic kidney 293 cells
HIV	human immunodeficiency virus infection
HP1	heterochromatin protein 1 binding domain
HRP	horseradish peroxidase
Hs	homo sapiens
IGF-1	insulin-like growth factor 1
IgG	immunoglobulin G
IKK	IκB kinase
IL-1	interleukin-1
IL-1β	interleukin-1 beta
IL-6	interleukin-6
kDa	kilo dalton
L	liter
LacZ	Lac-operon encoding for β-galactosidase
luc	luciferase
LZ	leucine zipper
m	milli
M	molar
M1P	*MuRF1* promoter
MCS	multiple cloning site
MEF	myocyte enhancer factor
MEF2A	myocyte enhancer factor 2A
MIKK	muscle-specific IKKβ transgenic mouse line
min	minutes
MiTF	microphthalmia-associated transcription factor
Mm	mus musculus

mRNA	messenger RNA
MuRF1	muscle specific ring finger 1
MyoD	myogenic differentiation 1
Myog	myogenin
n	nano
NaCl	sodium chloride
NES	nuclear export signal
NF-κB	nuclear factor kappa-light-chain-enhancer of activated B cells
NLS	nuclear localization signal
P	partial
p	statistical significance
p50	transcription factor p50
p65	transcription factor p65
PAGE	polyacrylamide gel electrophoresis
PBS	phosphate buffered saline
PCR	polymerase chain reaction
PEI	polyethylenimin
PH	pleckstrin homology-domain
PI3K	phosphatidylinositide 3-kinase
PKC	protein kinase C
PKD	protein kinase D
PKD1	protein kinase D1
PKD2	protein kinase D2
PKD3	protein kinase D3
PVDF	polyvinylidene difluoride
RAS	renin-angiotensin-system
RING	really interesting new gene
RIPA	radioimmunoprecipitation assay
RLB	reporter lysis buffer
RNA	ribonucleic acid
RP	regulatory particle
RT	reverse transcriptase
RT-PCR	real-time PCR
SD	standard deviation
SDS	sodium dodecyl sulfate
siRNA	small interfering RNA
SYBR®	SYBR® green, asymmetrical cyanine dye, used in RT-PCR
TE	tris and EDTA containing butter
TFE3	transcription factor binding to IGHM enhancer 3
TFEB	human transcription factor EB
Tfeb	mouse transcription factor EB
TFEC	transcription factor EC
TNF-α	tumor necrosis factor-alpha
TSS	transcriptional start site
TWEAK	TNF-related weak inducer of apoptosis

U	Unit (s)
Ub	ubiquitin
UPS	ubiquitin-proteasome system
WT	wild type
β-Gal	β-galactosidase
Δ	delta or deletion

1 Introduction

1.1 The skeletal muscle

The major function of a skeletal muscle is to contract and by that to generate force for most of the essential processes in a living organism. The functional commitment of muscle tissue is extremely broad, ranging from the very complicated neuromuscular orchestration of walking, to the mechanistic execution of breathing and the highly fine tuned sensual process of seeing. But generating motion is not the only crucial duty of skeletal muscles. Skeletal muscles generate heat during contraction and amongst other functions, they safe the appropriate temperature homeostasis and thereby prevent the individual's body hypothermia (sever undercooling). Even more important is the essential role of skeletal muscle tissue in energy allocation. Being the most abundant tissue in the human body (40 to 50 % of the total body mass in mammals, depending on gender, body height and fitness) the skeletal muscle is capable of releasing amino acids into the blood stream through intracellular catabolic processes. Thereby muscle mass degradation serves as a backup reservoir for various organs (including heart, brain and liver) in periods of fasting, during catabolic events or diseases, such as cancer, sepsis, AIDS and heart failure. The catabolic processes leading to skeletal muscle atrophy will be introduced in the following chapter in more detail. This study focuses on the identification of novel transcriptional regulators involved in degradation mechanisms leading to skeletal muscle atrophy. (Fanzani, Conraads, Penna, & Martinet, 2012a; Gundersen, 2011)

1.2 Skeletal muscle atrophy

The skeletal muscles are highly plastic organs, their structure and functional unity is tightly regulated by a multiplicity of pathways. Under normal conditions the pathways crosstalk assures a proper balance between protein synthesis and protein degradation and leads to a homeostatic muscle composition. This balance is influenced by external stimuli such as physical activity, availability of nutrients and growth factors as well as mechanical stresses. During the process of skeletal muscle atrophy, which is defined by a reduction of cross-sectional area (CSA) of the muscle fiber diameter and an impaired strength in the skeletal muscle, the ubiquitin related proteolytic systems are getting activated (Stewart H. Lecker, Solomon, Mitch, &

Goldberg, 1999; Tawa, Odessey, & Goldberg, 1997). The range of triggering events conducting to skeletal muscle atrophy is large. On the one hand, pathologic skeletal muscle atrophy can be provoked by external stimuli like immobilization (e.g. bed rest, fixation) or micro- to zero-gravity events (e.g. spaceflights) leading to severe and rapid degradation of contractile proteins and/or whole organelle structures. In contrast, more physiological triggers for skeletal muscle atrophy can be missing neuromuscular stimulation as caused by denervation or several neurological disorders as well as a series of systemic diseases (e.g. cancer, kidney diseases, heart failure, sepsis and infections as HIV/AIDS). (Bonaldo & Sandri, 2012a; Glass, 2005; Sartorelli & Fulco, 2004; Y. Wang & Pessin, 2013)

Additionally, the loss of muscle mass in the seniority, called sarcopenia, is a public health problem that can be a first cause of severe reduction in mobility and by that a reduction in an individual's life quality (Thomas, 2007). An ongoing and severe loss of muscle mass is often associated with poor prognosis in diseases survival of suffering individuals, in case of myopathies and muscular dystrophies, heart failure, chronic kidney disease (CKD), diabetes, sepsis and cancer. All these diseases share the chance of an end stage development of cachexia (definition: weight loss >5% or >2% with a body-mass-index, BMI <20), which is characterized by weakness and weight loss, including loss of fat and muscle mass. Expectedly, cachexia is a complex metabolic syndrome that can strongly increase morbidity as well as mortality and lead to a severe reduction in life quality. (Amitani et al., 2013; Lainscak et al., 2008; Thomas, 2007)

In the complex process of cachexia pro-inflammatory cytokines such as angiotensin II (AngII), tumor necrosis factor-alpha (TNF-α), TNF-related weak inducer of apoptosis (TWEAK), interleukin-1 (IL-1) and interleukin-6 (IL-6) are suggested to be involved in the induction of muscle wasting by enhancing the activation of the proteolytic degradation machinery (Amitani, Asakawa, Amitani, & Inui, 2013; Lainscak, Filippatos, Gheorghiade, Fonarow, & Anker, 2008; Tadashi Yoshida et al., 2013a).

1.2.1 Molecular mechanisms and pathways involved in skeletal muscle atrophy

In the past 20 years, the process and regulation of skeletal muscle atrophy has been drawn into focus by several scientific research groups. As pioneers in modern atrophy research, the laboratories of Alfred L. Goldberg and David J. Glass could independently identify the E3 ubiquitin ligase named muscle specific RING (really interesting new gene) finger 1 (*MuRF1* or *Trim63)* and the F-box protein family member 32 (*Fbxo32* or *atrogin1/MAFbx*). Expression of both *MuRF1* and *atrogin1* were highly increased in skeletal muscles of rats and mice upon immobilization, denervation or hind-limb suspension (a muscular disuse approach) induced atrophy (Bodine, Latres, et al., 2001a; Gomes, Lecker, Jagoe, Navon, & Goldberg, 2001a). In mice, gene deficiencies for either *MuRF1* or *atrogin1* lead to a strong reduction in denervation induced skeletal muscle weight loss and the reduction of muscle fiber diameter decrease (Bodine, Latres, et al., 2001a; Gomes et al., 2001a). During the following years, it has been proven that the expression of *MuRF1* as well as *atrogin1* is increased in various atrophy models (Bonaldo & Sandri, 2012a; Glass, 2005). Since then, both genes serve as atrophy markers and their specific regulating pathways where drawn into focus (Sandri, 2008).

IGF-1/Insulin-PI3K-Akt-FoxO Pathway

One of the best-characterized examples influencing muscle composition is the insulin-like growth factor 1 (IGF-1) triggered PI3K/Akt/FoxO signaling cascade. IGF-1 is involved in cell proliferation, differentiation, myofiber growth and regeneration (reviewed in Fanzani et al., 2012). It activates the phosphatidylinositol 3-kinase (PI3K) - protein kinase B (PKB or AKT) pathway, which in turn blocks the Forkhead box (FoxO) transcription factor family activity (Sacheck, Ohtsuka, McLary, & Goldberg, 2004; Y.-H. Song et al., 2005; Stitt et al., 2004). The FoxO family of transcription factors has been reported to induce *MuRF1* and *atrogin1* expression in different atrophy models (Reed, Sandesara, Senf, & Judge, 2011; Stitt et al., 2004). In contrast, low circulating IGF-1 levels, which have been associated with sarcopenia, CHF, cancer (Costelli et al., 2006) and other syndromes, can be a triggering event that leads to loss of muscle mass (reviewed in Fanzani et al., 2012). In addition, IGF-1 treatment reduces *MuRF1* and *atrogin1* mRNA expression in C2C12 myotubes (skeletal muscle mouse cell line) and blocks dexamethasone (Dexa) induced protein breakdown, probably by its strong negative influence on *atrogin1* expression (*atrogin1* mRNA expression at ~40% after 3h IGF-1 treatment) (Sacheck et al., 2004). The transcription factor FoxO1 binds to the *MuRF1*

promoter and increases its binding upon Dexa treatment (Waddell et al., 2008a). But it is of interest, that *in-vivo* gain of function approaches using FoxO3a could only show a ~2 fold increase of *MuRF1* activation in a luciferase promoter assay (Senf, Dodd, & Judge, 2009). Furthermore, a constitutive active mutant of FoxO1 (caFoxO1), was not sufficient to induce *MuRF1* mRNA expression in C2C12 myotubes (Stitt et al., 2004).

In conclusion, the involvement of the FoxO transcription factor family in the regulation of muscle atrophy is significant and seems to be relevant for the induction of *MuRF1* and *atrogin1* in skeletal muscle atrophy and in the IGF-1 mediated inhibition of protein degradation. However, the FoxO transcription factor family seems to be more important for *atrogin1* than for *MuRF1* regulation. These and other evidences led us to the assumption of the existence of other relevant transcription factors which could be involved in *MuRF1* regulation and thereby mediate skeletal muscle atrophy.

The NF-κB pathway

The classical NF-κB pathway is involved in the cellular response to stress, cytokines, UV-light irradiation mediated DNA damage, bacterial and viral infections, as well as to oxidative stress. The so called canonical NF-κB pathway can be triggered by TNF-α, TWEAK and IL-1β. The specific receptor stimulation of IL-1β activates and recruits different complex members (TAK1 complex) which in turn activate the central IκB kinase (IKK) complex (composed out of IKKα, IKKβ and the linking IKKγ subunit). The IKKβ kinase subunit marks the IκBα suppressor protein via phosphorylation, which in turn gets ubiquitinated and degraded in the proteasome. The unbound or de-suppressed transcription factor dimers (e.g. p50 and p65) translocate to the nucleus and activate gene transcription. (Gilmore, 2006; Jackman, Cornwell, Wu, & Kandarian, 2013; Perkins, 2007; Peterson, Bakkar, & Guttridge, 2011)

Being also expressed in skeletal muscle tissue, the activation of the NF-κB pathway has been reported in different states of atrophy/cachexia (Cai et al., 2004a; Hunter et al., 2002; Y.-P. Li & Reid, 2000; Penner, Gang, Wray, Fischer, & Hasselgren, 2001; Peterson et al., 2011). As mentioned before, the NF-κB cascade can be stimulated by TNF-α (Y.-P. Li & Reid, 2000), whose circulating levels were shown to be increased in patients suffering from cancer cachexia (Argilés & López-Soriano, 1999; Tisdale, 1997).

Supporting the involvement of NF-κB in systemic atrophy development, Ladner *et al.* showed that NF-κB is required for TNF-α induced atrophy by using an IκBα super-repressor (SR;

non-degradable form of IκBα) C2C12 cell line (Ladner, Caligiuri, & Guttridge, 2003). In the following year Cai *et al.* (Cai et al., 2004a) used a muscle-specific transgenic mouse line over-expressing an active form of IκB kinase β (called MIKK), which showed significant muscle wasting even without atrophying stimulus. In addition, a very interesting and important result of this study was that the NF-κB mediated muscle wasting affected only the expression of *MuRF1*, but showed no effect on *atrogin1* expression. *MuRF1* mRNA expression moderately increased in tibialis anterior (TA) muscles of MIKK mice (~3 fold) and *MuRF1* promoter fragments showed very low response to the NF-κB mediated signals in different luciferase assay approaches (Cai et al., 2004a). This means that in summary, the NF-κB pathway plays a central role for regulation and progression of skeletal muscle atrophy. Several loss-of-function approaches showed that the NF-κB pathway is crucial for denervation and immobilization induced atrophy. But gain-of-function approaches showed only little, if any, positive regulatory effects on *MuRF1* and *atrogin1* expression. Therefore, the induction of *MuRF1* and *atrogin1* observed in most of the skeletal muscle atrophy models cannot be completely explained by involvement of only one pathway.

The mTOR pathway, downstream of Akt

The "original" target of rapamycin (TOR) pathway components where first identified in yeast (Crespo & Hall, 2002). Major cellular processes regulated by the mammalian target of rapamycin complex 1 (mTORC1) are protein and lipid synthesis, lysosomal biogenesis, energy metabolism and autophagy (Hay & Sonenberg, 2004; Mathieu Laplante & Sabatini, 2012; Wullschleger, Loewith, & Hall, 2006). The mTOR pathway has been linked to a variety of diseases like atrophy, several cancers, obesity and type 2 diabetes (Bentzinger et al., 2013; Bodine, Stitt, et al., 2001). In more detail, the mTORC1 pathway integrates intra- and extracellular stimuli like growth factors and nutrient supplementation; moreover it participates in energy status regulation and senses other stress factors. The catalytic active protein of mTOR, a serine threonine kinase belonging to the phosphoinoside-3-kinase related (PI3K) family, interacts with several other proteins forming two different complexes, named mTOR complex 1 (mTORC1) and mTOR complex 2 (mTORC2). The better characterized mTORC1 is more sensitive to rapamycin inhibition, as it interacts directly with the "gain-of-function" complex formed from rapamycin and the FKBP12 protein (Brown et al., 1994; Mathieu Laplante & Sabatini, 2012; Sabatini, Erdjument-Bromage, Lui, Tempst, & Snyder, 1994).

The second mTOR complex (mTORC2) shows inhibition effects only after long term treatment and independent of FKBP12/rapamycin complex binding (Dos D. Sarbassov et al., 2004; Sarbassov et al., 2006). When active, mTORC2 is involved in regulation of cell survival, metabolism and cytoskeleton organization (M. Laplante & Sabatini, 2013; Mathieu Laplante & Sabatini, 2012).

In 2008 Bentzinger *et al.* showed that skeletal muscle specific ablation of the mTORC1 complex protein raptor (regulatory-associated protein of mTOR) resulted in smaller muscles and led to muscle dystrophy and a soon death shortly after birth (Bentzinger et al., 2008). Earlier studies presented evidences towards an involvement of the mTORC1 pathway in muscle size control (Rommel et al., 2001). Wan *et al.* were able to show that indirect inhibition of mTORC1 via transgenic overexpression of TSC1, which forms an upstream inhibitory complex with TSC2, resulted in muscle atrophy (Wan et al., 2006). In addition, a recent study of Bentzinger et al. (Bentzinger et al., 2013) underlined these previous results by analyzing TSC1-deficient mice in reference to hypertrophy and atrophy signaling events. The investigators could indicate that ongoing activation of the mTORC1 pathway by genetic deletion of the inhibitory *Tsc1* gene induced atrophy in all but the soleus muscle. Their biochemical analysis pointed out to a PKB/Akt mediated inhibitory feedback mechanism by mTORC1 that led to a subsequent induction of *MuRF1* and *atrogin1* (Bentzinger et al., 2013). The suggested crosstalk between Akt-FoxO and the mTORC1 pathway, which is important for lysosomal formation and autophagosomal biogenesis (Sardiello et al., 2009; Settembre et al., 2012), is supported by the findings of two independent groups in 2007. These groups showed that FoxO3 induces major lysosomal and autophagosomal genes as well as *atrogin1* (Mammucari et al., 2007; Zhao et al., 2007a). However, it has to be mentioned that in the same study of Zhao *et al.* rapamycin mediated mTOR inhibition faintly (~10%) increased protein breakdown in myotubes (Sandri, 2010). Given that, mTORC participates in skeletal muscle atrophy development, but was shown to be not the primarily responsible pathway.

The AMP-activated protein kinase (AMPK)

Serving as a general sensor for cellular energy balance, the 5'-adenosine monophosphate-activated protein kinase (AMPK) plays a central role in the skeletal muscle tissue as a key regulator of the oxidative capacity, cell growth and balances metabolic gene expression (Bonaldo & Sandri, 2012a; Sean L. McGee & Hargreaves, 2010).

Due to its critical participation in energy pathway regulation, it was taken into focus of the atrophy research field. Thus, in 2007 two independent groups could show that AMPK activation led to FoxO3 phosphorylation independent of the previously mentioned Akt pathway phosphorylation of FoxO3 (Greer, Dowlatshahi, et al., 2007; Greer, Oskoui, et al., 2007; Nakashima & Yakabe, 2007). The chemical activation of AMPK, using the adenosine analogue AICAR (5-Aminoimidazole-4-carboxamide ribonucleotide) led to an increase in protein degradation, but showed little effect on *MuRF1* and *atrogin-1* expression (Nakashima & Yakabe, 2007). In 2012, an adjacently published study showed the same moderate effect of AICAR on the *MuRF1* (~1.5 fold) and *atrogin-1* (~1.9 fold) expression in primary myotubes and assigned major parts of the observed protein degradation to the induction and transcriptional activation of autophagic components (e.g. *LC3*) and the autophagosomal formation in skeletal muscle cells (Sanchez et al., 2012). AMPK shares a connective point with the mTOR pathway, where it can inhibit mTORC1 activity via phosphorylation of the TSC2 complex (Langen, Gosker, Remels, & Schols, 2013).

A recent paper which investigated the regulating effect of AMPK on both atrogenes in the rodent heart showed in vivo data, which again indicated a faint mRNA expression increase of *MuRF1* and *atrogin-1* (~2.3 fold for both atrogenes) in AICAR treated NRVM cells (neonatal rat ventricular cardiomyocytes). The authors addressed the *MuRF1* induction to the myocyte enhancer factor 2 (MEF2) (Baskin & Taegtmeyer, 2011a). The MEF2 family of transcription factors is composed of four members A, B, C and D; they are central regulators of developmental processes, amongst other in skeletal muscle tissue (M. J. Potthoff & Olson, 2007). Focusing on muscle atrophy and the regulation of *MuRF1*, it is of interest that the *MuRF1* promoter from human as well as other mammalian species shows a highly conserved MEF2 binding site in nearest proximity to the transcriptional start of the *MuRF1* gene (Andrés, Cervera, & Mahdavi, 1995; Baskin & Taegtmeyer, 2011a). Baskin e*t al.* showed that mutation of the MEF2 binding site led to reduced induction by AICAR in H9C2 cells (mouse heart) in a luciferase assay system. Nutrient deprivation and active isoforms of AMPK, as well as its regulatory effects on *MuRF1* expression in connection with skeletal muscle atrophy development have not been investigated so far. It is important to note, that several publications have shown a strong regulatory connection between MEF2 and ClassIIa histone-deacetylases (HDACs), which have been proven to be negative regulators of skeletal muscle atrophy (Miska et al., 1999; Matthew J. Potthoff et al., 2007). The role and function of ClassIIa HDACs in muscle atrophy will be elucidated in a following specialized chapter.

The transcription factor myogenin

An important regulator of atrogene gene expression in denervation induced atrophy is the bHLH transcription factor myogenin (Macpherson, Wang, & Goldman, 2011; Viviana Moresi et al., 2010a; Tiffin, Adi, Stokoe, Wu, & Rosenthal, 2004). Myogenin is essential for skeletal muscle development, since mice with partial germ line deletion of the myogenin gene died immediately after birth and showed skeletal defects (Hasty et al., 1993; Nabeshima et al., 1993). Due to these findings, Moresi *et al.* used an inducible knockout strategy to investigate the role of myogenin in denervation induced atrophy (Viviana Moresi et al., 2010a). Moresi *et al.* showed that myogenin binds to conserved E-box sequences (CANNTG, Figure 2) in the *MuRF1* promoter and that overexpression of myogenin induced *MuRF1* (~10 fold) and *atrogin-1* (~3 fold) promoter constructs in C2C12 myoblasts in an E-box dependent manner. Myogenin deficient mice showed reduced *MuRF1* and *atrogin-1* mRNA induction upon denervation, but no effect after 48 h of fasting (Moresi et al., 2010). Supporting evidences from the lab of Daniel Goldman showed a reduced effect on denervation mediated reduction of muscle atrophy, at least for the soleus muscle (Macpherson et al., 2011).

Furthermore, Moresi *et al.* in 2010 as well as Bricceno *et al.* in 2012 showed that class IIa histone deacetylases (HDAC) 4 and 5 are both regulators of skeletal muscle atrophy, and that this process involves myogenin mediated atrogene induction (Bricceno et al., 2012; Viviana Moresi et al., 2010b).

The chemical blockade or genetic deactivation of individual pathway components has been shown to be able to block atrophy in denervation induced atrophy. This recently discovered connection of myogenin to denervation induced atrophy and the negative regulation of class IIa HDAC4 and 5 in that process added in a new optional pathway that influences *MuRF1* and *atrogin-1*.

Summing up these findings, the understanding of the crosstalk between signaling pathways participating in skeletal muscle maintenance widens up, but the complicated orchestration of various stimuli influencing the skeletal muscle structure and development of atrophy is not fully understood.

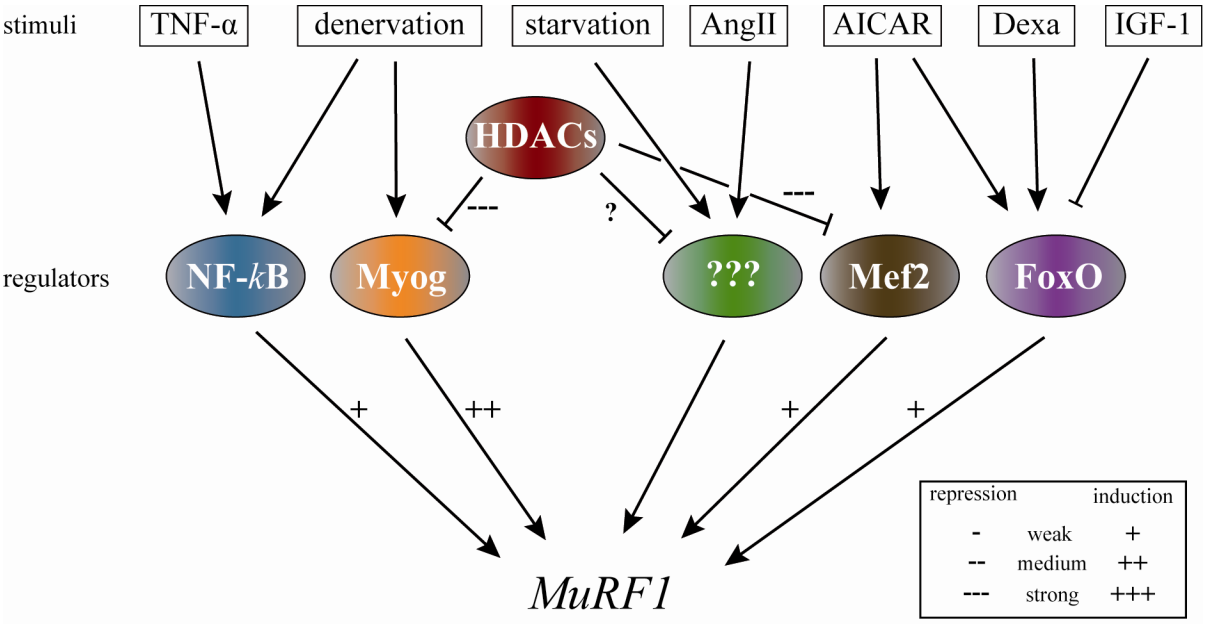

Figure 1: Regulators of *MuRF1* expression

The diagram summarizes atrophy stimuli and their influences via indicated regulators on *MuRF1* expression. Transcription factor families as well as class IIa histone deacetylases (HDAC) being involved in *MuRF1* regulation are indicated. Nuclear factor kappa-light-chain-enhancer of activated B-cells (NF-κB); myogenin (Myog); Forkhead box binding transcription factor (FoxO); Myocyte enhancer factor 2 (Mef2); interrogation mark represents unknown regulators supposedly being involved in *MuRF1* regulation.

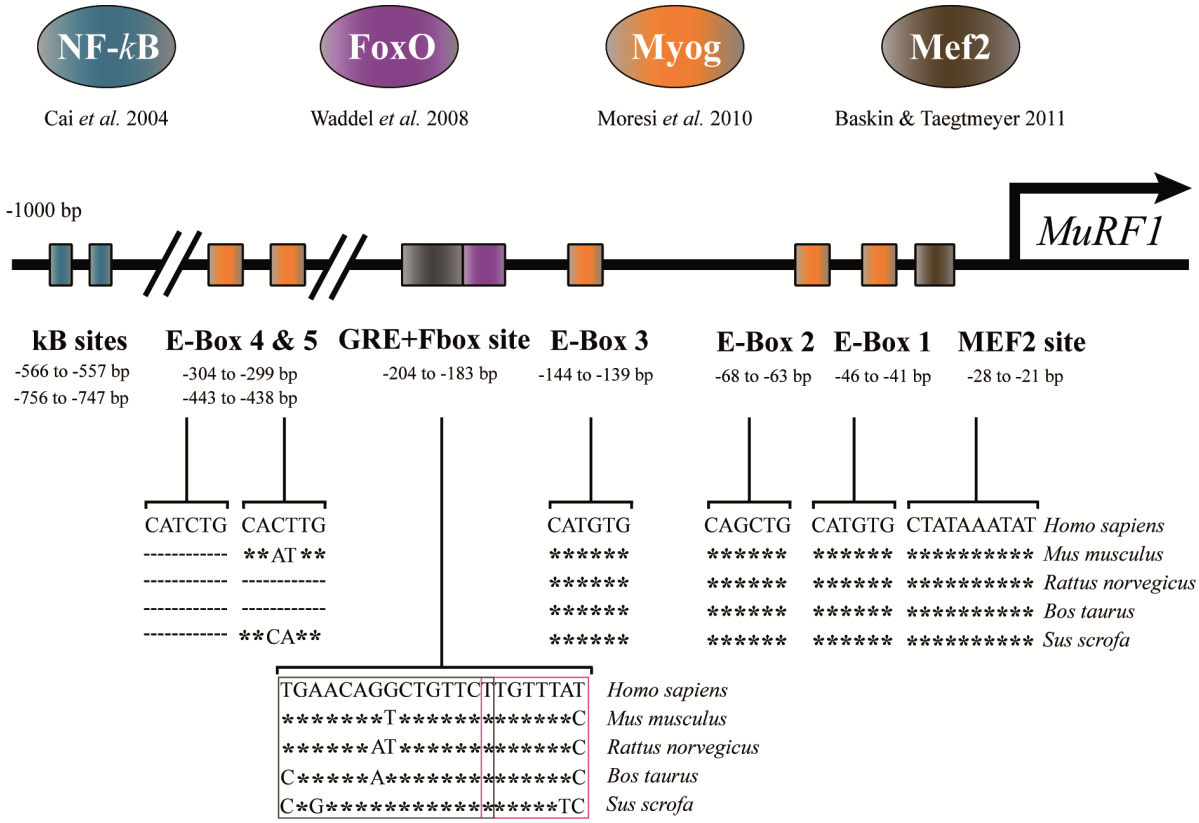

Figure 2: Transcription factor binding sites within the *MuRF1* promoter structure

The diagram shows an illustration of the human *MuRF1* promoter region, representing 1000 base pairs (bp) upstream of the transcriptional start site (Gene ID: 84676). Transcription factor families involved in *MuRF1* regulation are indicated. Myocyte enhancer factor 2 (Mef2); myogenin (Myog); Forkhead box binding transcription factor (FoxO); nuclear factor kappa-light-chain-enhancer of activated B-cells (NF-κB); subtitled publications indicate investigators of regulatory mechanisms. Binding sites for MEF2, E-Box positions 1 to 5, F-Box site; glucocorticoid response element (GRE) and the NF-κB sites are shown relatively to their indicated distance to human *MuRF1* transcription start. Lower panel shows sequence alignment of indicated species, with stars representing sequence coincidence and dotted lines for aberrations. GRE and Fbox site overlap at one position; both sequence elements are marked with corresponding colored boxes.

1.3 Protein degradation in cell biology

The two major mechanisms for protein degradation in eukaryotic cells are the ubiquitin-proteasome system (UPS) and the autophagy - lysosome pathway (Fanzani, Conraads, Penna, & Martinet, 2012; Sandri, 2013). In general and under normal conditions the UPS is mainly involved and responsible for the targeted degradation of short lived proteins, whereas the autophagic machinery degrades long lived proteins and whole organelle structures (Fanzani et al., 2012a). During the advance and acute state of skeletal muscle atrophy both degradational mechanisms have been reported to be activated and to differentially contribute to loss of muscle proteins (reviewed in Bonaldo and Sandri, 2012b; Fanzani et al., 2012; Schiaffino et al., 2013).

1.3.1 The ubiquitin-proteasome system

The muscle tissue includes a strong requirement for specific and profoundly regulated degradation of target proteins or selective subsets of proteins, e.g. as a process adaptation to different conditions in activity and maintenance. This target-oriented and precisely orchestrated protein disassembly is mainly performed by the UPS via a highly selective and target specific transfer of multiple ubiquitin peptide residues (76 amino-acids, 8 kDa) as marking signals for a subsequent degradation in the proteasome. Ubiquitin is expressed in all eukaryotic cell types and its sequence is conserved from yeast to human. To achieve highest specificity, the UPS is composed gradually of target recognizing enzymes at its cascade end. (S. H. Lecker, 2006)

The first process-related steps include an ATP consuming activation and binding of one ubiquitin (Ub) residue to the E1 ubiquitin-activating enzyme and the subsequent transfer of this Ub monomer to an E2 ubiquitin-conjugating enzyme. Successively, the Ub carrying E2 enzyme then binds to the specificity mediating E3 ubiquitin ligase. The intrinsic ubiquitin-marking procedure, which covalently binds the ubiquitin molecule to a lysine residue of the target protein, can be mediated directly by the E3 ligase, which transfers the ubiquitin on the target protein. The E3 ligase can also serve as a linker for an indirect E2 enzyme mediated labeling. Repeated elongation of the ubiquitin chains to at least four ubiquitin residues, linked via lysine 48, demonstrate the “classical” recognition signal for subsequent degradation in the proteasome. All seven lysine residues within the ubiquitin protein can serve as potential conjugating sites and lead to different types of chains (Lys 6, 11, 27, 29, 33, 48 and 63). Some

ubiquitylation positions function as regulatory modifications, while others lead to degradation. (Glickman & Ciechanover, 2002; Stewart H. Lecker, 2003; Pickart, 2000; Weissman, 2001; Wilkinson, 2000)

The human genome encodes for more than 650 different ubiquitin ligases. These E3 ligases are involved in the regulation of metabolism, cell cycle, transcription and muscle mass control. Considering a tissue specific expression of E2s and E3s, different E2-E3 pairs degrade different proteins and by that enhance the preciseness of the UPS (Bonaldo & Sandri, 2012b). It is necessary to mention, that the transfer of single ubiquitin residues (mono-ubiquitylation) can have different effects concerning the targeted protein and influence e.g. its function or its sub-cellular localization. Besides that, ubiquitin residues can be removed by de-ubiquitinating enzymes (DUBs), which negatively regulate the effect of the ubiquitin cascade (Glickman & Ciechanover, 2002).

Summing up, the specified mechanism of targeted degradation of muscle proteins via the UPS is arranged by the interplay of ubiquitin activating (E1), conjugating (E2) and transferring or ligating enzymes (E3), but the 26S proteasome complex performs the ultimate proteolytic degradation process.

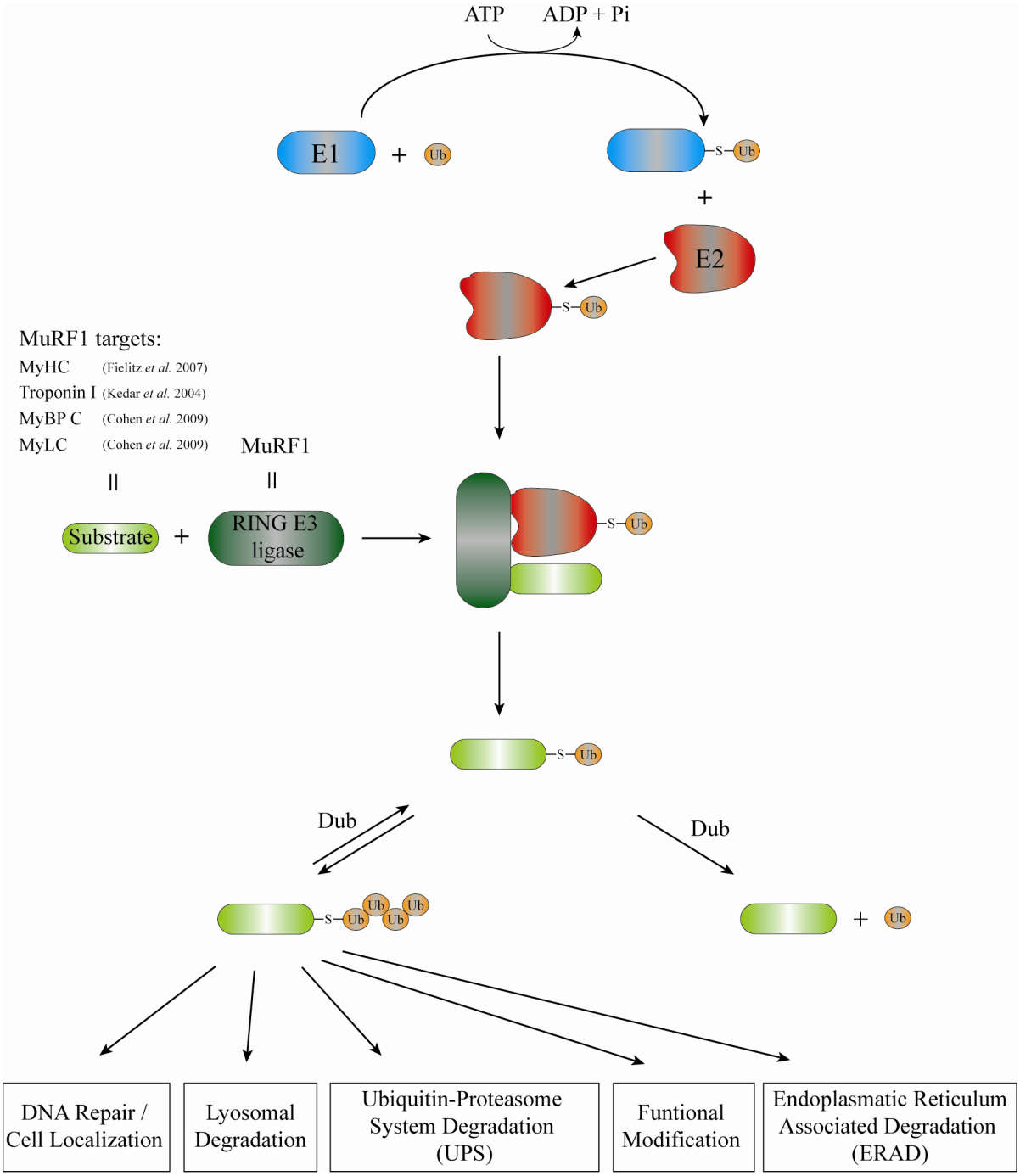

Figure 3: The ubiquitylation cascade

This schematic illustration shows the process of ubiquitylation and the connected mechanisms. Ubiquitin (Ub) gets activated by the E1 enzyme via using ATP hydrolyzing energy, Ub is then passed to an E2 Ub-conjugating-enzyme. The Ub is adjacently transferred to a target or substrate protein, this process is supported by a target specific E3 ligase. RING (really interesting new gene) E3 ligases act as scaffold proteins, which pass the Ub from the E2 to the substrate protein. More Ub residues can be added via repeated “normal” ubiquitylation or by covalent coupling of pre-assembled polyUb chains from an E4 ligase (not illustrated). Covalently bound Ub residues can be cleaved off the substrate protein at any point in the process by de-ubiquitylating enzymes (DUBs). Graphical information and layout have been adapted from McDowell and Philpott 2013 and Bonaldo and Sandri 2012.

1.3.2 The proteasome

The proteasomal degradation is a stepwise mechanism with distinct and specialized functions for each section of the proteasome complex. It consists of two general subunits: a central core structure with hydrolysis activity called the core particle (CP) or 20S proteasome and the regulatory particle (RP) or 19S particle subunit. The RP is the substrate recognition subunit and responsible for the ATP-dependent unfolding of the target protein, removal of the ubiquitin chain and the subsequent translocation into the CP. In a progressive mechanism, the linearized protein enters the CP and gets degraded into peptide fragments. (Finley, 2009; Schmidt & Finley, 2013)

The CP is assembled out of 28-subunits; two alpha-rings are covered at both sides with two beta-rings forming together a barrel like core, which catalyzes the peptide bond cleavage at the end of the proteolytic process. The RP complex can bind to either side of the CP and contains 10 subunits forming a base and a lid sub-complex, whereas the base includes six ATPases, which utilize ATP energy for the unfolding process. On the other hand, the lid part is suggested to recognize and de-ubiquitinylate the target proteins. The molecular architecture of the 26S proteasome complex can be reviewed in Nickell *et al.* (2009).

The proteasome is the final executing part of the UPS. The involvement of the UPS in skeletal muscle atrophy and many other diseases has been reported by others (Murton, Constantin, & Greenhaff, 2008; Pagan, Seto, Pagano, & Cittadini, 2013; Petroski, 2008; Schmidt & Finley, 2013; Sohns, van Veen, & van der Heyden, 2010).

By the matter of fact, the specificity of degradation is mediated by the E3 ligases of the ubiquitin system. This marking section moved into focus of research as potential interfering point for the prevention of diseases and drug development.

1.3.3 The autophagy-lysosome system

Autophagy is a central part of the cells recycling and turnover system. The autophagy-lysosome system digests whole cell components, long-lived proteins and vesicular proteins via fusion of the vesicles with lysosomes. Autophagic dysfunction has been associated with skeletal muscle atrophy in humans and other diseases like cancer, microbial infections, neuron-degeneration, myopathies and heart disease. (Bonaldo & Sandri, 2012b; Mizushima, Levine, Cuervo, & Klionsky, 2008)

Core machinery of the autophagy process is the lysosome, a vesicular structure present in mammalian cells with an acidic pH of 4-5, raised by ATP-consuming proton pumps. Lysosomes import proteases, lipases, nucleases, phosphatases, hydrolases and glycosidases via the endoplasmic reticulum and the Golgi apparatus; all together execute the digestion process. In general, the lysosomal degradation is fed by three different substrate-delivering mechanisms: the micro-autophagy, the macro-autophagy and the chaperone-mediated autophagy (CMA). In addition, extracellular proteins and other substances can be digested in the lysosome as well via endocytotic internalization and vesicle fusion. Small portions of cytoplasm can directly be transferred into the lysosome via invagination of its membrane, representing the micro-autophagy. This mechanism has not been described in skeletal muscle cells so far. In the CMA degradation process the cytoplasmic target protein gets recognized by heat-shock protein hsc73 via sequence recognition of the amino acid motive Lys-Phe-Glu-Arg-Gln and bound to the lysosomal membrane via the receptor protein LAMP2. During macro-autophagy big protein complexes and whole cytoplasmic organelles get surrounded by a double membrane vesicle generating the autophagosome. Beforehand, the formation of the so called pre-autophagosomal structure, assisted by several multi-complex associated proteins, is necessary before fusion with the lysosome and subsequent target degradation. Macro-autophagy has been observed and investigated in skeletal muscle tissue and seems to be very relevant for the healthy maintenance of skeletal myofibers. Various myopathies and dystrophies have been linked to an impairment of lysosomal function or autophagy dysfunction due to mutations in different lysosomal/autophagosomal genes including chloroquine induced myopathy, Pompe disease, Danon disease, Bethlem myopathy and Ullrich congenital muscular dystrophy. (Bechet, Tassa, Taillandier, Combaret, & Attaix, 2005; Bonaldo & Sandri, 2012b; Mizushima et al., 2008)

1.4 The E3 ubiquitin ligase *MuRF1* and the F-box protein *atrogin1*

The dual discovery of the muscle-specific E3 ubiquitin ligases *MuRF1* (or *Trim63*) and the muscle-specific F-box protein a*trogin1* (or *MAFbx*), following transcript profiling of rodent fasting and immobilization atrophy models, raised great expectations in the development of new therapeutics for a more specified treatment of skeletal muscle atrophy events (Bodine, Latres, et al., 2001b; Gomes, Lecker, Jagoe, Navon, & Goldberg, 2001b). During the following years after discovery their importance in skeletal muscle atrophy strengthened by functional characterization and identification of individual target proteins. On the one hand, both gene expressions where observed to be increased in various models of skeletal muscle atrophy including cancer, rheumatoid cachexia, diabetes, denervation, renal failure and glucocorticoid or cytokine treatment. On the other hand, rodent knockout models showed resistance to denervation induced muscle atrophy for both proteins (Bodine, Latres, et al., 2001b). (Foletta, White, Larsen, Léger, & Russell, 2011)

Continuing molecular characterizations highlighted completely different targets for both proteins. For atrogin1, only a few targets were identified as substrates for degradation. In addition to myogenic differentiation 1 (MyoD), which is a key transcription factor in muscle differentiation (Tintignac et al., 2005), it arranges degradation of eukaryotic translation initiation factor 3 subunit F (eIF3f), an activator of protein synthesis (Csibi et al., 2010). In the heart atrogin1 reduces calcineurin A levels, which is an important factor in response to pressure overload induced hypertrophy (H.-H. Li et al., 2004).

In contrast, the E3 ubiquitin ligase MuRF1 mediates degradation of proteins associated within the sarcomere. Early *in-vitro* studies in the lab of Siegfried Labeit showed that MuRF1 binds to the giant myofibrillar protein titin and is assumed to have regulatory influence on titans' kinase activity (Centner et al., 2001). MuRF1 also regulates stability of troponin I, myosin heavy chain proteins (Clarke et al., 2007a; Fielitz, Kim, et al., 2007; Kedar et al., 2004a), myosin binding protein C and myosin light chain (Cohen et al., 2009). All together, the degradational targets so far known for atrogin1 seem to be more growth, synthesis and survival associated. However, the targets of MuRF1 are functional relevant for the muscle maintenance (Bonaldo & Sandri, 2012b). These findings implicate a separate functional involvement of MuRF1 and atrogin1 in skeletal muscle atrophy. Considering the differences in target arrangement, the study was aimed to the identification of factors regulating *MuRF1* expression.

1.4.1 Involvement of angiotensin II in skeletal muscle atrophy

The renin-angiotensin system (RAS) is a hormone system regulating blood pressure, water balance and cardiac hypertrophy. The process involves multiple conversions of the liver secreted angiotensinogen propeptide to angiotensin I (AngI), catalyzed by renin, which is secreted from the kidney. Finally, AngI is converted by the angiotensin-converting enzyme (ACE) into fully active angiotensin II (AngII) which influences a multiplicity of body functions. AngII activates multiple pathways, which regulate muscle mass, and has been linked to muscle wasting. (Tadashi Yoshida et al., 2013b)

Individuals suffering from CHF, CKD or myocardial infarction have increased AngII levels (Anker et al., 2003; Jin et al., 2004; Roig et al., 2000). AngII treatment in rats leads to a loss of body weight by increased proteolysis in skeletal muscle and reduced food intake (M Brink, Wellen, & Delafontaine, 1996). Brink *et al.* showed in rats that AngII induced protein degradation in muscle tissue was mainly mediated by the UPS (Marijke Brink et al., 2001).

Expression levels for *MuRF1* and *atrogin1* have been shown to be elevated in AngII-induced muscle wasting (Semprun-Prieto et al., 2011; Y.-H. Song et al., 2005; T. Yoshida, Semprun-Prieto, Sukhanov, & Delafontaine, 2010a). Surprisingly, activation of the IGF-1/Akt/FoxO pathway only abolished AngII induced *atrogin1* but not *MuRF1* expression (T. Yoshida et al., 2010a). These results show that FoxO transcription factors are not responsible for *MuRF1* regulation in AngII induced atrophy.

1.5 The transcription factor EB - TFEB

The basic helix-loop-helix (bHLH) leucine zipper (LZ) domain containing transcription factor EB (TFEB) was first identified in a cDNA screen (Carr & Sharp, 1990). Shortly after, Fisher *et al.* confirmed the DNA binding ability of TFEBs bHLH domain and additionally identified the leucine zipper (LZ) domain as essential for homo- or heterodimerization with other transcription factors, e.g. its family member TFE3 (Fisher, Carr, Parent, & Sharp, 1991).

TFEB is one of four family members of the micropthalmia-related family of transcription factors (MiTF/TFE), including MiTF, TFEB, TFE3 and TFEC (Figure 4). The different family members show tissue specific expressional and alternative splicing patterns (Kuiper, Schepens, Thijssen, Schoenmakers, & van Kessel, 2004), high structural homology in their family spanning and family characteristic activation domain (AD), bHLH and LZ domains (Haq & Fisher, 2011). Kuiper et al. showed that human TFEB is expressed in skeletal and heart muscle tissue and that is alternatively spliced at its 5'- end. Since, the resulting different splicing products did not show any in-frame start codon, the final gene product was supposed to be unaffected (Kuiper et al., 2004).

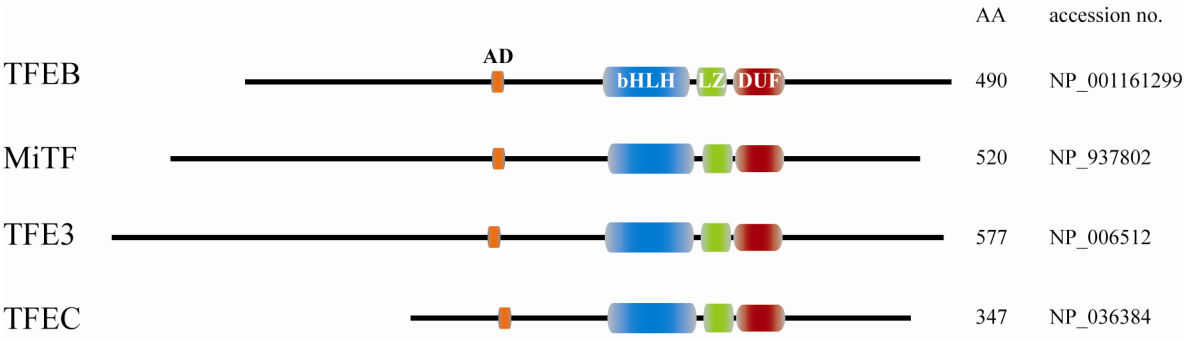

Figure 4: Illustration of human micropthalmia transcription factor (MiTF/Tfe) family members

Schematic illustration of human TFEB, MiTF, TFE3 and TFEC with conserved domain structures: activation domain (AD), basic helix-loop-helix domain (bHLH), leucine-zipper domain (LZ) and DUF3371 domain. Shown are the longest isoforms of TFEB, MiTF, TFE3 and TFEC with number of amino acids and accession numbers labeled at the right side. Positions of domains are shown relative to sequence length, position and size.

The MiTF/TFE family regulates cell growth, differentiation and survival. Genetic deletions, including targeted knockouts, show severe developmental aberrations. More specifically, TFEB plays an essential role for placental vascularization in mice (Steingrímsson, Tessarollo, Reid, Jenkins, & Copeland, 1998). MiTF also participates in the eye development in dro-

sophila (Hallsson et al., 2004). Mutations within genes of family members have been reported in connection with a variety of different cancers, e.g. MiTF in connection with melanoma cancers (Steingrímsson, Copeland, & Jenkins, 2004), TFE3 and TFEB can provoke renal cell carcinomas (Camparo et al., 2008), and TFE3 additionally accounts for alveolar soft part carcinomas (Steingrímsson et al., 2004). A genomic fusion of alpha (locus neighbor) to TFEB was found and described in renal tumors (Davis et al., 2003). (Haq & Fisher, 2011)

Most importantly, TFEB was linked to the lysosomal biogenesis and the regulation of autophagosomal formation in different tissues and cell types, such as bone and heart tissue (Ferron et al., 2013; Ma, Godar, Liu, & Diwan, 2012; Palmieri et al., 2011; Sardiello et al., 2009a; Settembre et al., 2012a). These findings, and the results of this study, highlight a central regulatory position for TFEB in the cells degradational processes.

1.6 The histone-deacetylase family

The histone deacetylases (HDAC) are a family of post-translational modifying enzymes, which can deacetylate histone and non-histone proteins. In general, the acetylation process of histone proteins releases them from DNA and enables transcriptional activation of target genes. HDACs regulate the basal composition of muscle tissue and mediate stimuli dependent changes in gene expression, which can lead to increased proteolysis in skeletal muscle or heart depending on the participating sub-class of HDACs (Viviana Moresi et al., 2010a; Rick B. Vega et al., 2004). The mammalian HDAC family is divided into four different (sub)-classes. Class I HDACs (HDAC1, 2, 3 and 8) are widely expressed in different tissues and were associated with regulation of skeletal muscle homeostasis (V. Moresi et al., 2012). Class II HDACs are separated into two sub-classes, including class IIa HDACs (HDAC4, 5, 7 and 9; Figure 5), mainly expressed in muscle tissues, and class IIb HDACs (HDAC6 and 10). (Alamdari, Aversa, Castillero, & Hasselgren, 2013; Kee & Kook, 2011; S. L. McGee & Hargreaves, 2010; Timothy A. McKinsey, Zhang, & Olson, 2001)

As shown by Moresi *et al*. (2010), class IIa HDAC4 and 5 function as negative-regulators of *MuRF1* and *atrogin1* during denervation induced atrophy using knockout mice, working via an inhibitory cascade finally regulating *myogenin* expression (Bricceno et al., 2012; Viviana Moresi et al., 2010a). HDAC4 was first identified and characterized by Miska *et al.* in 1999. In the same study the interaction and functional repression of MEF2A was published, which is one of the *MuRF1* regulating transcription factors. The knowledge of this connection has

been expanded by several researchers, especially in the lab of Eric N. Olson, who added in the findings of a 14-3-3 dependent nuclear export not only of HDAC4, but also HDAC5, including an upstream signaling cascade of the stress dependent serine/threonine kinase protein kinase D1 (PKD1) (Fielitz et al., 2008; Kim et al., 2008; Martin, Kettmann, & Dequiedt, 2007; T. A. McKinsey, Zhang, & Olson, 2001; R. B. Vega et al., 2004).

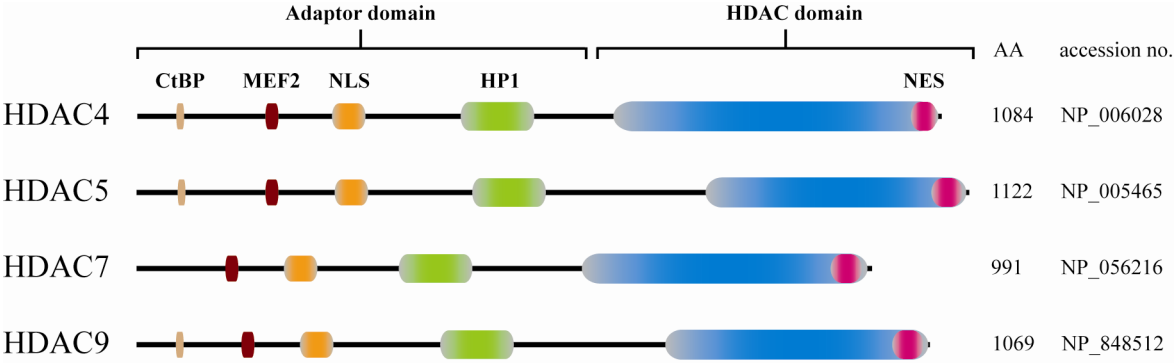

Figure 5: Illustration of the human ClassIIa Histone-Deacetylase (HDAC) family members

Schematic illustration of HDAC4, HDAC5, HDAC7 and HDAC9, showing the longest isoform for each protein, with total amino acid residues and database accession number at the right side. The CtBP, MEF2 and HP1-binding regions are illustrated in colored boxes together with the NLS and NES sites. CtBP: C-terminal-binding protein; HP1: heterochromatin P1; NLS: nuclear localization signal; NES: nuclear export signal. Positions and total length (AA; amino acids) are shown relative to sequence and element size, graphical information and layout where partially adopted from Martin *et al.* 2007 and Zhang *et al.* 2002.

1.7 Protein kinase D family

The protein kinase D (PKD) family of serine/threonine kinases includes three isoform members: PKD1 (Valverde, Sinnett-Smith, Van Lint, & Rozengurt, 1994), PKD2 (Sturany, 2000) and PKD3 (Hayashi, Seki, Hattori, Kozuma, & Saito, 1999). The family members share structural characteristics as the catalytic domain (kinase domain), the pleckstrin homology (PH-domain) domain and two N-terminal cysteine-rich domains (C1a and b-domain) (Fielitz et al., 2008; LaValle et al., 2010; Rybin, Guo, Harleton, Zhang, & Steinberg, 2012; Q. J. Wang, 2006). PKD proteins are involved in the regulation of a multiplicity of cellular functions like protection from oxidative stress, regulation of cell shape, proliferation, motility, adhesion, cancer and, most of interest, in gene transcript regulation (Eiseler et al., 2009; Fu & Rubin, 2011; Karam, Legay, Auclair, & Ricort, 2012; LaValle et al., 2010). (Fu & Rubin, 2011)

Several publications analyzed the regulatory mechanisms controlling PKD activation, demonstrating a direct phosphorylation of at least two conserved serine residues by different PKC

isoforms, which in turn get activated by different triggering stimuli over G-protein coupled receptors (Tan, Xu, Ohba, Ogawa, & Cui, 2003; Q. J. Wang, 2006; Yuan, Bae, Cantrell, Nel, & Rozengurt, 2002; Zugaza, Sinnett-Smith, Van Lint, & Rozengurt, 1996).

One of the well investigated regulatory mechanisms, influencing gene expression in the heart as well as skeletal muscle is the PKD1 – ClassIIa histone deacetylases (HDAC) – MEF2 axis. This axis has influence on the endurance and maintenance status of muscle tissue. As described in special HDAC chapter, the ClassIIa family of HDACs coordinately represses gene expression with cell-type-specific functions. When activated by an external stimulus (e.g. endothelin-1 or angiotensin II) over PKC signaling, PKD1 translocates into the nucleus and phosphorylates HDAC5, which binds to 14-3-3 nuclear export proteins and gets exported from the nucleus and gene transcription can be enabled by MEF2 and other suppressed transcription factors. (Fielitz et al., 2008; rev. Fu and Rubin, 2011; Kim et al., 2008; Vega et al., 2004)

Investigating muscle atrophy, it is of interest that the conflictive hypertrophic phenotype is strongly reduced in cardiac specific PKD1 knockout mice upon pressure overload or angiotensin II treatment, implying a central role of the PKD1-HDAC5 axis in muscle tissue protection and maintenance (Fielitz et al., 2008).

Considering these frame conditions, class IIa HDAC repression as well as the positive PKD family regulatory aspect was included in this study and their influences on the newly identified *MuRF1* inducing transcription factor was analyzed.

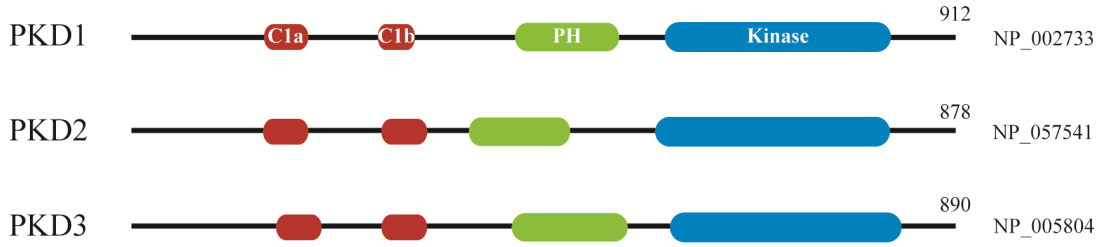

Figure 6: Illustration of human protein kinase D (PKD) family members

Schematic illustration shows domain organization of human protein kinase D family. PKD1, PKD2 and PKD3 show highly homologue and species conserved C1a and C1b sites (red), pleckstrin homology domain (PH; green) and kinase domains (kinase; blue). The number of amino acids according to illustrated accession numbers for the individual PKD isoforms is shown on the right. Positions of domains are shown relatively to sequence length.

Table 1: Knockout mouse phenotypes of skeletal muscle atrophy involved genes

Gene	Mouse model	Phenotype	Reference
atrogin-1	KO	no abnormal baseline phenotype protection from denervation-induced atrophy	Bodine *et al.* 2001
MuRF1	KO	no abnormal baseline phenotype protection from denervation-induced atrophy	Bodine *et al.* 2001
Tfeb	KO	embryonic lethal	Steingrímmson *et al.* 1998
HDAC4	Muscle-specific KO	protection from denervation-induced atrophy	Moresi *et al.*2010
HDAC5	KO	protection from denervation-induced atrophy	Moresi *et al.*2010
HDAC4/5	Muscle-specific KO	protection from denervation-induced atrophy	Moresi *et al.*2010
PKD1	Cardiac-specific KO	diminished cardiac hypertrophy upon TAC, AngII and Isoproterenol	Fielitz *et al.* 2007
Myogenin	Inducible KO	protection from denervation-induced atrophy	Moresi *et al.* 2010
FoxO1	Muscle-specific transgenic	muscle atrophy	Kamei *et al.* 2004
FoxO1	Muscle-specific KO	myofiber switch from slow to fast twitch fibers	Kitamura *et al.* 2007
FoxO3	Inducible KO	no abnormal phenotype	Paik *et al.* 2007
MEF2A	KO	mitochondrial defects, sudden death after birth and cardiac deficiencies	Naya *et al.* 2002
MEF2C	Muscle-specific KO	disorganized myofibers and perinatal lethality	Potthoff *et al.* 2007
MEF2D	Muscle-specific KO	reduction of slow fibers in the soleus muscle	Potthoff *et al.* 2007

1.8 Aim of the study

Skeletal muscle atrophy is a severe problem for individuals suffering from this disease and can occur as a result of a variety of different causes like cancer, sepsis, diabetes, AIDS as well as renal and heart failure. The diversity of triggering events and stimuli show the complex orchestration of skeletal muscle maintenance and point out to the participation of several parallel pathways working together in the regulation of skeletal muscle structure and the development of muscle atrophy. Many questions concerning the regulation of muscle atrophy are still unanswered. The skeletal muscle specific E3 ubiquitin ligase *MuRF1* has been described to be important in skeletal and heart muscle atrophy. Since MuRF1 marks structural sarcomeric proteins and initiates their degradation via the UPS its expression level is often used in diagnostics as marker in skeletal and heart muscle atrophy. Because MuRF1 plays a central role in the degradation process of structural proteins its transcriptional regulation was primarily investigated in this study. Currently known pathways and associated transcription factors influencing *MuRF1* expression were shown not to be responsible for all *MuRF1* inductions observed in muscle atrophy. Especially the AngII triggered induction of *MuRF1*could not be explained until know. In addition to the identification of a new transcriptional regulator of *MuRF1*, its possible functional contribution in AngII triggered atrophy as well as its participation in pathways influencing skeletal muscle atrophy was addressed as secondary aims of this work.

2 Material and Methods

2.1 Human adult skeletal muskle cDNA library screening

A human male skeletal muscle cDNA library (Invitrogen, #11327-012) was titrated to achieve 100 expressing cDNA plasmids per well. Titrated plasmid cDNA pools were co-transfected with the human -5002 bp (first screen) or 1006 bp (second screen) Hs_*MuRF1*-luc and pCMV-*LacZ* construct in COS-7 cells. For each well (96 format) 15000 COS-7 cells were transfected with 130 ng of pooled cDNA library together with 50 ng of Hs_*MuRF1*-luc reporter construct and 10 ng of pCMV-*LacZ* by using Fugene6 (Roche) according to the manufacturer's instructions. 24 h after transfection the luciferase and fluorescence expressions were quantified as described in the next chapter (Luciferase and fluorescence quantification). Subsequently, Sib-selection was performed to isolate single inducers of the Hs_*MuRF1*-luc construct (illustrated in Figure 7, Results chapter). The number of used cDNAs per well was gradually reduced to 10 and finally one single cDNA per well to validate the initially observed induction potentials. Inducing cDNA clones with induction levels over the plate's double positive SD mean value (2xSD+) were selected for further analysis. Single cDNAs activating the Hs_*MuRF1*-luc construct over 2xSD+ were verified by sequencing.

2.2 Luciferase and fluorescence quantification

Transfected cells (e.g. COS-7, HEK293 or C2C12, as indicated) were washed once with ice cold 1xPBS w/o $MgCl_2$ (PAA H15-002), rinsed in 200 µL Reporter Lysis Buffer (RLB; Promega, E3971) and additionally lysed by snap freezing at -80°C for 10 min. The cell lysates were collected in 96 well plates and centrifugated at 1000 g for 2 min to pellet cell debris. The supernatant was transferred into new 96 well plates and used for quantification of luciferase activity and β-Galactosidase in a Fluostar Optima instrument (BMG-Labtech). For Luciferase analysis 50 µL of supernatant were mixed with 50 µL of luciferase substrate solution (Promega E1501) within the Fluostar Optima instrument and for β-Galactosidase analysis 10 µL lysates were analyzed with FluoReporter LacZ Galactosidase Quantification Kit (Invitrogen, F2905) according to the manufacturer instructions.

2.3 Indirect immunofluorescence microscopy

For immunofluorescence microscopy cells were cultured onto glass cover slips, fixed with 4% Para-Formaldehyde (20 min 4°C), permeabilized with 0,1% Triton X-100 in 1x PBS 20 min RT, blocked with 5% serum corresponding to the secondary antibodies host and incubated with specific primary antibody at 4°C over night in H_2O saturated atmosphere. After three times washing with 1xPBS, sections as well as cells were incubated with fluorescence coupled secondary antibody. Pictures were recorded with the Leica CTR 6500HS and analyzed with Leica software LASAF 2.3.5 build 5379 Version 2010. Confocal microscopy was performed with a Zeiss LSM 700 microscope and analyzed with Zeiss ZEN 2009 software.

2.4 Protein extraction from tissue and Western blot analysis

Briefly, biopsy specimens were homogenized in ice-cold extraction buffer (1:3 wt/vol; 10 mM Tris HCl, pH 7.5, 140 mM NaCl, 1 mM EDTA, 25% glycerol, 0.5% sodium dodecyl sulfate (SDS), 0.5% Nonident P-40, 0.1 mM dithiothreitol, 0.5 mM phenylmethylsulfonyl fluoride, 100 ng/ml protease inhibitor cocktail) using FastPrep-24 instrument (MP Bio) according to the manufacturer's instructions (30 s, 2000 rpm). After centrifugation at 18,700 x g (4 °C, 10 min) protein concentration in the resulting supernatant was measured using a protein assay (Bio-Rad), before samples were stored at -80°C. Protein samples were separated by size using 8, 10 or 15 % SDS polyacrylamide gel electrophoresis (SDS-PAGE) and blotted onto PVDF membranes (Amersham Pharmacia Biotech).

2.5 Antibodies

Following antibodies were used (for Western blot, Co-IP and ChIP analyses): anti-Tfeb goat (Abcam, ab2636 and ab122910), anti-Goat-HRP (Abcam, ab6741), anti-GAPDH mouse (Millipore, MAB 374), anti-MuRF1 mouse (Abcam, ab57865), anti-MYC mouse (Millipore, 05-419), anti-MYC rabbit (Upstate, 06-549), anti-FLAG rabbit (Cell Signaling, 2368), anti-Mouse HRP (Cell Signaling, 7076), anti-rabbit HRP (Cell Signaling, 7074), anti-mouse AlexaFluor488 (Invitrogen, A11001) and anti-rabbit AlexaFluor488 (Invitrogen, A11008) antibody.

2.6 RNA Isolation, cDNA synthesis and real-time RT-PCR analysis

RNA's were isolated using Trizol™ Reagent (Invitrogen, 15596-026) according to manufacturer instructions.

Detailed protocol with variations of the manufacturer's instructions: Cells from cell culture experiments or organ fragments isolated from animals were lysed after washing once with ice-cold 1xPBS, by adding 1 mL (per 6 well) of Trizol reagent and passing several times through a 1 mL pipette tip. Resulted extract solutions from muscle cells and muscle tissue were pre-cleared by an additional centrifugation strep at 4°C with 12,000 g for 10 min. The cleared supernatant was transferred to a fresh RNAse free tube, incubated for 5 min at RT. Phase separation has been started by supplementation with 200 µL pure chloroform per 1 mL of initially used Tritol and ongoing hand shaking for 15 seconds and incubation at RT for 2 to 3 minutes. Separation was proceeded by centrifugation at 4°C with 12,000 g for 15 min. The resulting clear upper aqueous phase was transferred to a fresh RNAse free tube, RNA was precipitated by adding 0,5 mL of isopropyl alcohol (isopropanol) per 1 mL of Trizol Reagent used for initial homogenization, resulting samples were mixed by hand shaking and incubated for 10 min at RT. After centrifugation at 4°C with 12,000 g for 10 min the resulting pellet was washed with 1 mL 75% EtOH and again centrifuged at 4°C with 7,500 g for 5 min. RNA pellet was resolved in RNAse-free water after air-drying in sterile conditions and used for further analysis or stored at -80°C. RNAs from C2C12 myotubes following Tfeb siRNA treatment were isolated with RNeasy Mini Kit (Quiagen) according to the manufacturer instructions.

For cDNA synthesis 1 µg of total RNA was transcribed using Superscript II reverse transcriptase (Invitrogen, 18064-022) according to manufacturer instructions.

Detailed protocol with variations of the manufacturer's instructions: Transcription of 1 µg of total RNA in a final volume of 20 µL was started by adding 1 µL of 50 – 250 ng/µL random Oligos or Oligo dT 12-18mer (500 ng/µL) and 1 µL of dNTP Mix (10 mM each) to the RNA and filling up at 12 µL with RNAse free distilled water. Mixture was incubated at 65°C for 5 min quick chilled on ice and 4 µL of 5x First Strand buffer, 2 µL of 0.1 M DTT and 1 µL of RNaseOUT (40 units/µL) were added and mixed. When using Oligo dT primers solution was incubated at 42°C for 2 min, or when using radom primers at 25°C for 2 min; after adding 1 µL of SuperScriptII (200U) the mixture was incubated at 42°C for 50 min; when using random primers an additional pre-incubation at 25°C for 10 min was added. To deactivate the SuperScriptII enzyme an incubation at 70°C for 15 min was performed. The resulting cDNA

was used for further analysis or stored at 4°C for short term storadge or -20°C for long term storadge.

For real-time RT-PCR analysis 10 ng of cDNA were used in a SYBR Green (ABI) based approach in a StepOnePlus™ Real-Time PCR System (Applied Bio Systems) according to the manufacturer's instructions. Expression levels were correlated to *Gapdh* expression, aberrations are indicated. Primer sequences are listed in table 1.

Table 2: Real-Time PCR Primers used in this study

Primer name		Sequence (5' – 3')
Mm_*Gapdh*	sense	ATGGTGAAGGTCGGTGTGA
	anti-sense	AATCTCCACTTTGCCACTGC
Mm_*Tfeb*	sense	GAGCTGGGAATGCTGATCC
	anti-sense	CTTGAGGATGGTGCCTTTGT
Mm_*MuRF1*	sense	GATTATAAATCTAGCCTGATTC
	anti-sense	TTGGTGTTCTTCTTTACCCTC
Mm_*MuRF2*	sense	AGCACTTCTCTGAATTACAAG
	anti-sense	TTCATTTAGGGAATTCAACCAG
Mm_*MuRF3*	sense	AACTTCACGGTGGGTTTCAAGC
	anti-sense	GTGCAGGCCTGAGCCTTCTGGC

2.7 Mammalian expression vectors

Table 3: Mammalian expression vectors used in this study

Vector description	Vector card
pcDNA™3.1/*myc*-His(-) vectors (Invitrogen) Mammalian expression vector, the multiple cloning site (MCS) is driven from a CMV promoter to obtain high expression of inserted gene transcript. The vector includes coding sequences (CDS) for Neomycin (for mammalian selection) and ampicillin (for bacterial selection). The vector card is shown on the right side including the MCS and primers for sequencing. This vector was used as template for the manufacturing of the N-terminal FLAG tagged version, obtained from Jens Fielitz.	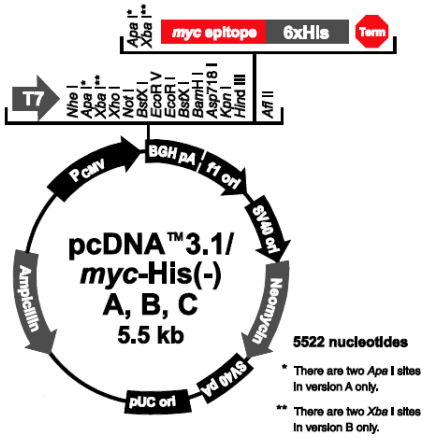
pCMV SPORT6 (Invitrogen) Mammalian expression vector for SuperScript Pre-made cDNA library integration via Gateway Cloning procedure. The Gateway cloning site in between attB2 and attB1 is driven from a CMV promoter to obtain high expression of inserted gene transcript. The vector includes a CDS Ampicillin (for bacterial selection). The vector card is shown on the right side including the MCS and primers for sequencing.	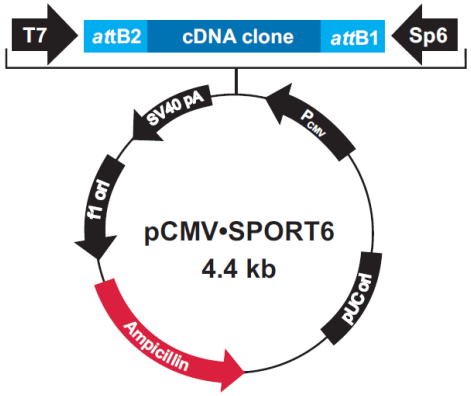
pCMV-LacZ (Clontech) Mammalian expression vector encoding the β-Galactosidase gene which is regulated from the CMV promoter for high expression rates. The vector includes a CDS Ampicillin (for bacterial selection). In this study this vector was used as transfection control plasmid in luciferase assay co-transfection approaches. The vector card is shown on the right side including the MCS and primers for sequencing.	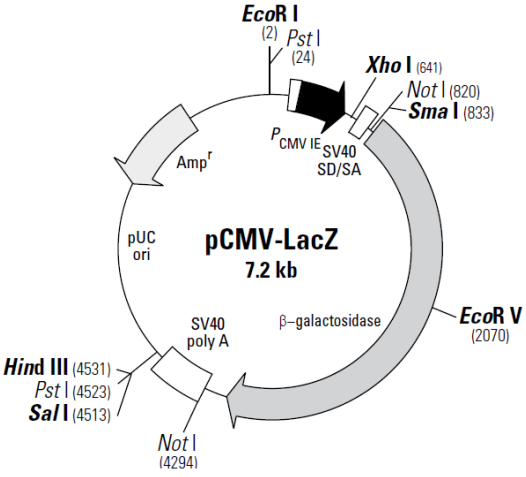

pZsGreen1-N1 (Clontech)

Mammalian expression vector for fusion expression with the *Zoanthus* sp. green fluorescent protein, ZsGreen1 (excitation maximum = 496 nm; emission maximum = 506 nm). The gene of interest is cloned into the MCS and regulated from the CMV promoter; the resulting protein contains an N-terminal fusion to the ZsGreen1 protein. The vector includes a CDS of the Ampicillin gene (for bacterial selection). The vector card is shown on the right side including the MCS.

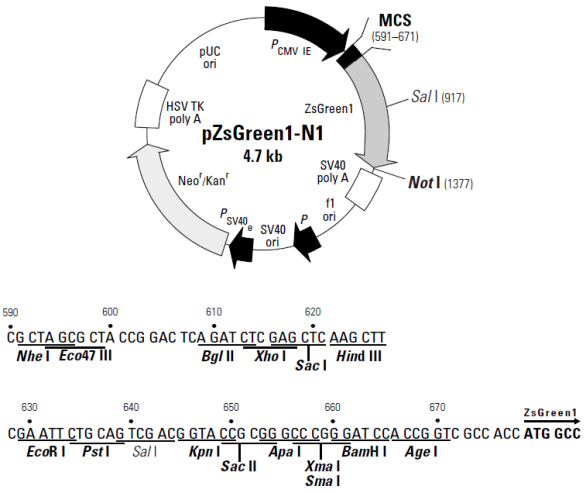

pGL3-Basic vector (Promega)

This vector lacks eukaryotic promoter and enhancer sequences enabling the analysis of regulatory elements, cloned into the MCS, driving the firefly luciferase gene (*luc*+). The vector includes a CDS for Ampicillin (for bacterial selection). The vector card is shown on the right side including single cutting restriction enzymes within the MCS.

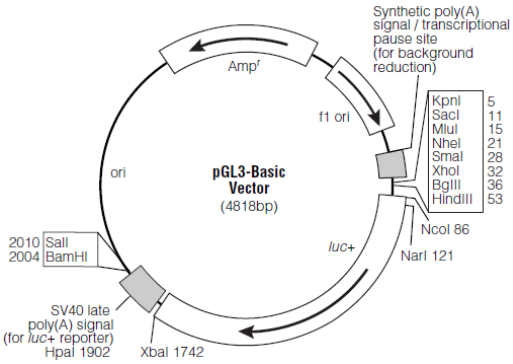

2.8 Eukaryotic expression constructs

Table 4: Eukaryotic expression constructs used in this study

Name	Insert	Backbone	Tag	Source/Reference
Hs_*MuRF1*-luc	Human *MuRF1* promoter sequence; mostly used size 543 bp upstream of the ATG	pGL3-basic	none	self made
Hs_*MuRF1*-luc additional sizes	Human *MuRF1* promoter sequence; different clones with sizes from -5002 bp to -100 bp upstream of the ATG	pGL3-basic	none	self made
Hs_*MuRF1*-luc E-Box 1, 2, 3 and 4 mutations	Human *MuRF1* promoter sequence; size 543 bp; individual mutations of the E-box motifs 1, 2, 3 and 4 (CANNTG to ATNNTG)	pGL3-basic	none	self made
FLAG-Tfeb	Mouse full length isoform 1 of the transcription factor EB	pcDNA3 N-FLAG (Jens Fielitz)	FLAG N-terminal	full length Tfeb from imaGenes sub-cloning self made
FLAG-Tfeb deletion clones	deletion clones manufactured via deletion-PCR of the full length FLAG-Tfeb construct; deletion clones: 128-C, Δ129-237, Δ238-400, Δ299-352	pcDNA3 N-FLAG (Jens Fielitz)	FLAG N-terminal	full length Tfeb from imaGenes sub-cloning self made
Tfeb Myc-His	Mouse full length isoform 1 of the transcription factor EB	pcDNA3.1/*myc*-His(-) A	Myc – 6x His C-terminal	Tfeb CDS from imaGenes sub-cloning self made
TFEB And other screening hits	Partial sequence of the human transcription factor EB coding sequence from cDNA library	pCMV-SPORT6	none	cDNA library from Invitrogen
Tfeb-GFP	Mouse full length isoform 1 of the transcription factor EB;	pZsGreen1 N1	Green fluorescent protein (GFP) (*Zoanthus* sp.) C-terminal	full length Tfeb from imaGenes sub-cloning self made
FLAG-HDAC4	Full length coding sequence of human ClassI-	pcDNA3 N-FLAG (Jens Fielitz)	FLAG N-terminal	(Rick B. Vega et al., 2004)

	Ia HDAC4			
FLAG-HDAC5	Full length coding sequence of human ClassIIa HDAC5	pcDNA3 N-FLAG (Jens Fielitz)	FLAG N-terminal	(K. Song et al., 2006)
HDAC5-Myc	Full length coding sequence of human ClassIIa HDAC5	pcDNA3.1 c-*myc* (Invitrogen)	Myc C-terminal	(K. Song et al., 2006)
HDAC5-Myc deletion clones	Diverse indicated deletion mutants of human ClassIIa HDAC5	pcDNA3.1 c-*myc* (Invitrogen)	Myc C-terminal	(K. Song et al., 2006)
FLAG-HDAC7	Full length coding sequence of human ClassIIa HDAC7	pcDNA3 N-FLAG (Jens Fielitz)	FLAG N-terminal	(Shurong Chang et al., 2006)
FLAG-HDAC9	Full length coding sequence of human ClassIIa HDAC9	pcDNA3 N-FLAG (Jens Fielitz)	FLAG N-terminal	(S. Chang et al., 2004)
Myc-PKD1	Full length coding sequence of human PKD1	no information available	Myc C-terminal	(Kim et al., 2008)
Myc-PKD1 ca and dn	Full length coding sequence of human PKD1; with	no information available	Myc C-terminal	(Kim et al., 2008)
FLAG-PKD2	Full length coding sequence of human PKD2	pcDNA3 N-FLAG (Jens Fielitz)	FLAG N-terminal	Jens Fielitz, unpublished
FLAG-PKD2 ca and dn	Full length coding sequence of human PKD2	pcDNA3 N-FLAG (Jens Fielitz)	FLAG N-terminal	Jens Fielitz, unpublished
FLAG-PKD3	Full length coding sequence of human PKD3	pcDNA3 N-FLAG (Jens Fielitz)	FLAG N-terminal	Jens Fielitz, unpublished
FLAG-PKD3 ca and dn	Full length coding sequence of human PKD3	pcDNA3 N-FLAG (Jens Fielitz)	FLAG N-terminal	Jens Fielitz, unpublished
FLAG-MEF2A	Full length coding sequence of human MEF2A	pcDNA3 N-FLAG (Jens Fielitz)	FLAG N-terminal	(Kim et al., 2008)

Expression constructs encoding for ClassIIa HDAC 4, 5, 7 and 9 as well as PKD1 and its isoforms were described recently as shown on the right side and were a kind gift from Eric N. Olson, Kunhua Song and Johannes Backs.

2.9 Expression plasmids and reporter gene assay construction

The human *MuRF1* promoter was amplified from genomic DNA, isolated from female human blood. The *MuRF1* -5000 bp promoter fragment was cloned into pGL3 basic luciferase vector (Promega E1751) using the primers listed in table 5. The smaller *MuRF1* promoter fragments were generated using the -5000 bp fragment as template.

The *MuRF1* promoter E-box mutations were generated using Phusion® Site-Directed Mutagenesis Kit (Finnzymes, #F-541). Primers were designed according to manufacturer's instructions to mutate the consensus E-box motif CANNTG to ATNNTG, primer sequences in primer table. All positive clones were verified by sequencing.

Table 5: PCR Primers for cloning of human *MuRF1*-promoter and E-Box mutation PCRs

Primer name		Sequence (5' – 3')
Hs_E-Box 1 mut.	sense	CCTCCTGGGGCTATTGTGACCAAGATC
	anti-sense	GATCTTGGTCACAATAGCCCCAGGAGG
Hs_E-Box 2 mut.	sense	CATCGGAATGCTATGCTGGTCCCCTC
	anti-sense	CCAAGCGGCTGGTGGGGCTTGAG
Hs_E-Box 3 mut.	sense	GATTGCTCATCCCTGATTGTGATTTGAGAG
	anti-sense	CTCTCAAATCACAATCAGGGATGAGCAATC
Hs_E-Box 4 mut.	sense	CTTGAATCCCCGTGGCTATCTTGCTGGGTCCCATCC
	anti-sense	GGGTTAATAGCCAATGCTATGATGAAAATGTTCGATGAATGA
Hs_*MuRF1*-luc -5002 bp	sense (NheI)	CTAGCTAGCAACAGGGCCATGTGAATGGC
Hs_*MuRF1*-luc -3938 bp	sense (NheI)	GTGCTAGCGCTGGGATTATAGGTGTGAGC
Hs_*MuRF1*-luc -3500 bp	sense (NheI)	GTGCTAGCGAGAATCATCAGCATATGG
Hs_*MuRF1*-luc -2960 bp	sense (NheI)	GTGCTAGCCTGAGGTCCCATGAGCAAGGAAG
Hs_*MuRF1*-luc -1565 bp	sense (NheI)	GTGCTAGCCAGGCGTGAGTCACTGTGCCC
Hs_*MuRF1*-luc -1006 bp	sense (NheI)	GTGCTAGCCCATTTCAAAATCTGTAAGATG
Hs_*MuRF1*-luc -543 bp	sense (NheI)	GTGCTAGCGTACTCAGAAAAATGTCTGATG
pGL3 basic general reverse primer (XhoI)	anti-sense	CCGCTCGAGCATTCTGTGGGAAGGAATGA
Hs_*MuRF1*-luc -400 bp	sense	GTGCTAGCGACCAATTTCTGGAGGAAG
Hs_*MuRF1*-luc -300 bp	sense	GTGCTAGCGATTGCTCATCCCTGCATGTG
Hs_*MuRF1*-luc -200 bp	sense	GTGCTAGCCTCCTGGGGCTCATGTGAC
Hs_*MuRF1*-luc -100 bp	sense	GTGCTAGCACCCGGTGTTTTGTGACAAAG

Mouse Tfeb cDNA was purchased from imaGenes (IRAVp968G09140D) and cloned into pcDNA™3.1*myc*-His_6 (-A) (Invitrogen) providing a C-terminal myc-$(His)_6$ tag fused to Tfeb with primers listed in table 6 as well as into pcDNA™3.1 FLAG providing an N-terminal FLAG-tag. For pZS-Green1N1 vector (Clontech) cloning, providing a ZsGreen1 fluorescent

fusion protein, Tfeb was amplified using primers also listed in table 6. Deletion mutants of Tfeb were generated by using Phusion® Site-Directed Mutagenesis Kit (Finnzymes) with the full length FLAG-Tfeb clone as template and primer sequences listed in table 6 as well. Positive clones were verified by sequencing.

Table 6: Primers for Tfeb and deletion mutant construction cloning used in this study

Primer name		Sequence (5' – 3')
Tfeb pcDNA3.1 *myc*-His (-) A	sense (EcoRI)	TGAATTCATGGCTCAGCTCGCTCAG
	anti-sense (KpnI)	CAGGTACCCAGAACATCACCCTCCTCCATGCT
Tfeb pcDNA N-FLAG	sense (EcoRI)	GGAATTCGCTCAGCTCGCTCAGTGGTCT
	anti-sense (KpnI)	GGGTACCTCACAGAACATCACCCTCCTCCATGC
Tfeb pZsGreen1-N1	sense (NheI)	CTAGCTAGCATGGCTCAGCTCGCTCAGTGG
	anti-sense (XhoI)	CCGCTCGAGCAGAACATCACCCTCCTCCA
Tfeb 1-128	sense	AAGGTGCAGTCCTACCTGGAGAAC
	anti-sense	ATCGATTTTATCGTCATCGTCTTTGTAGTCCAT
Tfeb Δ129-237	sense	ATGCCTAACACGCTGCCCCTG
	anti-sense	CAGCACCTCCCCGGGCACA
Tfeb Δ238-400	sense	CAGCAGGTGGTGAAGCAAGAGTTG
	anti-sense	CTGCATCTCAGGGTTGATGTAGCCCA
Tfeb Δ299-352	sense	TCCCGGCGCCTGGAGATGACT
	anti-sense	GTGATTGTCTTTCTTCTGCCGCTCCT

2.10 Cell lines

COS-7 cells (ATCC, CRL1651) and C2C12 cells (ATCC, CRL1772) were cultured in low glucose DME-Medium (PAA, D6046) HEk293 in high glucose DME-Medium (PAA,D5796) both supplemented with 10% FBS (PAA, A15-104) and penicillin and streptomycin (PAA, P11-010) in a humidified 5% CO2 atmosphere at 37°C. For differentiation of C2C12 myoblasts $2x10^5$ cells per well of a 6well-plate were seeded in 10%FBS DME-medium which was replaced 24h later by low glucose DME-Medium containing 2% FBS with penicillin and streptomycin (PAA, P11-010). Differentiation was performed for indicated time points with daily medium exchange. COS-7 cells were transiently transfected using FuGENE-6 (Roche) following manufacturers' instructions, HEK293 cells were transiently transfected using polyethylenimine (Polyscience Inc., #24313 linear MW2500) with DNA/PEI ratio of 1/3.

2.11 siRNA transfection

The mouse Tfeb ON-TARGETplus SMARTpool siRNA (Dharmacon, L-050607-01-0020) was used, optimization was performed using 5 to 100 ng (data not shown), and transfected

with Dhramafect3 reagent (Dharmacon, T-2003) according to the manufacturer's instructions. As negative control the ON-TARGETplus Non-targeting siRNA Pool (Dharmacon, D-001810-10-05) was used in the same concentration.

2.12 Co-Immunoprecipitation (Co-IP)

For Co-IP analysis HEK293 cells were transfected with 2 µg of total expression plasmid DNA per six-well, diluted in 200 µL serum-free medium (DMEM Low glucose) and 6 µL of polyethylenimin (PEI Stock 1µg/µL), well mixed solution's were incubated for 30 min at RT. Transfected cells were washed with ice cold 1xPBS and isolated after 24 h of over expression by scraping cells in 200 µL precooled (4°C) potasium phosphat buffer (Co-IP buffer: potassium-phosphate buffer pH 7,4; 150mM NaCl; 0,5% Triton X-100). Lysing was achieved by a following incubation at 4°C for 30 min in an overhead shacer. After centrifugation at 4°C with 10,000 g the resulting supernatend was transfered into a fresh, precooled 1,5 mL tube, whereof 10% were seperated as input control. The precipitation was assembeled using equal amounts of each lysate, 30 µL prewashed and equilibrated M2-FLAG agarose resolved in 100 µL Phosphat buffer containing 0,2 % Triton X-100 (Co-IP buffer 0,2%); mixture was filled up with Co-IP buffer w/o triton X-100 up to 1 mL and incubated at 4°C in an overhead shacer at low speed (10 rpm) for 2 h. After washing 3 times with Co-IP buffer w/o triton X-100 by centrifugation at 4°C with 800 g for 3 min, the resulting agarose beats were sucked dry with a fine (40 gauge) needle, supplemented and resuspend with 2 x Lämli without beta-mercaptoethanol and boiled for 3 min at 95°C. After short centrifugation, the eluate containing supernatant was transferred into a fresh tube, supplemented with 3 µL of 100% beta-mercaptoethanol and boiled for additional 7 min at 95°C. Input and Co-IP eluate of each experiment were analyzed using SDS-PAGE protein separation and following antibody detection.

2.13 Chromatin-Immunoprecipitation (ChIP)

For ChIP experiments, $7{,}5x10^5$ C2C12 cells were seeded into 10 cm dishes and after 24 h a transient transfection or indicated treatment were performed. After incubation for indicated time of treatment or over expression, cells were cross-linked with 1% formaldehyde for 8 min at room temperature. Fixation was stopped by adding 2.5 M glycine to a final concentration of 100 mM and incubation of 10 min at room temperature. Cells were harvested and washed three times with ice cold 1xPBS containing proteinase inhibitors (Roche) and centrifuged at

4000 x g for 5 min at 4 °C. Cell pellets were resuspended in SDS ChIP lysis buffer (10 mM EDTA, 50 mM Tris pH 8.1, 1% SDS) to a final concentration of $5*10^6$cells/mL. For cell lysis cell-suspension was passed 10 times through a 27 gauge needle (Braun, size 20) and sonicated (Hielscher, UP50H) with conditions that consistently lead to DNA fragment sizes of 100-500 Bp. Following centrifugation (13,000 x g, 10 min and 4 °C) 50 µL of clarified chromatin was used as Input control and 100 µL for immunoprecipitation. Clarified chromatin was diluted 1:10 with of ChIP RIPA buffer containing 0,1% SDS and incubated with 30 µL of prewashed anti-FLAG M2 agarose beats (Sigma, A2220) for 2 h at 4°C. Coupled protein-DNA complexes were washed twice in low salt buffer (0,1% SDS, 1% Triton X-100, 2mM EDTA, 20mM Tris-HCl pH 8.1, 150mM NaCl), twice in high salt buffer (as low salt, but 500mM NaCl) and twice in TE buffer (10mM Tris HCl pH 8.8, 1mM EDTA). Elution was performed by using 55 µL TE buffer with 1% SDS at 65°C and shaking at 1200 rpm for 10 min. 50 µL of eluate and input were supplemented with 150 µL TE, 5µL 10% SDS and 1µL RNAse (Fermentas, EN0541) and incubated for 30 min at 37C°. Proteins were afterwards digested by adding 5 µL of Proteinase K (20 µg/µL, VWR, 1.245.680.500) and lysates were incubated for 6 h at 37 °C and 6 h at 65 °C. DNA was isolated using DNA purification columns (Macheray Nagel, 740609, NT buffer 740595) as described by the manufacturer. Input DNA was eluted in 200 µL and ChIP DNA was eluted in 50 µL H_2O whereof 5 µL were used for each Real-Time PCR detection.

Table 7: Primers for Real-Time detection of ChIPed mouse *MuRF1*-promoter E-Box sites

Primer		Sequence (5' – 3')
Mm_*MuRF1* E-box 1 (-30 bp)	sense	GTGGGTTTGGAGACAAAGAC
	anti-sense	ATTGCTTTGAAATGCGACTGT
Mm_*MuRF1* E-box 2 (-151 bp)	sense	TCCTGGGGCTCATGTGAC
	anti-sense	CCCTCTGATATTTATAGCTGCAC
Mm_*MuRF1* E-box 3 (-173 bp)	sense	CTCAAGCCCTGCCAGCAG
	anti-sense	CAGGAGGGGACCAGCTG
Mm_*MuRF1* E-box 4 (-250 bp)	sense	CAACAGCGATTGCTCATCCC
	anti-sense	AAGATTTGGCCCTCTCAGATC

Base indications of E-box primer positions refer to the genomic mouse sequences of *MuRF1*-promoter upstream of the ATG start codon. These positions do relatively differ from human E-box positions.

3 Results

3.1 *MuRF1*-promoter screening

The main focus of this research project was to identify new transcriptional regulators of the *MuRF1* gene. To identify novel regulators of *MuRF1* two independent screening procedures, using 5002 base pairs (bp) and 1006 bp of the human *MuRF1* promoter (*M1P*, Table 4), were separately performed using a human skeletal muscle derived cDNA library. After screening a total number of about 114,000 cDNA clones by sib selection (fractionation based isolation of a particular cDNA library clone which shows positive induction; working scheme illustrated in Figure 7). Finally purified and isolated cDNAs were identified by sequencing. A total number of 34 cDNA clones activating the *M1P* construct, with partial (P) or full-length (FL) coding sequences (CDS), were obtained from both screening procedures. In total, five identified clones were previously described as transcription factors or linked to transcriptional activation. One hit was previously described as transcriptional repressor.

Following the studies main focus, the strongest inducers were analyzed in dose dependent verification assays. The most interesting looking candidates, which showed dose dependent *M1P* construct inductions, were cloned into expression plasmids as full-length isoforms. During the screening process the transcription factor EB (TFEB) was identified as most potent regulator of the *M1P* construct and was found six times in both screenings.

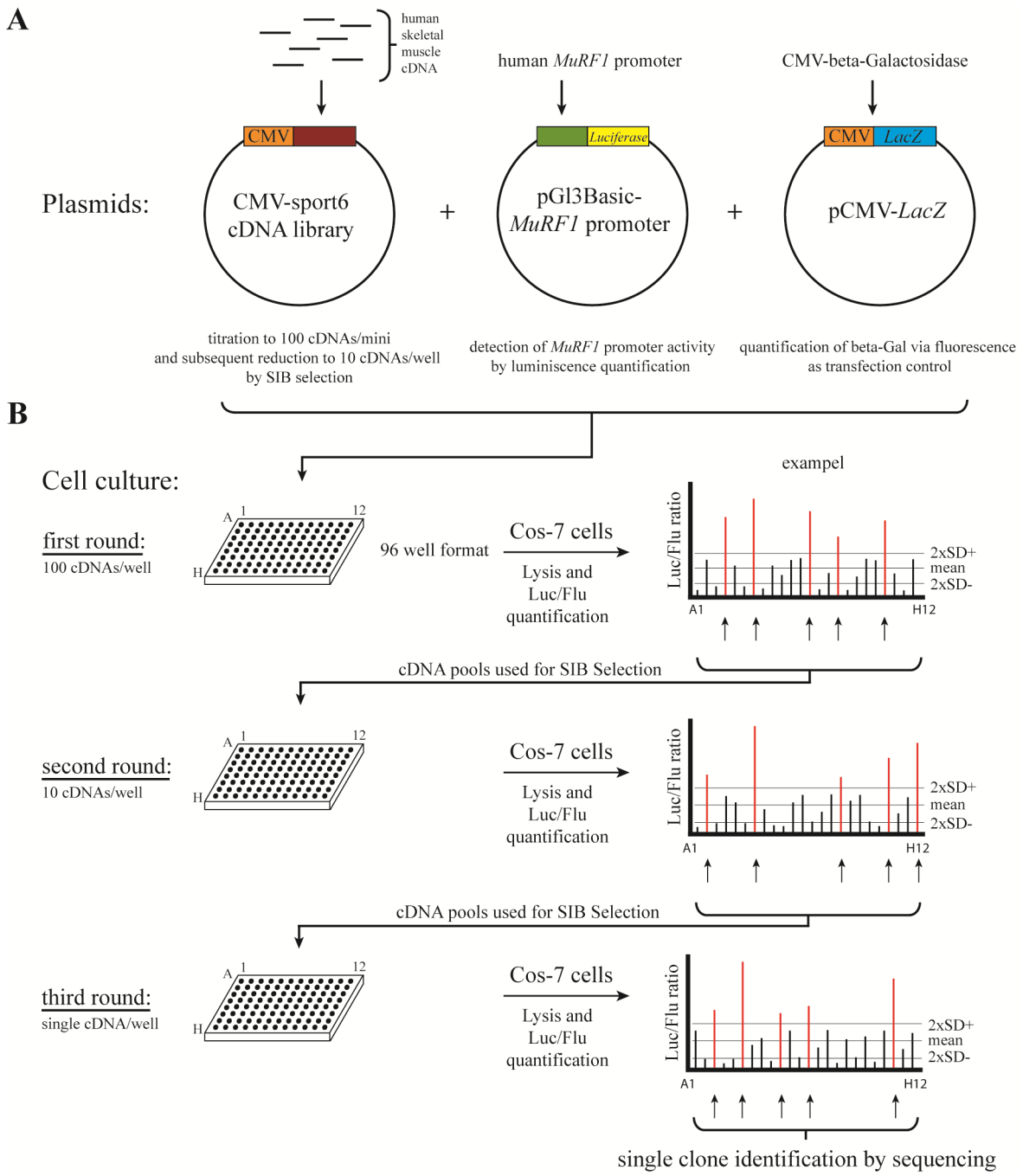

Figure 7: Schematic illustration of cDNA library screening procedure

The upper figure panel (**A**) shows the general plasmids used in the screening transfection approach. Left plasmid: CMV-promoter driven, containing cDNA library derived from adult human skeletal muscle mRNA transcripts (from Invitrogen); Middle plasmid: pGl3basic vector (Promega), containing *MuRF1* promoter sequence amplified from human genomic DNA driving *luciferase* gene, used for quantification of promoter activity; Right plasmid: CMV-promoter, controlling *beta-Galactosidase* gene expression, used as constitutive active transfection control, measured via fluorescence quantification. Lower panel (**B**) shows the underlying cell culture procedure. The cDNA library was titrated to an initial average concentration of 100 CFU/well (or different cDNA clones/mini-prep) during plasmid preparation from BAK clone library. For detailed transfection information see Material and Methods. After subsequent cDNA count reduction single clone candidates were identified by sequencing.

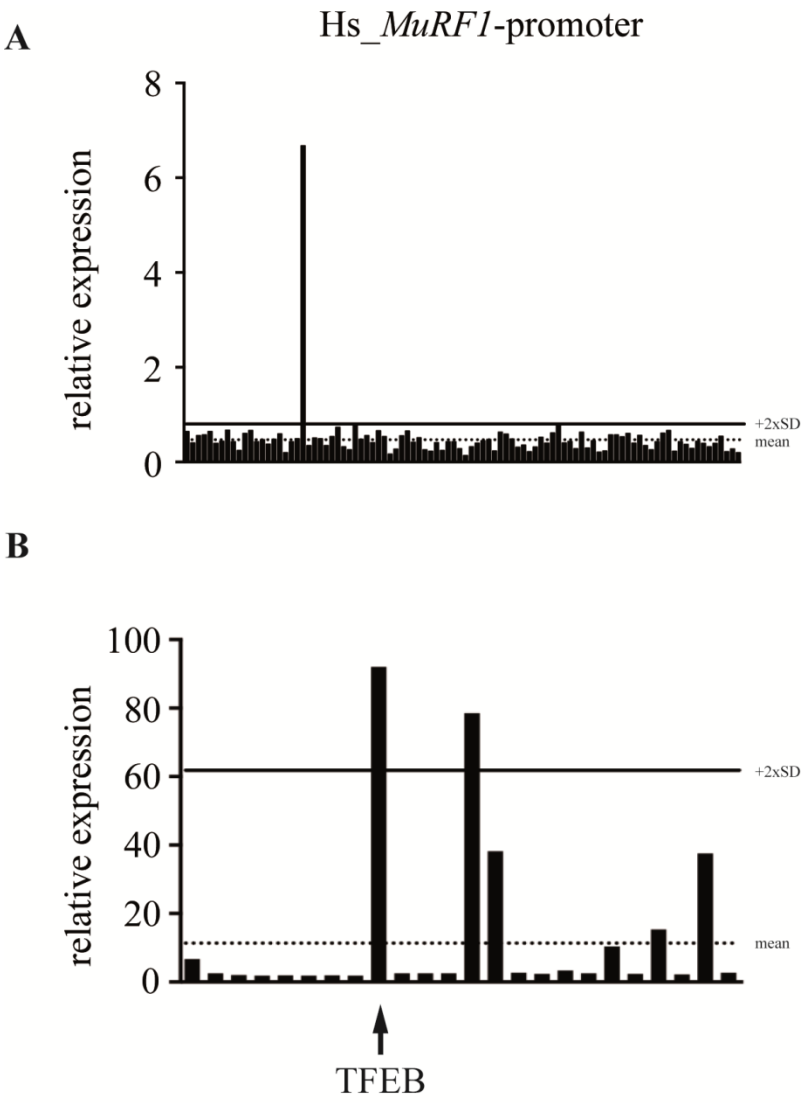

Figure 8: Luciferase assay read-outs from cDNA library screening procedure of human *MuRF1*-promoter

(**A**) Graph shows representative quantifications of one initial screening plate, corresponding to ~100 cDNAs per well of cDNA library derived from human skeletal muscle mRNA. (**B**) Graph shows final screening phase, after sib selection, whereas each bar represents *M1P* construct inductions by a single cDNA clone, subsequently extracted from initial round shown in A. Arrow indicates well/peak containing a sequence-verified partial TFEB cDNA clone. Relative calculations are shown in luciferase/fluorescence ratio, corresponding to cDNA clone induced *M1P* construct and the fluorescence quantification of the transfection control plasmid pCMV-*LacZ*. Black continuous lines indicate the plates doubled average SD values (+2xSD) whereas dotted lines indicate the plates mean values. (Ref.: Figure data are included in manuscript in preparation/submission)

Sequencing of the cDNA library encoded pSPORT6-TFEB constructs revealed that two different isoforms of TFEB were isolated during the screening process. One encoded a full length version in accordance with the human TFEB Isoform 1. The second isoform encoded for a partial cDNA fragment ranging from amino acids 96 to the C-terminal end of the full length human TFEB protein (Figure 9), when compared with the longest human TFEB iso-

form 2 (accession NM_1167827.2; (Carr & Sharp, 1990)). However, the shorter isoform identified here contains all of the annotated domains, such as the activation (AD), basic helix-loop-helix (bHLH), leucine-zipper (LZ) and DUF3371 (DUF) domain.

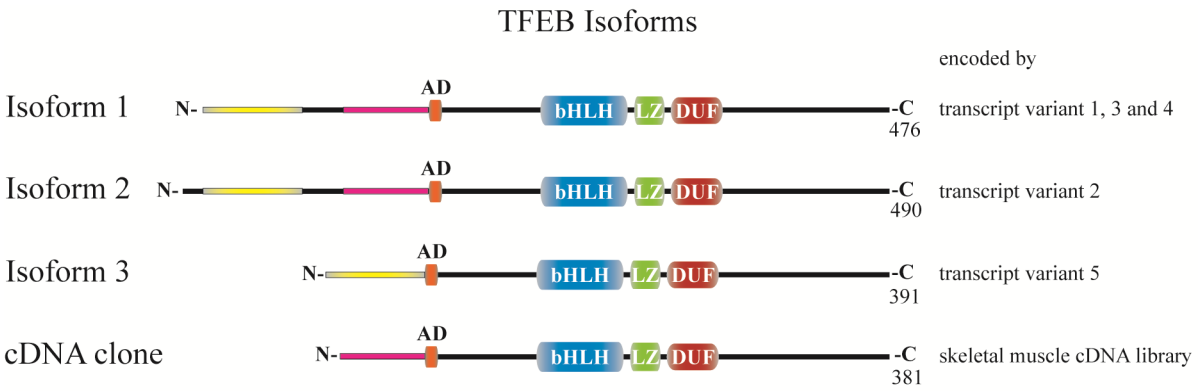

Figure 9: Illustration of the human TFEB Isoforms 1, 2 and 3 plus the identified clone from cDNA library screening.

The human TFEB Isoforms 1, 2 and 3 encoding transcript variants 1 to 5 are indicated at the right side. Graphical explanations: (AD) activation domain, (bHLH) basic helix-loop-helix domain, (LZ) leucine-zipper domain and DUF3371 domain. Number of amino acids is shown under the C-terminal end of each isoform. Sections in yellow and violet are marked for better orientation and do not represent annotated domains or regulatory regions.

3.2 Identification of binding site for Tfeb of *MuRF1* promoter

Comparing the longest isoforms of human TFEB Iso 2 (490 AA) and mouse Tfeb isoform A (534 AA), both protein sequences disclosed a 93 % sequence identity (Sequence-alignment in appendix figure 1). Since direct amplification of the full length mouse Tfeb from muscle tissue derived cDNA was without any result, a purchased Tfeb (mouse isoform A) from ImaGenes was used. The obtained full length Tfeb was cloned in an N-terminal FLAG tag expression vector (FLAG-Tfeb, Table 3 and 4). Tfebs' ability to dose dependently induce the *M1P* construct (size -543 bp, Table 4) could be confirmed when co-transfected in COS-7 cells (Figure 10). Luciferase assays, utilizing subsequently size-reduced *M1P* fragments from -5002 bp to -543 bp upstream of the *MuRF1* transcriptional start codon, showed comparable fold activations (Figure 11 A). Further decrease of the *M1P* fragment from -300 bp to -200 bp strongly reduced Tfeb induced *M1P* expression declining from ~100 to ~10 fold (Figure 11 B). These results pointed towards a strong Tfeb regulatory element close to the transcriptional start codon of *MuRF1*. It is noteworthy, that differences observed in maximum *M1P* construct inductions are partially based on variations in transfection efficiencies of differentially used cell lines.

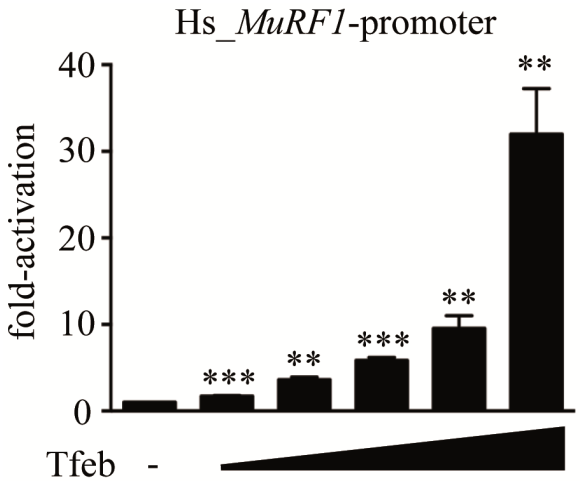

Figure 10: Dose dependent *MuRF1*-promoter activation by Tfeb

(**A**) COS-7 cells were co-transfected with the *M1P* construct (size -543 bp), pCMV-*LacZ* control plasmid and increasing amounts of FLAG-Tfeb expression plasmid (dose: 6, 25 – 100 ng). Values were normalized to basal expression of the *M1P* construct and calculated as fold-activation ratio (set to 1) of FLAG-Tfeb induced reporter (luciferase) to pCMV-*LacZ* (β-*Gal*). Graph shows representative experiment in triplicates, experiment has been performed at least three times. Error bars represent SD. Students T-Test, ** $p < 0.005$; *** $p < 0.001$. (Ref.: Figure data are included in manuscript in preparation/submission)

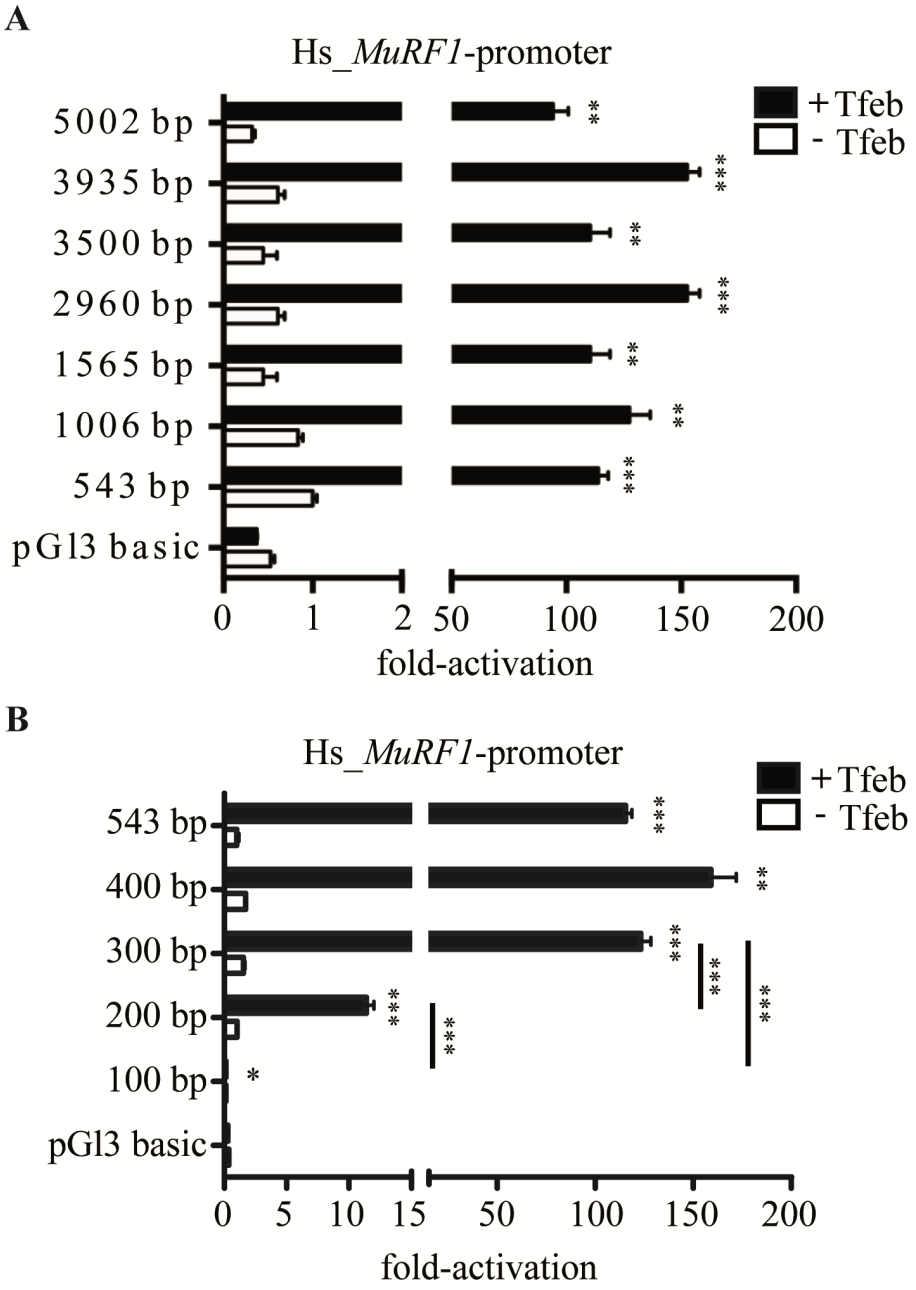

Figure 11: Size dependent *MuRF1*-promoter activation by Tfeb

(**A**) Graph shows luciferase assay readouts, performed in HEK293 cells, of decreasing Hs_*MuRF1*-luc promoter fragment lengths (-5002 to -543 bp of Hs_*MuRF1*-promoter; pGL3basic equates empty luciferase reporter plasmid), co-transfected with 100 ng of FLAG-Tfeb expression plasmid. Values were normalized to basal expression of the *M1P* construct (size -543 bp) and calculated as fold-activation ratio of FLAG-Tfeb expression plasmids induced reporter relative to pCMV-*LacZ* (β-*Gal*). Graph shows representative experiment in triplicates, experiment has been performed at least three times. Error bars represent SD. Students T-Test, ** $p < 0.005$; *** $p < 0.001$. (**B**) Graph shows luciferase assay readout from HEK293 cells, co-transfected with Tfeb expression plasmids (FLAG-Tfeb), pCMV-*LacZ* transfection control plasmid and indicated decreasing *M1P* constructs (-543to -100 base pairs of Hs_*MuRF1*-promoter; pGl3 basic equates empty luciferase reporter plasmid). Values were normalized to basal expression of the *M1P* construct (size -543 bp) and calculated as fold-activation ratio of Tfeb expression plasmids induced reporter relative to pCMV-*LacZ* (β-*Gal*). Graph shows representative experiment in triplicates, experiment has been performed at least three times. Error bars represent SD. Students T-Test, * $p < 0.05$; ** $p < 0.005$; *** $p < 0.001$. (Ref.: Figure data are included in manuscript in preparation/submission)

Tfeb contains a bHLH DNA binding domain (Figure 9), which mediates E-box specific promoter binding (E-box motive CANNTG; Figure 12 A). After literature reviewing (Fisher, Carr, Parent, & Sharp, 1991; Kuiper, Schepens, Thijssen, Schoenmakers, & van Kessel, 2004) and additive analysis of the *MuRF1* promoter*'s* structure, including various mammalian species, the conserved E-box binding motives within the *M*1P construct (size -543 bp) were individually mutated (Figure 12 B; mutation CANNTG to ATNNTG). Mutation of the first and third E-box motives lead to a strong reduction of Tfeb mediated *M*1P expression. In contrast, mutation of the second E-box motif only moderately reduced luciferase expression. Surprisingly, mutation of the lesser conserved forth E-box motif at position -299 to -304 in the human *M1P* construct produced an increase in Tfeb mediated *M*1P expression (Figure 12 B). This forth E-box position was excluded from further analysis due to lower species conservation and the main focus of this study, the investigation of positive regulators of *MuRF1* expression.

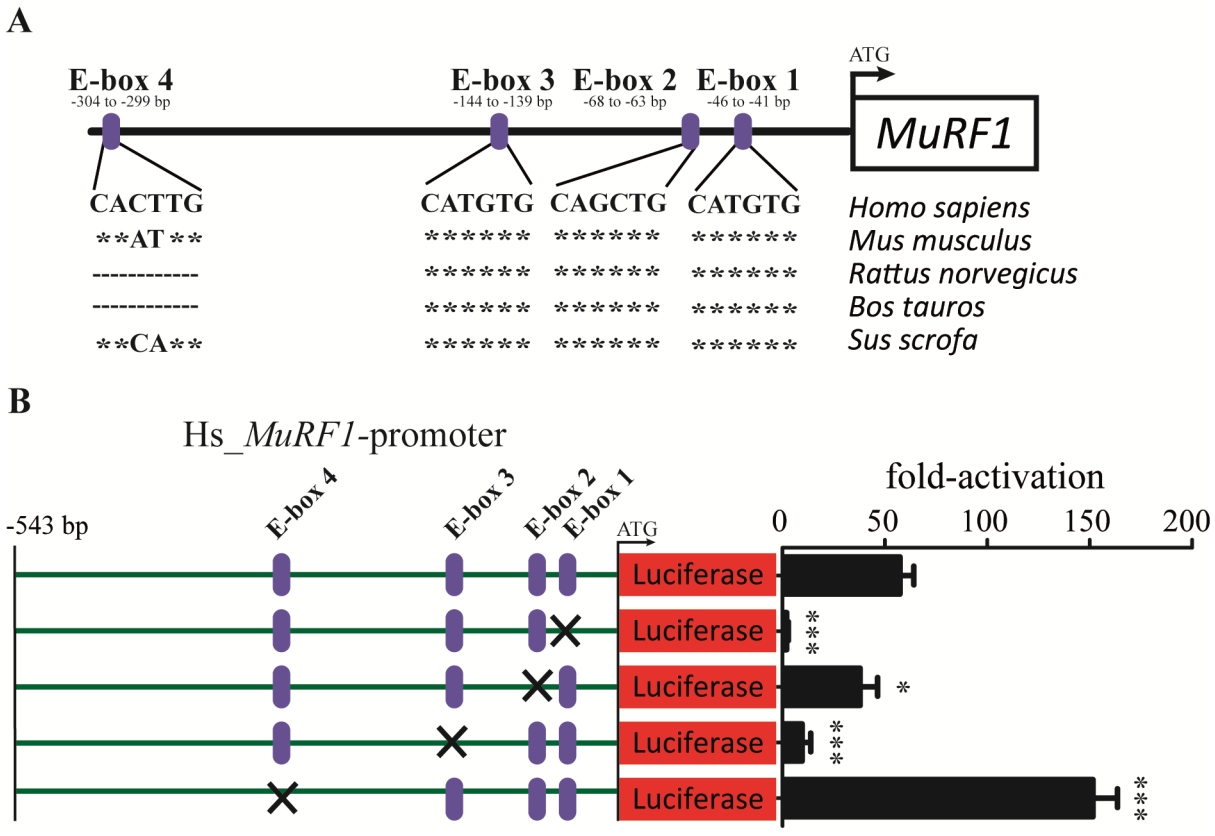

Figure 12: Tfeb regulates *MuRF1* expression via E-box motives

(**A**) Schematic diagram of *MuRF1* promoter E-box conservation. E-box elements in the human *MuRF1* promoter are indicated in purple relative to the transcription start codon (ATG). Underlying alignment shows genomic homology of individual E-box motifs in the *MuRF1* promoter sequence of *Homo sapiens*, *Mus musculus*, *Rattus norvegicus*, *Bos tauros* and *Sus scrofa*. (**B**) Luciferase assay readouts from COS-7 cells co-transfected with FLAG-Tfeb construct, wild type (upper lane) and E-box mutated *M1P* constructs and the pCMV-*LacZ* (β-*Gal*). Values were normalized to basal expression of WT *M1P* construct expression (set to 1, not shown) and calculated as fold-activation ratio of luciferase to β-*Gal.* Each well contained same amounts of FLAG-Tfeb expression

plasmid. Mutations of the E-box motives (E-box 1 to E-box 4; CANNTG to mutant ATNNTG) are indicated. Error bars represent SD; n = 3; Students T-Test; * $p < 0.05$; ** $p < 0.005$; *** $p < 0.001$. (Ref.: Figure data are included in manuscript in preparation/submission)

3.3 Tfeb: Gain-of-function

Potential influence of Tfeb over-expression onto the gene expression of the other MuRF family members *Trim55* encoding *MuRF2* and *Trim54* encoding *MuRF3* was quantized by Real-Time PCR (RT-PCR). Transfection of C2C12 myoblasts with a cDNA expression plasmid encoding FLAG-Tfeb resulted in a significant increase in *MuRF1* expression (~10 fold), whereas no change was observed for *MuRF2* or *MuRF3* (Figure 13 A). In addition, lysates of identical treated C2C12 myoblasts showed increased MuRF1 protein content after 24 h of Tfeb over-expression in Western blot analysis (Figure 13 B). The increase in gain-of-function experiments of *MuRF1* mRNA and MuRF1 protein contents confirmed that Tfeb regulates endogenous *MuRF1*.

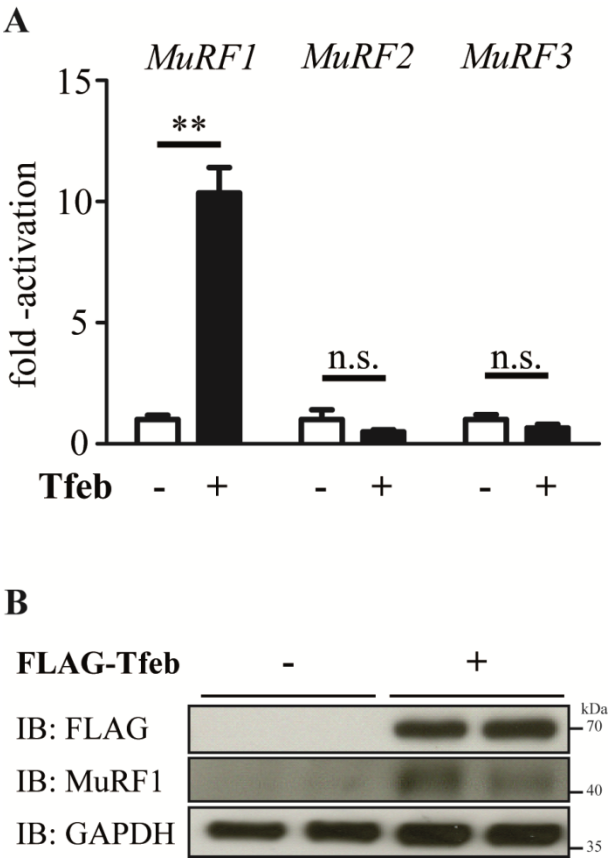

Figure 13: Tfeb regulates endogenous *MuRF1* expression in C2C12 myoblasts

(**A**) RT-PCR analysis of *MuRF1*, *MuRF2* and *MuRF3* expression in C2C12 myoblasts following overexpression of FLAG-Tfeb plasmid or a control plasmid for 24 h. *Glyceraldehyde-3 phosphate dehydrogenase* (*GAPDH*) expression was used as reference. Gene expression following control plasmid transfection was set to 1. Error bars represent SD. n.s. = not significant. ** $p < 0.005$; $n = 3$ for each sample. (**B**) C2C12 myoblasts were transfected with expression plasmids encoding FLAG-Tfeb or a control protein for 24 h, and immunoblot analysis was performed with the antibodies indicated. (Ref.: Figure data are included in manuscript in preparation/submission)

3.3.1 Tfeb binds to the *MuRF1* promoter via E-box motives

To confirm Tfebs' binding to the endogenous *MuRF1* promoter sequence, Chromatin-Immunoprecipitation (ChIP) experiments were performed in C2C12 myoblasts. ChIP analysis followed by RT-PCR showed that over-expressed N-FLAG or C-terminally Myc tagged full length Tfeb (Table 4) binds to the endogenous *MuRF1* promoter sequence in C2C12 myoblasts (Figure 14 A and B). Both ChIP experiments showed an enrichment of the mouse *MuRF1* promoter sequence when Tfeb was present, compared to the empty vector transfections. Due to the very close proximity of the E-box motives in the *MuRF1* promoter sequence a clear distinction between individual E-box motifs was impossible (Figure 14 A, upper illustration).

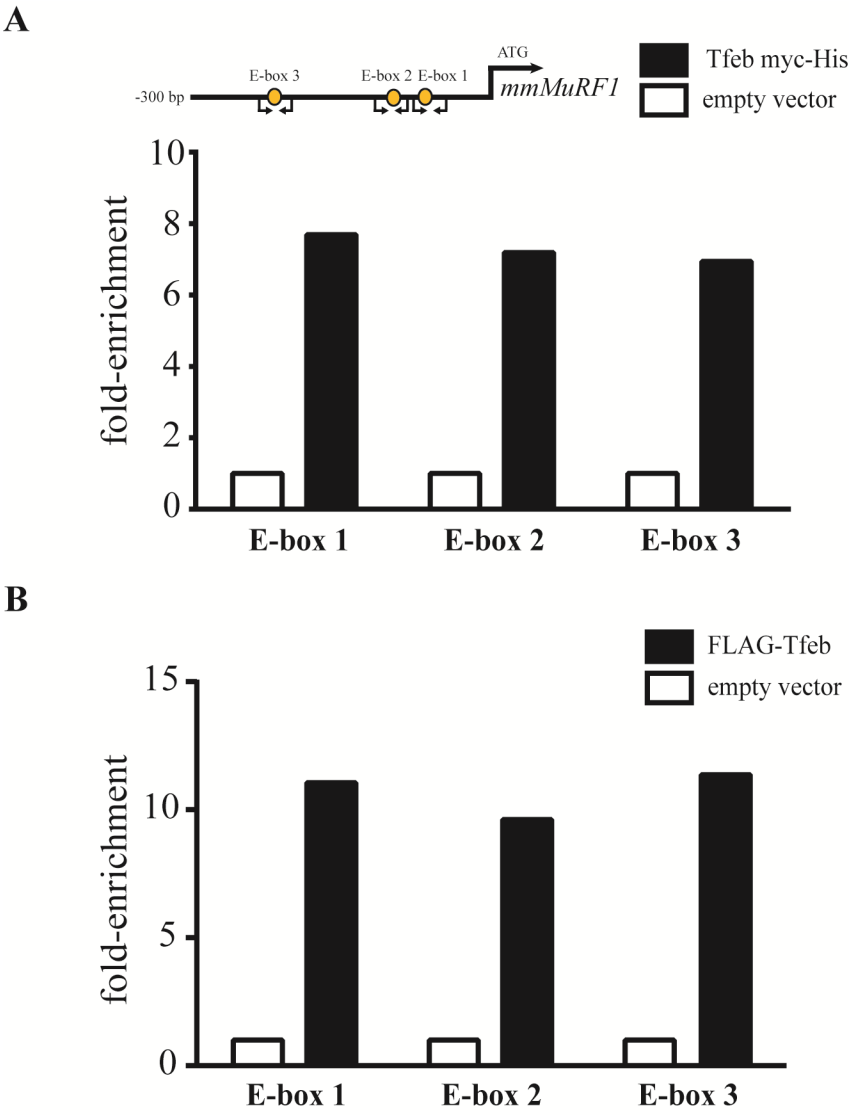

Figure 14: Tfeb binds to the endogenous *MuRF1* promoter sequence

(**A**) Representative Chromatin-Immunoprecipitation (ChIP) experiment performed with chromatin from C2C12 myoblasts after overexpression of Tfeb Myc-His construct for 24 h (Tfeb Myc-His, Table 4). Chromatin was

immunoprecipitated with anti-Tfeb vs. IgG rabbit antibody (1 µg per IP) and Agarose-G beats. For eluate analysis, E-box flanking primers (positions illustrated above) specific for the mouse *MuRF1* promoter were used in Real-Time PCR based quantification. Results were calculated using $delta^{Input}$ - $delta^{IgG}$ - $delta^{vector}$ cT method. (**B**) Representative ChIP experiment of chromatin from C2C12 myoblasts after overexpression of FLAG-Tfeb construct for 24 h (FLAG-Tfeb, Table 4). Cells were grown in normal growth DME-Medium (10 % FBS). Chromatin was immunoprecipitated using M2 FLAG-Agarose. For eluate analysis, E-box flanking primers (positions illustrated in Figure 14 A) specific for the mouse *MuRF1* promoter were used in Real-Time PCR based quantification. Results were calculated using $delta^{Input}$ - $delta^{vector}$ cT method. (Ref.: Figure data are included in manuscript in preparation/submission)

3.4 Tfeb loss-of-function and functional involvement in starvation induced myotube formation

Loss-of-function approaches, using siRNA mediated knock-down of Tfeb mRNA, in C2C12 myoblasts and differentiated myotubes were performed to confirm the results from gain-of-function and ChIP experiments. Knock-down of Tfeb for 24 h via specific siRNA transfection (100 nM each) in C2C12 myoblasts led to a decrease in *MuRF1* mRNA and protein contents compared to siScr control treated cells (Figure 15 A and B).

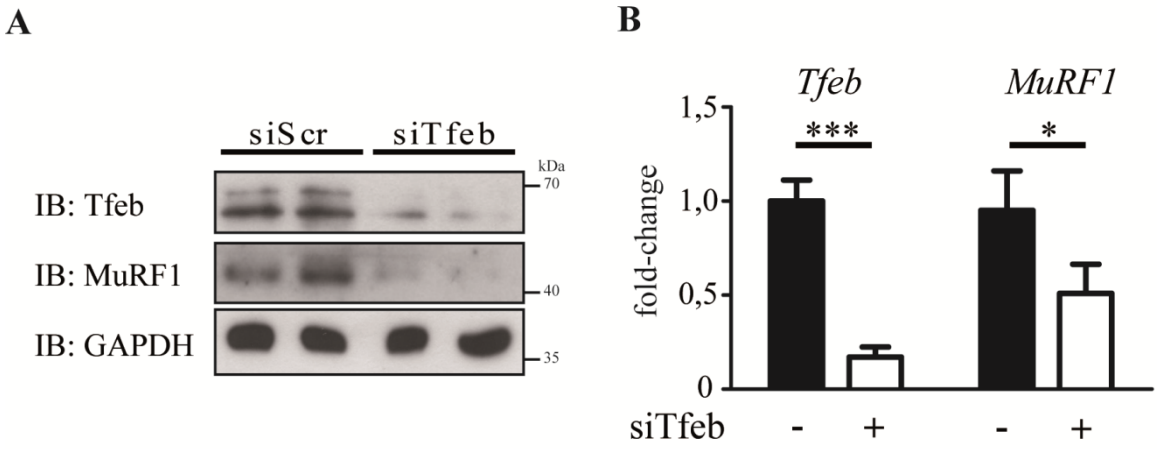

Figure 15: Knockdown of Tfeb influence endogenous *MuRF1* expression

(**A**) C2C12 myoblasts were transfected with scrambled control siRNA (siScr) or siRNA against Tfeb (siTfeb*;* 100 nM each. Cells were harvested 24 h after transfection for immunoblot analysis of Tfeb, MuRF1 and Glyceraldehyde-3 phosphate dehydrogenase (GAPDH) protein content. (**B**) C2C12 myoblasts were treated as described for A. Cells were harvested 24 h after transfection and *Tfeb* and *MuRF1* expression were quantified using RT-PCR analysis. *GAPDH* expression was used as reference. Error bars represent SD. * $p < 0.05$; *** $p < 0.001$; $n = 3$. (Ref.: Figure data are included in manuscript in preparation/submission)

When identically treated C2C12 myoblasts were subsequently treated with differentiation medium (2 % FBS containing DME-medium) for 5 days, a diminished tube formation was observed, as determined by counting of myotubes (Figure 16 A and B). Reduced myotube formation was supported by a decrease in myosin fast protein content detected by Western-blotting (Figure 17 A), which is observed only in differentiated myocytes.

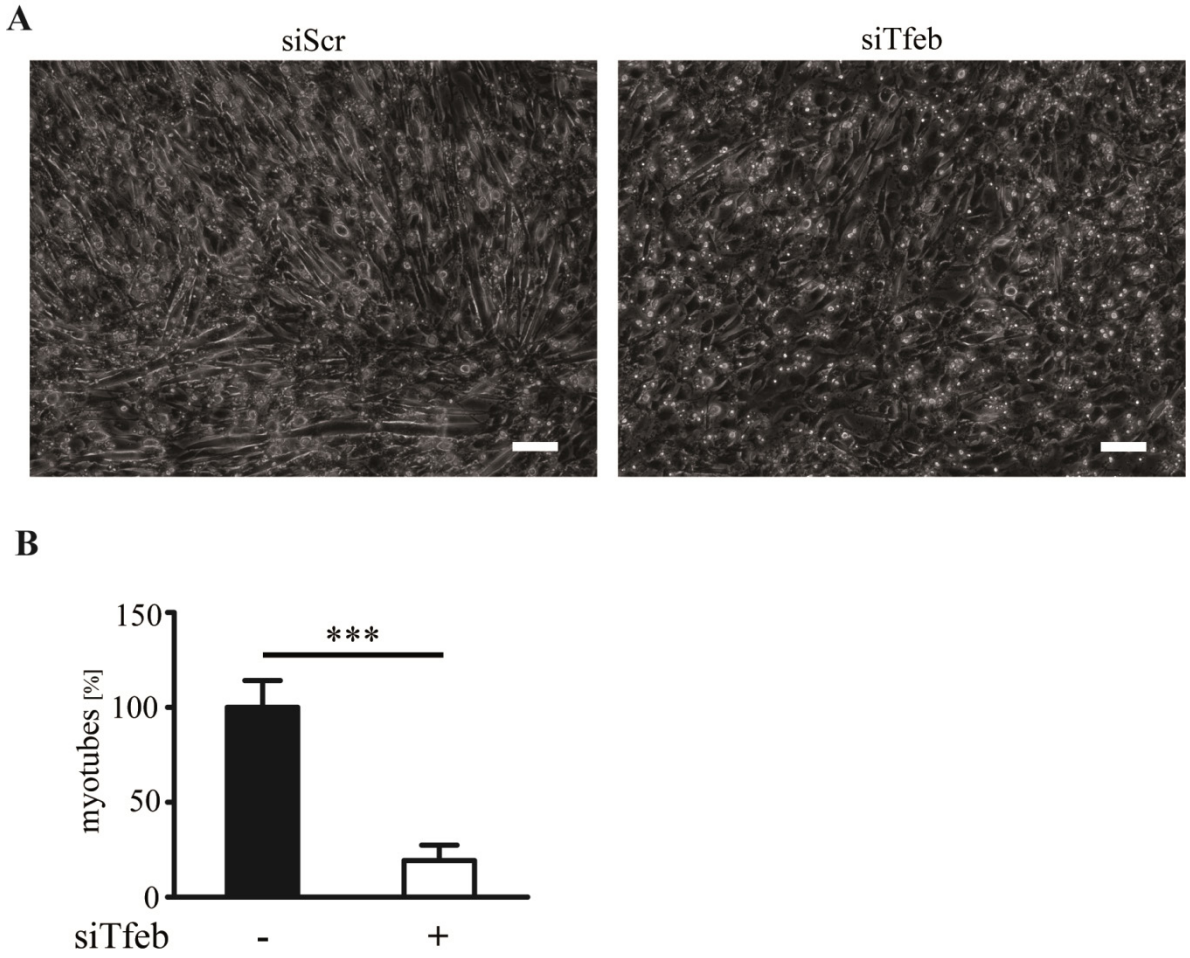

Figure 16: Knock-down of Tfeb reduces C2C12 myotube differentiation

(**A** and **B**) C2C12 myoblasts were transfected with scrambled control siRNA (siScr) or siRNA against *Tfeb* (siTfeb*;* 100 nM each), as indicated. Cells were switched to differentiation conditions 24 h after transfection and diff. Medium (2 % FBS DME-medium) was changed every day. After 5 days of differentiation, cells were harvested and analyzed. (**A**) Representative graphical representation of C2C12 cells after siRNA knock-down described above. Scale bar represents 100 µm. (**B**) Graph shows myotube quantification from ten randomly taken pictures per group from same experimental setup as described above. Error bars represent SD. Student T-Test; *** $p < 0.001$. (Ref.: Figure data are included in manuscript in preparation/submission)

In addition, siTfeb pre-treated and differentiated C2C12 myotubes showed a decreased *MuRF1* mRNA expression when compared with siScr control after 5 days of differentiation (Figure 17 B). This finding was supported by ChIP analysis. An enriched binding of endogenous Tfeb to the endogenous *MuRF1* promoter sequence was observed in ChIP analysis of 6 hr serum starved (2 % FBS containing DME-medium) C2C12 myoblasts (Figure 18).

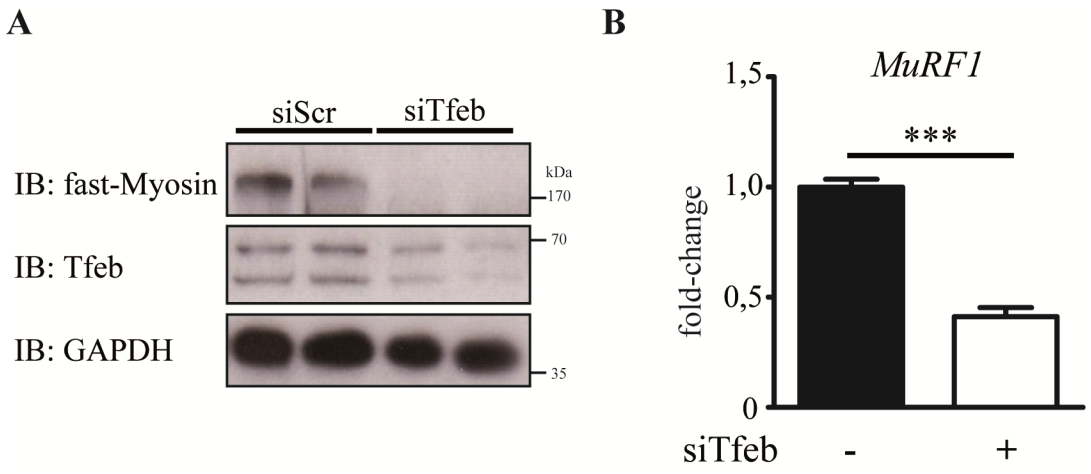

Figure 17: Tfeb knock-down reduces fast myosin and *MuRF1* expression during C2C12 myotube differentiation

(**A and B**) C2C12 myoblasts were transfected with scrambled control siRNA (siScr) or siRNA against *Tfeb* (siTfeb*;* 100 nM each), as indicated. Cells were switched to differentiation conditions 24 h after transfection and diff. Medium (2 % FBS DME-medium) was changed every day. After 5 days of differentiation, cells were harvested and analyzed. (**A**) Western-blot analysis of differentiated C2C12 cells, proteins were detected by immunoblot analysis against fast-myosin, Tfeb and Gapdh. (**B**) Real-Time PCR analysis of *MuRF1* expression in C2C12 cells, treated as described above. *GAPDH* expression was used as reference. Error bars represent SD. Students T-Test; *** $p < 0.001$; $n = 3$. (Ref.: Figure data are included in manuscript in preparation/submission)

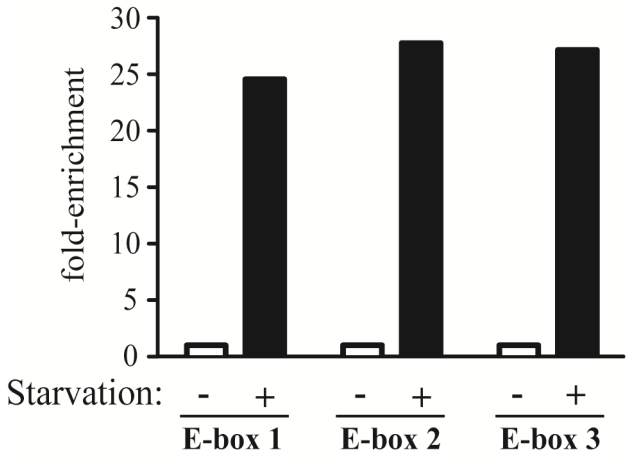

Figure 18: Enhanced Tfeb binding to the *MuRF1* promoter after serum starvation

Graph shows representative ChIP analysis of C2C12 myoblast chromatin of control cells, grown in normal growth DME-medium (10 % FBS) or serum starved cells (6 h; 2 % FBS DME-medium). Chromatin was incubated with anti-Tfeb vs. IgG rabbit antibody (1 µg per IP) and immunoprecipitated using Agarose-G beats. For analysis, E-box flanking primers, specific for the mouse *MuRF1* promoter, were used in RT-PCR quantification. Calculation was carried out using $delta^{Input}$ - $delta^{IgG}$ - $delta^{starvation}$ cT method. (Ref.: Figure data are included in manuscript in preparation/submission)

3.5 Tfeb is negatively regulated by class IIa HDACs

Now assuming that Tfeb plays a role in the regulation of *MuRF1* expression, participation of Tfeb in known regulation pathways of skeletal muscle atrophy was taken into focus. One of the major and most potent regulators described for *MuRF1* expression are the class IIa HDAC, shown to inhibit *MuRF1* expression under different conditions (Viviana Moresi et al., 2010b). All class IIa HDACs (HDAC4, 5, 7 and 9) were found to reduce basal expression of the *M1P* construct (size -543 bp) when co-transfected in COS-7 cells (Figure 19 A). To investigate if class IIa HDACs inhibit Tfeb induced *MuRF1* expression (Hs_*MuRF1*-luc also *M1P*; size -543 bp) FLAG-Tfeb expression plasmid was transfected together with increasing amounts of HDAC4, 5, 7 and 9 expression plasmids and reporter assays were performed. The strongest negatively regulating effects unto the Tfeb mediated *M1P* inductions were observed for HDAC4 and 5 (Figure 19 B).

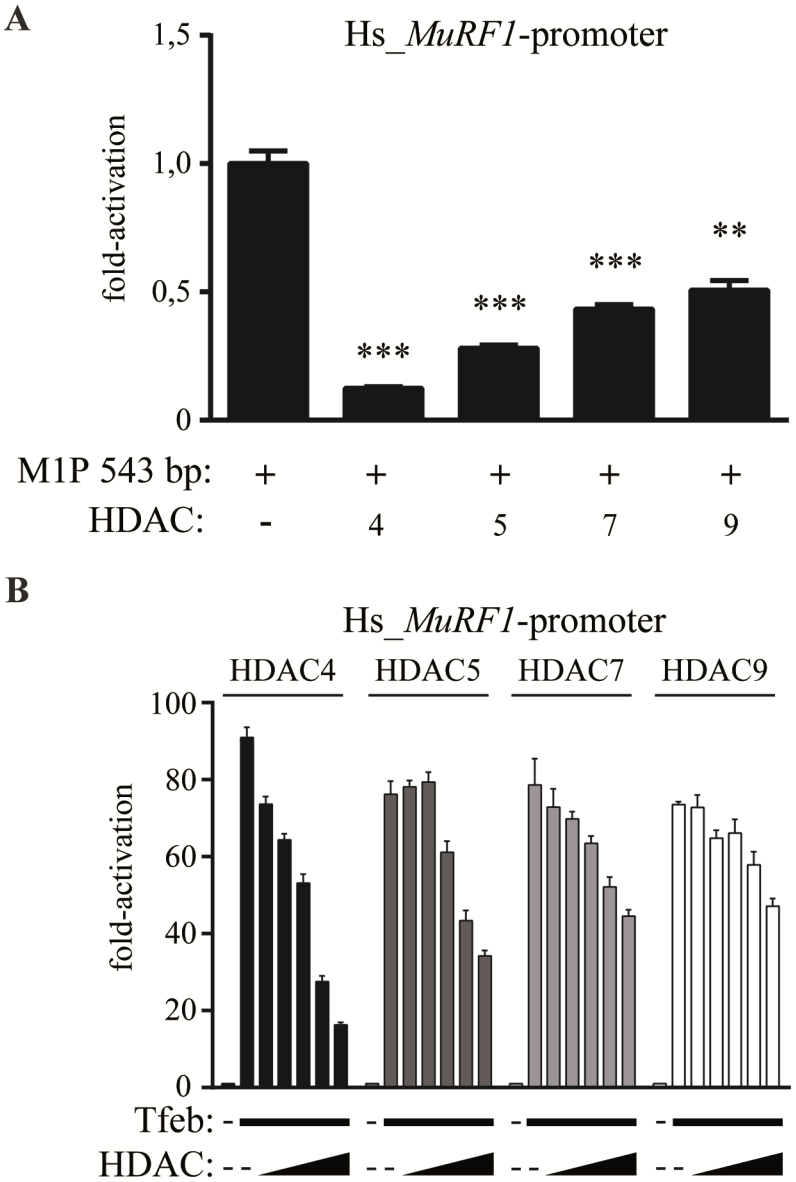

Figure 19: Repressive effect of ClassIIa HDACs on *MuRF1* basal expression and Tfeb mediated induction

(**A**) Graph shows luciferase assay quantification of co-transfected COS-7 cells with the *M1P* construct (size -543 bp), pCMV-*LacZ* transfection control plasmid and indicated ClassIIa HDAC4, 5, 7 and 9 expression plasmids. Values were normalized to basal expression of *M1P* construct and calculated as fold-activation ratio of reporter to pCMV-*LacZ* (β-*Gal*). Graph shows representative experiment in triplicates, experiment has been performed at least three times. Error bars represent SD. Student T-Test; ** $p < 0.005$; *** $p < 0.001$. (**B**) Graph shows luciferase assay quantification of co-transfected COS-7 cells with the *M1P* construct (size -543 bp), pCMV-*LacZ* transfection control plasmid, FLAG-Tfeb expression plasmid (100 ng per well) and increasing doses of indicated ClassIIa HDAC4, 5, 7 and 9 expression plasmids (dose range from 5 to 100 ng per well). Values were normalized to basal expression of *M1P* construct and calculated as fold-activation ratio of reporter to pCMV-*LacZ* (β-*Gal*). Graph shows representative experiment in triplicates, experiment has been performed at least three times. Error bars represent SD. Students T-Test; ** $p < 0.005$; *** $p < 0.001$. (Ref.: Figure data are included in manuscript in preparation/submission)

If the repression of Tfeb induced *MuRF1* expression was mediated due to direct binding of Class IIa HDACs to Tfeb co-immunoprecipitation (Co-IP) experiments were performed of lysates from HEK293 cells co-transfected for 24 h with Tfeb Myc-His construct and FLAG-

HDAC constructs. Indeed, Tfeb physically interacted with the ClassIIa HDAC5 (Figure 20 A and Figure 21 B). Next, it was investigated if this interaction could also be observed in cells, using co-localization studies performed in C2C12 myoblasts. It was found that Tfeb-GFP co-localized with FLAG-HDAC4 and FLAG-HDAC5 (stained with Alexa 555), respectively. This co-localization occurred in nuclei (Figure 20 B) and in cytoplasmic vesicular structures (Figure 21 C; constructs in Table 4).

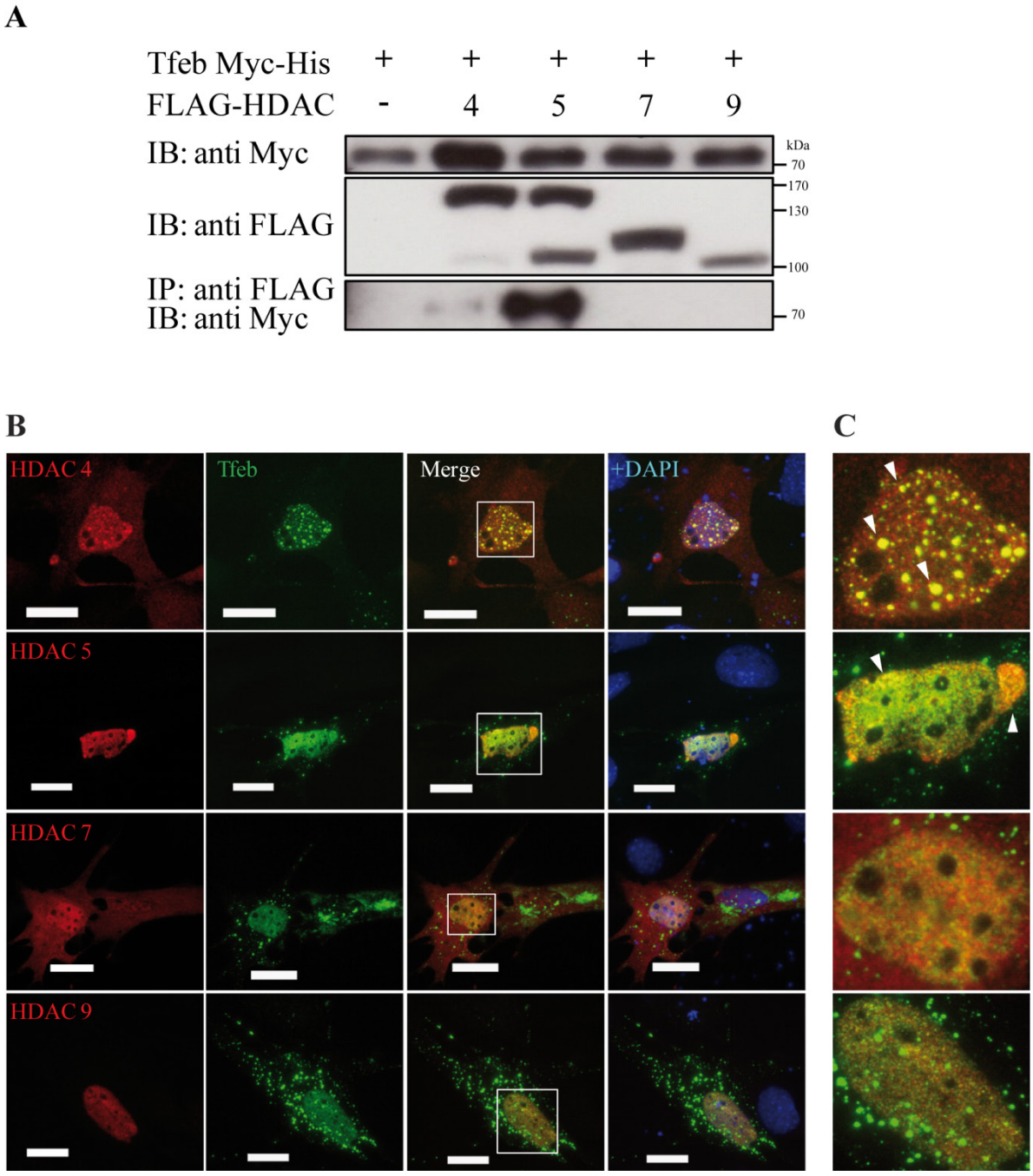

Figure 20: Interaction and Co-localization of Tfeb with ClassIIa HDAC family members

(**A**) Western-blot analysis showing inputs (both upper panels, anti Myc and anti FLAG) and eluates (lower panel, anti Myc) of co-immunoprecipitation experiment performed in HEK293 cells, over-expressing Tfeb Myc-His

expression plasmid and FLAG-HDAC4, 5, 7 or 9 expression plasmids (used constructs in Table 4). Inputs represent 10% of total lysates. Left panel represents negative control with empty FLAG vector. (**B**) Graphical representation of co-localization study performed in C2C12 myoblasts, over-expressing Tfeb-GFP and FLAG-tagged HDAC4, 5, 7 and 9 expression plasmids as indicated. Left panel (red signal) shows HDAC signal detected by immunostaining (secondary antibody Alexa 555, primary anti FLAG M2). Green signal shows GFP signal from Tfeb-GFP construct. The third panel from left represents merged overlays of red and green channels with marked nuclei in white boxes representing magnified area shown in C. Right panel in B shows merged channels plus DAPI signal overlay. Scale bars represent 10 µm. (**C**) Magnifications of marked nuclei shown in B. White arrowheads indicate areas of co-localization. (Ref.: Figure data are included in manuscript in preparation/submission)

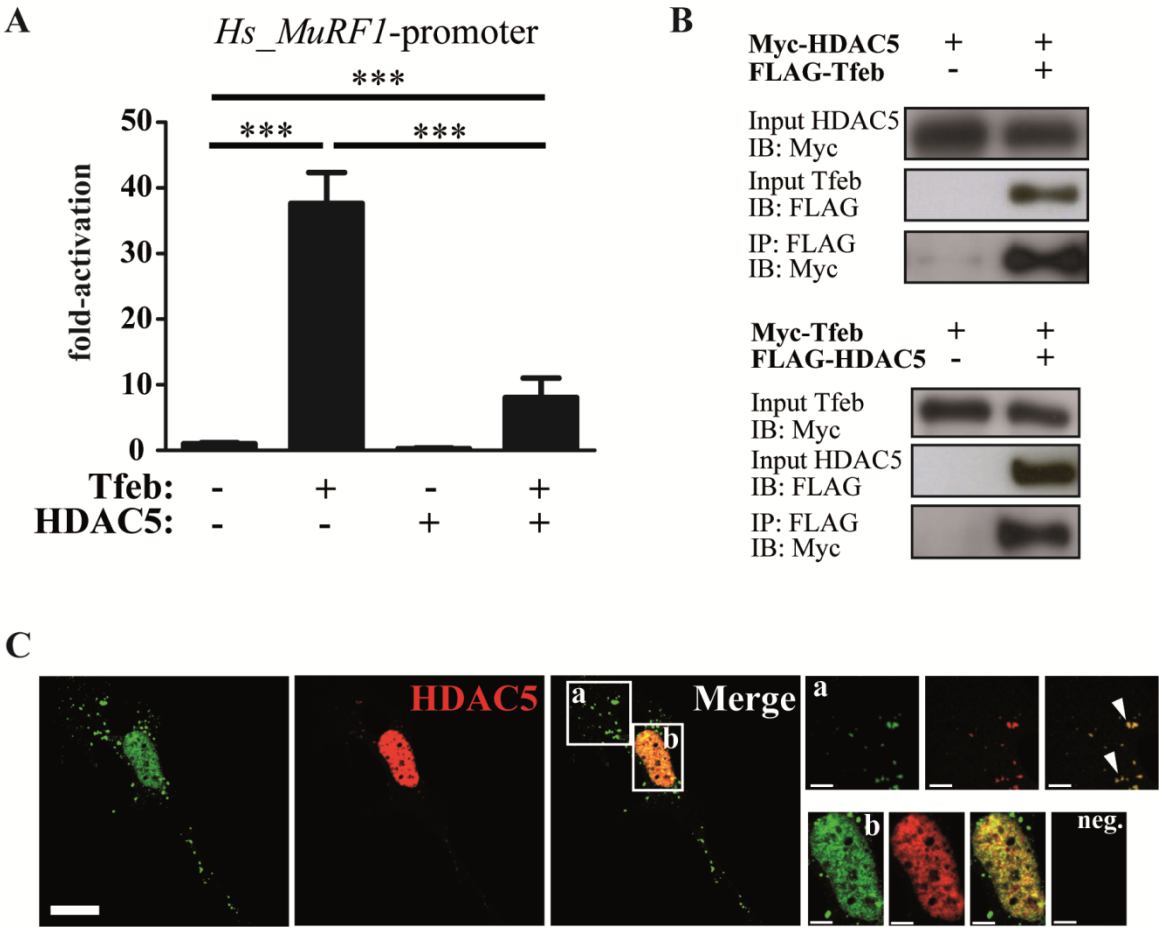

Figure 21: Inhibition of the Tfeb mediated *MuRF1* induction by ClassIIa HDAC5

(**A**) HEK293 cells were transfected with expression plasmids encoding full length Tfeb and HDAC5 together with the *M1P* construct (size 543 bp), as indicated. Values were normalized to pCMV-*LacZ* transfection control vector expression and calculated as fold-activation in luciferase to pCMV-*LacZ* ratio compared to the reporter alone. Error bars represent SD. Students T-Test; *** $p < 0.001$. $n = 3$. (**B**) HEK293 cells were transfected with expression plasmids encoding FLAG-Tfeb and HDAC5-myc (above panel) and Tfeb-myc and FLAG-HDAC5 (lower panel). Inputs of Tfeb and HDAC5 proteins detected by immunoblot (IB) are shown in the top and middle panels. Inputs represent 10% of total lysates. Co-immunoprecipitated proteins are shown in the bottom panels. (**C**) C2C12 myoblasts were co-transfected with expression plasmids encoding Tfeb-GFP and HDAC5-myc. HDAC5 was detected by immunostaining (Alexa 555) and Tfeb by GFP fluorescence using confocal microscopy. Scale bar in left picture represents 10 µm. Augmentations of indicated regions (**a** and **b**) are shown in smaller panels to the right. Scale bar represents 5 µm. Arrowheads in **a** indicate areas of co-localization. (Ref.: Figure data are included in manuscript in preparation/submission)

3.6 Mapping of Tfeb and HDAC5 interaction

To characterize the interaction between Tfeb and HDAC5 in more detail, deletion mutants of both cDNAs were generated and used in Co-IP and luciferase assays. Co-IP experiments indicated that the HDAC5/Tfeb interaction was mediated via the N-terminal end of HDAC5 (Figure 22 A and B; constructs in Table 4). Because interaction of HDAC5 and Tfeb was still present when deletion mutant HDAC5 51-C was used, but disappeared with HDAC5 mutant 100-C, it was assumed that amino acids 51 to 100 of the HDAC5 protein are responsible for interaction with Tfeb (Figure 22 A and B). These findings are further supported by luciferase assay analysis. More specifically, deletion of the first 51 amino acids of HDAC5 did not influence its ability to inhibit Tfeb mediated *MuRF1*-luc induction (Figure 22 C). However, larger deletion of the N-terminal region in HDAC5, using HDAC5 100-C and HDAC5 175-C expression plasmids, abolished Tfeb induced *MuRF1* expression (Figure 22 C). In addition, when the HDAC domain in HDAC5 was deleted (using the C-terminal deletion clone HDAC5 1-664) no decrease of Tfeb mediated *MuRF1* expression was observed, indicative for the importance of the HDAC domain for its repressive function (Figure 22 C). Interaction of full length Tfeb with HDAC5 1-664 could still be observed (Figure 22 B). These findings implicate a direct interaction of both proteins mediated by amino acids 51 to 100 of HDAC5. These data also show that HDAC5 mediated inhibition of Tfeb induced *MuRF1* expression is mediated by its HDAC domain.

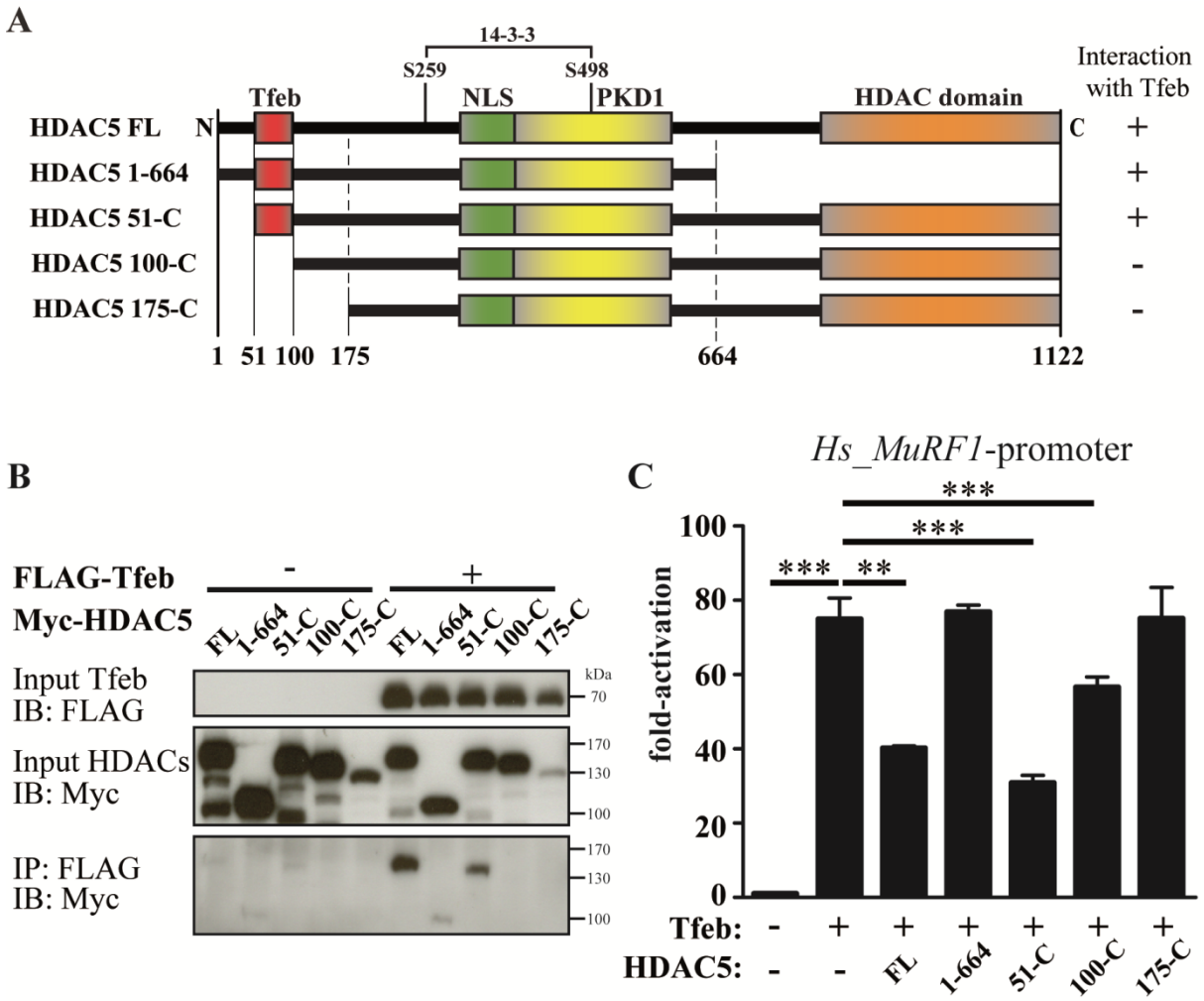

Figure 22: Functional mapping of HDAC5 deletion mutants with full length Tfeb

(**A**) Schematic illustration of HDAC5 deletion mutant clone design. Binding domains for Tfeb (red) and PKD1 (yellow) as well as nuclear localization signal (NLS, in green) and HDAC family domain (orange) are plotted. Figure's information were partially adopted from Zhang *et al.* 2002 and from own manuscript in preparation. Interaction of individual deletion clones with full length Tfeb in Co-IP assay, shown in B, is indicated at the right side. (**B**) HEK293 cells were transfected with expression plasmids encoding full length FLAG-Tfeb and HDAC5-myc full length or deletion clone plasmids as indicated. Input Tfeb and HDAC5 proteins detected by immunoblot (IB) are shown in the top and middle panels. Inputs represent 10% of total lysates. Co-immunoprecipitated eluates representing HDAC5 deletion clones are shown in the bottom panel. (**C**) HEK293 cells were transfected with expression plasmids encoding FLAG-Tfeb and full length or mutant HDAC5 expression plasmids, as indicated, and *M1P* (size -543 bp). Values were normalized to expression of pCMV-*LacZ* and calculated as the fold-activation in luciferase to pCMV-*LacZ* ratio compared to the reporter alone. Error bars represent SD. * $p < 0.05$; ** $p < 0.005$; *** $p < 0.001$; $n = 3$. (Ref.: Figure data are included in manuscript in preparation/submission)

Next step was the determination of the region in Tfeb which mediates its interaction with HDAC5 (Figure 23 A, constructs in Table 4). Tfeb deletion mutants were designed according to the known domain structure of mouse Tfeb; this included the bHLH and the LZ domain. The N-terminal deletion clone, lacking the first 127 amino acids (Tfeb 128-C), which includes a glycine rich region with unknown function, did not interact with full length HDAC5 in Co-

IP experiments (Figure 23 B). This clone showed a reduced effectiveness in *M1P* construct (size -543 bp) induction, and was less sensitive to HDAC5 in luciferase assays (Figure 23 C). Similar results were observed for the Tfeb deletion mutant Δ129-237, showing no interaction with HDAC5 and comparable induction of the *MuRF1*-luc activity (Figure 23 B and C). The other two internal deletion clones Tfeb Δ238-400 and Tfeb Δ299-352 were amongst others designed to confirm Tfebs' *MuRF1* induction via the bHLH DNA binding domain. Tfeb Δ238-400, which comprised the bHLH and the LZ domain, showed stable interaction with HDAC5 in Co-IP experiments (Figure 23 B). As expected, this deletion mutant was unable to induce *MuRF1* expression (Figure 23 C). Tfeb Δ299-352, missing the amino acids encoding for the bHLH domain, retained its interaction capacity with HDAC5 (Figure 23 B) and was also unable to increase *MuRF1* expression (Figure 23 C). In addition, this expression plasmid did not induce MuRF1 at protein level when transfected in C2C12 myoblasts compared to wild type full-length Tfeb (Figure 23 D).

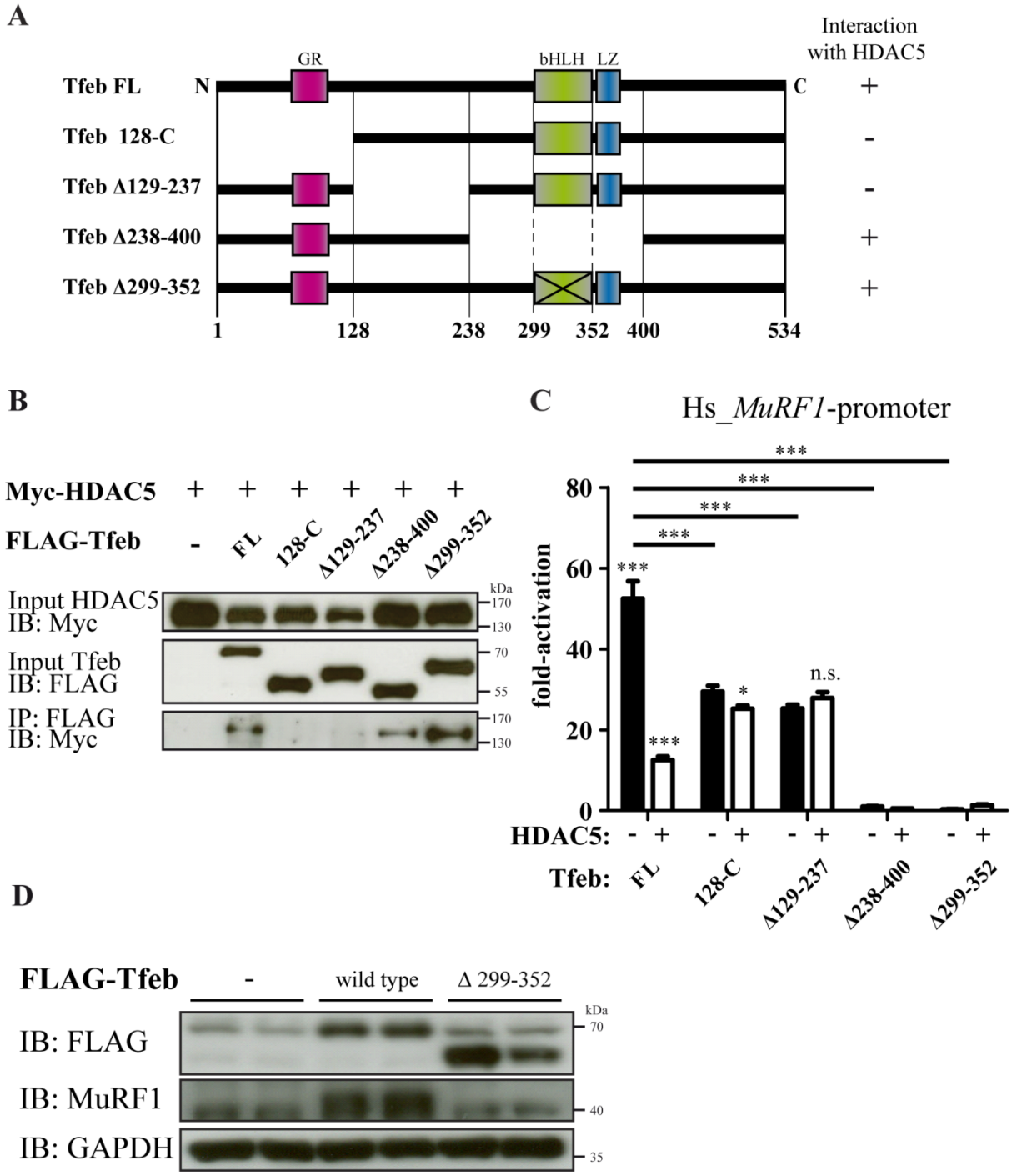

Figure 23: Functional mapping of Tfeb deletion mutants with full length HDAC5

(**A**) Schematic illustration of full length mouse Tfeb isoform A (Q6P203) and deletion mutants used in this study. Deletion-clone nomenclature is shown on left side. Indicated domains and regions: GR = Glycine-rich, violet box; bHLH = basic Helix-Loop-Helix domain, green box; LZ = Leucine Zipper domain, blue box. (**B**) HEK293 cells were transfected with expression plasmids encoding full length HDAC5-myc and full length or mutant FLAG-Tfeb proteins as indicated. Input HDAC5 and full length and mutant Tfeb proteins detected by immunoblot (IB) are shown in the top and middle panels. Inputs represent 10% of total lysates. Co-immunoprecipitated eluates representing HDAC5 are shown in the bottom panel. (**C**) HEK293 cells were transfected with expression plasmids encoding full length or mutant Tfeb or full length histone deacetylase (HDAC) 5 at equal amounts and the *M1P* reporter construct (size -543 bp). Values were normalized to expression of pCMV-*LacZ* and calculated as the fold-activation in luciferase to pCMV-*LacZ* ratio compared to the reporter

alone. Error bars represent SD. n.s. = not significant; * $p < 0.05$; *** $p < 0.001$; n = 3. (Ref.: Figure data are included in manuscript in preparation/submission)

Subcellular localization of the N-terminal Tfeb deletion clone 128-C and Δ129-237 did not change when over-expressed in C2C12 myoblasts and compared with the full-length FLAG-tagged Tfeb isoform (Figure 24). Both clones and wild type Tfeb were localized to nucleus, cytosol and vesicular structures according to previous publications (Sardiello et al., 2009a; Settembre et al., 2012a). In contrast, Tfeb Δ238-400 and Tfeb Δ299-352, both lacking the bHLH domain (Figure 23 A), were localized to the cytoplasm and not found in the nucleus of C2C12 myoblasts (Figure 24).

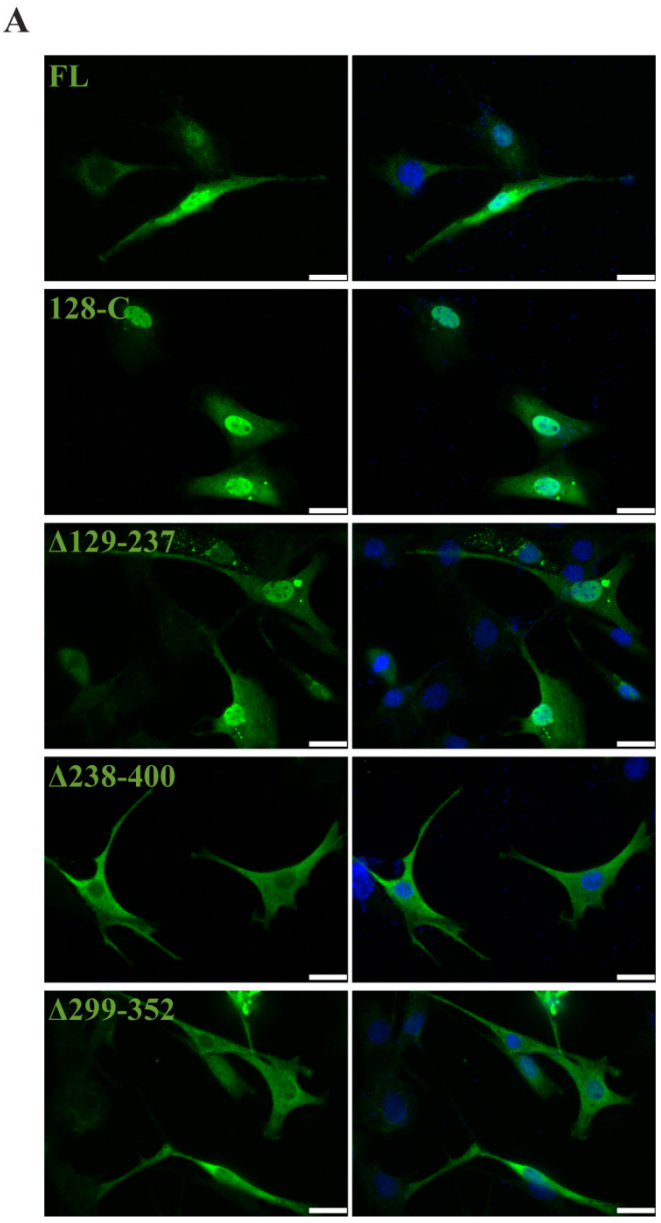

Figure 24: Subcellular localization of Tfeb deletion mutants in C2C12 myoblasts

Fluorescence images showing the subcellular localization of full length FLAG-Tfeb and indicated deletion mutants of Tfeb in transfected C2C12 myoblasts, detected by immunofluorescence (24 h after transfection). Left panel shows immunostaining against FLAG tag and secondary antibody Alexa 488, right panel shows merged pictures with DAPI channel. Scale bars represent 20 μm. (Ref.: Figure data are included in manuscript in preparation/submission)

In summary, Tfeb and HDAC5 interact with each other at their individual N-termini respectively. HDAC5 inhibits Tfeb induced *MuRF1* expression, most likely via its HDAC domain. Tfeb induced *MuRF1* expression requires Tfebs' bHLH DNA-binding domain.

3.7 Regulatory participation of PKD family

Earlier studies showed that the stress-dependent protein-kinase D family (PKD) of serine/threonine kinases regulates the activity of ClassIIa HDACs. Therefore, it was investigated if PKD is involved in regulation of the here identified HDAC5/Tfeb/*MuRF1* axis.

First goal was to confirm physical interaction between HDAC5 and PKD family members. Both full length FLAG-HDAC5 and Myc-PKD1 showed strong interaction in Co-IP procedure when co-expressed in HEK293 (Figure 25 A). In addition, full length FLAG-PKD2 interacted with full length Myc-HDAC5 (Figure 25 B). In contrast, no interaction was detected between FLAG-HDAC5 and Myc-PKD3 (Figure 25 B).

Secondly to confirm functional correlation between PKDs and the HDAC5/Tfeb axis was to over-express PKD cDNA expression plasmids in luciferase assays. Co-transfection of the *M1P* construct (size -543 bp) together with full length Tfeb showed increased *M1P* expression, which was inhibited by HDAC5 presence in HEK293 (Figure 25 C, third bar from left). In this setup wild type (WT), constitutive active (CA) or dominant negative (DN) isoforms of PKD1, 2 or 3 expressing constructs were used to investigate if PKDs can affect the repression of Tfeb by HDAC5. Both CA isoforms of PKD1 and PKD2 restored the HDAC5 mediated reduction of Tfeb induced *MuRF1* expression (Figure 25 C). In contrast, the CA isoform of PKD3 showed no recovering effect in luciferase assay setup when co-transfected with HDAC5, Tfeb and the *M*1P (size -543 bp) constructs in HEK293 cells (Figure 25 C).

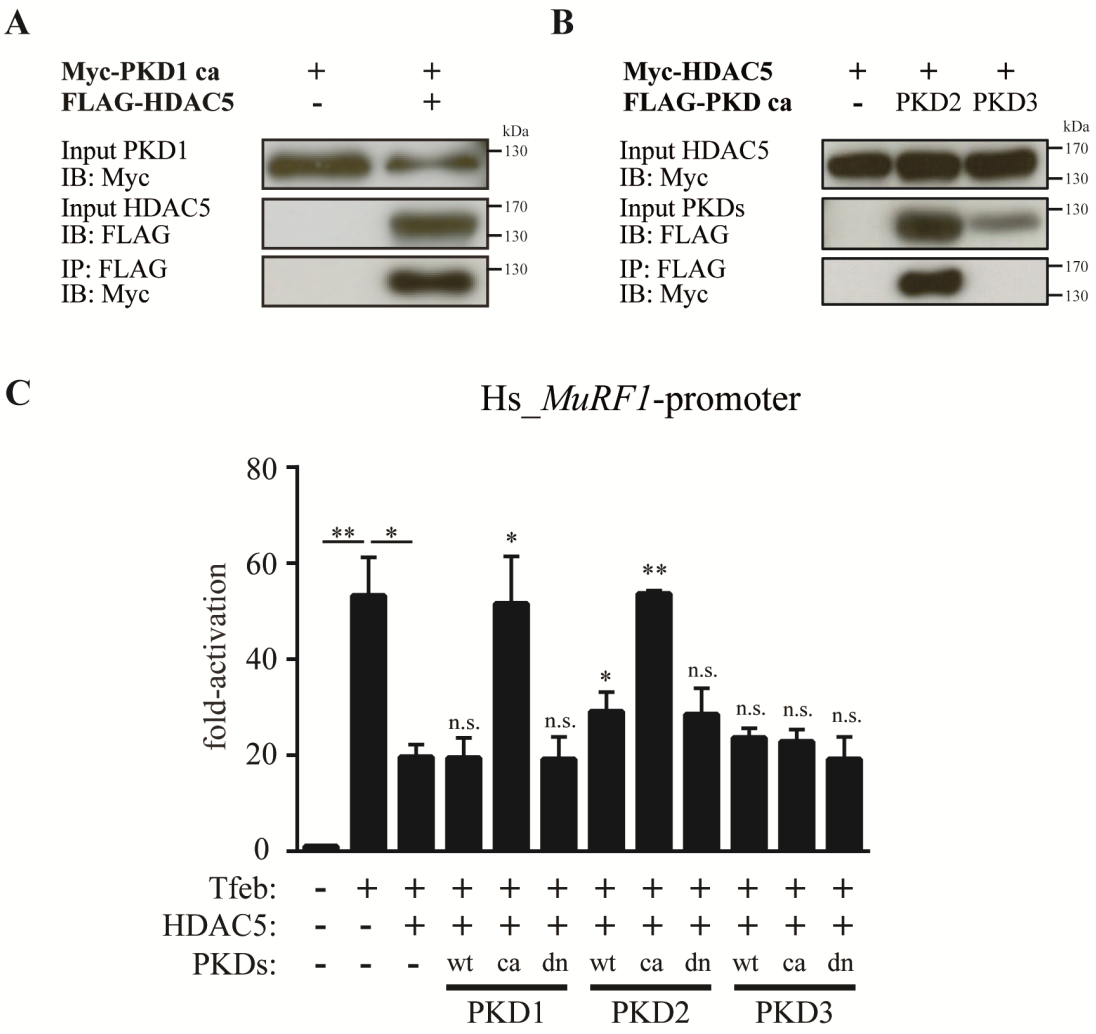

Figure 25: Interaction of PKD family members with HDAC5 and their regulatory influence on Tfeb induced *MuRF1* expression

(**A** and **B**) HEK293 cells were transfected with expression plasmids encoding full length wild type FLAG-HDAC5 and constitutive active (ca) isoform of myc-PKD1 or FLAG-PKD2 or 3 constitutive active (ca) isoforms as indicated. Inputs of PKDs and HDAC5 proteins detected by immunoblot (IB) are shown in the top and middle panels. Inputs represent 10% of total lysates. Co-immunoprecipitated eluates representing PKD1 (A) or HDAC5 (B) protein are shown in the bottom panel. (**C**) HEK293 cells were transfected with expression plasmids encoding FLAG-Tfeb (wt) and HDAC5 (wt) and PKD1, 2 or 3 wild type (wt), constitutive active (ca) or dominant negative (dn) isoforms, as indicated, and the *M1P* reporter construct (size -543 bp). Values were normalized to expression of pCMV-*LacZ* and calculated as the fold-activation in luciferase to β-Gal ratio compared to the reporter alone. Error bars represent SD. n.s. = not significant; * $p < 0.05$; ** $p < 0.005$; n = 3. (Ref.: Figure data are included in manuscript in preparation/submission)

Previous studies of others and own findings of the Fielitz Lab showed that PKD1 gets activated by AngII and mediates translocation of HDAC5 out of the nucleus. To analyze the atrophying effect of AngII in skeletal muscle tissue in connection with PKD1, members of the Fielitz Lab used AngII perfusion via mini pumps in skeletal muscle specific PKD1 knock-out mice (PKD1 cKO) (Data are not included in this Thesis, but are included in manuscript in

preparation). The obtained results clearly showed that muscles (soleus and gastrocnemius/plantaris) from PKD1 cKO animals were less atrophied than those from wild type animals.

Knowing that PKD1 is sensitive to and gets activated by AngII, the role of Tfeb in AngII induced atrophy was analyzed. To investigate if knock down of Tfeb inhibits AngII induced myotube atrophy, siRNA mediated knock-down of Tfeb in differentiated C2C12 myotubes and was performed. Differentiated myotubes (day 8) were transfected with siTfeb or scrambled control (100 nM each) for 24 h. Transfection with siTfeb resulted in a slight but significant increase in myotube diameter compared to siScr control treated cells (Figure 26 C, black bars). AngII treatment (500 nM for 20 h) of identically treated myotubes showed reduced atrophy compared with siSCR control cells (Figure 26 A to C). To validate that Tfeb is involved in AngII induced *MuRF1* expression, ChIP analysis of chromatin from AngII and vehicle treated C2C12 myoblasts were performed. Treatment of C2C12 myoblasts with 500 nM AngII for 3 h resulted in an enhanced binding of Tfeb towards E-box motifs of the *MuRF1* promoter compared to vehicle treated cells (Figure 26 D). These results showed that Tfeb is involved in AngII induced muscle atrophy by regulating expression of *MuRF1*.

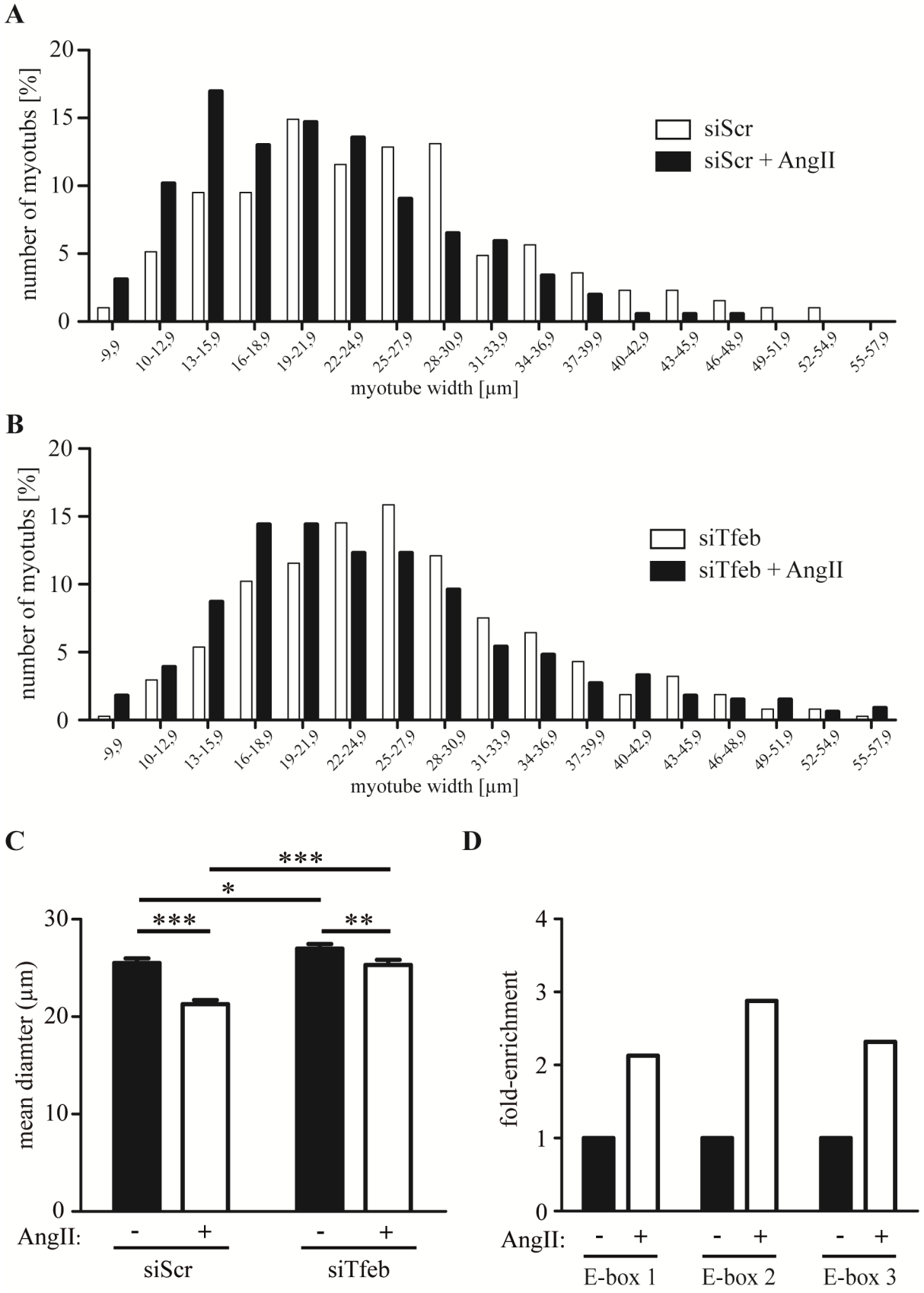

Figure 26: siRNA knock-down of Tfeb prevents AngII induced atrophy in C2C12 myotubes

(**A**, **B** and **C**) Differentiated C2C12 myotubes (8 days) were transfected with scrambled control siRNA (scr) or siRNA against Tfeb (siTfeb; 100 nM each), and treated with vehicle or Angiotensin II (AngII, 500 nM, for 20 h), as indicated. Pictures were taken and myotube width was analyzed from at least 100 myotubes per condition and

at three random positions per myotube. Graphs show frequency histograms plotting the number (or percentage) of myotubes against the myotube diameter. Frequency histograms of scrRNA and Tfeb siRNA transfected C2C12 myotubes treated with vehicle or AngII are shown in **A** (siScr) and **B** (siTfeb); respectively. (**C**) Diagram shows statistical quantifications of measured mean diameters of 8 days differentiated C2C12 myotubes, treated and quantified as described above, with or without AngII treatment (AngII, 500 nM, for 20 h) after previous 24 h siRNA knockdown. Experiment has been repeated two times, showing the same trend. Graph shows tube diameter distribution of one experiment. For analysis myotube widening of ten randomly taken pictures were quantified. Error bars represent SEM. * $p < 0.05$; ** $p < 0.005$; *** $p < 0.001$. (**D**) Chromatin immunoprecipitation (ChIP) assay in C2C12 myoblasts showing Tfeb binding to mouse *MuRF1* promoter E-boxes. Cells were grown in normal 10 % FBS DME-Medium before angiotensin II (AngII) treatment (500 nM) or vehicle for 3 h. Chromatin was immunoprecipitated with antibodies against immunoglobulin G (IgG) or Tfeb. Primers flanking the E-boxes on the *MuRF1* promoter were used for amplifying DNA by real-time PCR. Calculation was carried out using delta- delta- cT method. (Ref.: Figure data are included in manuscript in preparation/submission)

In summary, based on the data presented in this study and *in-vivo* data obtained from other lab members, a working model was postulated, which will be published in the near future and is shown in figure 27, at the end of the discussion part of this thesis. In an untreated condition, Tfeb can bind to the conserved E-box elements in the genomic *MuRF1* promoter sequence. In this stage HDAC5 localizes to the nucleus, binds to and inhibits Tfeb mediated expression of *MuRF1*. When AngII is present, it binds to its receptor (AT1R) and activates PKD1 which than translocates to the nucleus, and binds to and phosphorylates HDAC5. Phosphorylation of HDAC5 leads to binding of the 14-3-3 chaperon protein mediating CRM1 dependent nuclear export of HDAC5. This relives inhibition of Tfeb which can now activate the expression of its target genes, such as *MuRF1*. Tfeb activates *MuRF1* expression most likely via binding to the E-box motifs 1 and 3. In case of starvation the author assumes that Tfeb translocation in the nucleus gets enhanced, as findings of others showed for human TFEB.

4 Discussion

Regulation of muscle function is complex and involves well orchestrated protein synthesis as well as fine tuned protein degradation. When protein degradation overvalues protein synthesis, muscle atrophy can arise and critically influences sick individuals suffering from a variety of atrophy releasing diseases. Findings from the last two decades revealed that the E3 ubiquitin ligase MuRF1 takes a crucial stand in the process control and mediation of muscle atrophy. Given that regulation of *MuRF1* was not fully understood, the aim of this study was to identify new regulators of *MuRF1* gene expression. This decision was based on the knowledge that MuRF1 is directly involved in and responsible for the degradation of structural proteins in skeletal and in heart muscle tissue. (Clarke et al., 2007b; Cohen et al., 2009; Fielitz, van Rooij, et al., 2007; Kedar et al., 2004b)

4.1 TFEB was identified as the strongest *MuRF1* inducer

The proximal regulatory promoter sequence of the human *MuRF1* gene was screened for potential candidates with a focus on activating transcription factors. A skeletal muscle derived cDNA expression library was screened, with a total sampling rate of more than 100,000 clones. To obtain reliable read-outs, the screening procedure was repeated twice, using a 5 kb and a 1 kb genomic DNA fragment of the human *MuRF1* promoter sequence, respectively. The findings received from first screening procedure were verified in the second screening that also reduced effects of variable DNA amounts resulting from DNA isolation during sib-selection process.

To find new transcriptional activators of *MuRF1*, the most potent and promising candidate was chosen. In this case it was the transcription factor EB (TFEB).

Altogether, overall gene transcripts identified revealed a broad variety of genes potentially involved in regulation of *MuRF1* expression. The majority of sequencing results revealed partial cDNA fragments (23 out of 34). This result can be explained by the manufacturing procedure of the applied cDNA library. The library contained cDNA fragments with an average size of ~1600 bp (purchased from Invitrogen).

4.2 TFEB regulates *MuRF1* expression

TFEB has been isolated separately six times in total during both screening processes, indicating to be a relevant candidate with high probability. The fact that two different forms of TFEB were isolated (a full length isoform as well as a partial unknown fragment) could be explained on the one hand by differential splicing of the inserted mRNA and on the other hand by truncation during the manufacturing process. Since sequencing did not reveal a start codon it is most likely that the obtained clone was truncated during the manufacturing process. Anyway, the partial clone strongly induced the Hs_*MuRF1*-luc construct.

Because the following analyses were planned in C2C12 mouse myoblasts, it was decided to use the mouse isoform of Tfeb. Since cloning from cDNA was without any result, it was decide to buy the full length Tfeb mouse isoform A. The assembled Tfeb expression plasmid (FLAG-Tfeb, table 4) dose dependently induced the human *MuRF1*-luc construct. This result could be expected as protein sequences of human and mouse Tfeb are highly similar (93% total sequence identity, alignment shown in appendix figure 1).

The fact that Tfeb over-expression resulted in endogenously increased *MuRF1* mRNA levels and protein content in C2C12 myoblasts gave further reference towards an actual participation of Tfeb in the transcriptional regulation of *MuRF1*.

4.3 Tfeb binding sites in the *MuRF1*-promoter are identified

To indentify the specific region in the *MuRF1* promoter at which Tfeb binds to the *MuRF1* promoter and increases its expression, first of all subsequent length reductions of the Hs_*MuRF1*-luc construct were performed.

Tfeb binds to E-box motives (CANNTG (Carr & Sharp, 1990)) in the promoter regions of various genes (Sardiello et al., 2009b). It was shown by Moresi *et al.* that E-box motives are also present in the mouse *MuRF1* promoter (Viviana Moresi et al., 2010b). Therefore a detailed sequence analysis of the human *MuRF1* promoter used in this study for luciferase assay analysis was performed, revealing multiple E-box sites in the human *MuRF1*-luciferase construct located close to the transcriptional start site (TSS). To eliminate side effects of more distant E-box motives in the Hs_*MuRF1*-luc construct, length reduced variants of this construct were used in luciferase assays. Results showed constant induction of the inserted *MuRF1* promoter constructs, ranging down gradually from -5002 bp to -543 bp, when co-

expressed with Tfeb expression plasmid. Further decline of the *MuRF1* promoter construct reduced the Tfeb mediated induction gradually when reduced from -300 bp to -200 bp and subsequently to -100 bp upstream of the TSS. These results confirmed the existence of at least two potent binding sites close to the TSS of *MuRF1*. Findings from Ballebio *et al.* in 2011 supported the presumption of a TSS near binding of Tfeb. Ballebio *et al.* used an over-expression based ChIP-Seq method with a triple FLAG-tagged human TFEB in HeLa cells and revealed that a TSS near binding of TFEB is very important for the inducing effects of its target genes.

Site directed E-box motive mutation confirmed their importance for Tfeb mediated *MuRF1* regulation. The first three E-box positions, out of the four positions identified in the Hs-*MuRF1*-luc construct, are highly homologues throughout mammalian species. As shown be Moresi *et al.* another bHLH domain containing transcription factor, myogenin, binds to and regulates *MuRF1* expression in mice upon denervation, most likely via the second and third E-box motive (Viviana Moresi et al., 2010b). Investigations of the E-box motives revealed that E-box position 1 and 3 seem to be more relevant for the Tfeb mediated induction than position 2 or 4. ChIP analysis performed in this study confirmed binding of endogenous and over-expressed Tfeb to the endogenous *MuRF1* promoter sequence near the TSS, very likely via the amplified E-box motives. Using ChIP experiments, it was not possible to dissect Tfeb binding to different E-box sites, due to their very close proximity.

Surprisingly, site directed mutagenesis of the fourth E-box motive resulted in an increase in Tfeb sensitivity, leading to the assumption of the presence of a regulatory element negatively influencing *MuRF1* expression at this position, at least in the human promoter.

Considering the data of Moresi *et al.* and own results it was reasoned that the E-box position 3 in the *MuRF1* promoter is used dually by myogenin and Tfeb. Whereas Tfeb individually uses E-box 1 and myogenin autonomously uses E-box 2, presumably.

These three conserved E-box motives are located in between the FoxO transcription factor binding site (Waddell et al., 2008b) (Figure 2) and the MEF2 site close to the TSS of *MuRF1* (Baskin & Taegtmeyer, 2011b). Due to potential homo- and heterodimerization of Tfeb, it is most likely that multiple E-box binding sites are necessary for a maximum induction of *MuRF1* expression. Different binding positions may have different effects on the formation of a transcriptional start complex, potentially with other transcription factors. Interestingly, pre-liminary data point to a co-operational effect of MEF2A and Tfeb in the transcriptional regu-

lation of *MuRF1* (Appendix Figure 4). Further analyses are required to validate the functional relevance of these results.

In summary, Tfeb induces *MuRF1* expression via binding to conserved E-box motives in the *MuRF1* promoter.

4.4 Tfeb is required for starvation induced *MuRF1* induction and its basal expression

Using siRNA based loss-of-function approaches the connection between endogenous Tfeb and basal *MuRF1* expression was investigated in C2C12 myoblasts. Reduction of Tfeb subsequently reduced endogenous *MuRF1* mRNA and protein levels, indicating a participation of Tfeb in basal *MuRF1* regulation. ChIP results support this assumption, due to proved binding of Tfeb to the endogenous *MuRF1* promoter.

Since Moresi *et al.* showed that bHLH transcription factor binding of myogenin to E-box motives in the *MuRF1* promoter is relevant in denervation induced atrophy, this study investigated the role of the newly identified *MuRF1* regulator and also bHLH transcription factor Tfeb in reference to AngII induced atrophy and starvation initiated C2C12 myoblast to myotube differentiation (Viviana Moresi et al., 2010b). Myogenin was shown to regulate *MuRF1* expression in case of denervation induced atrophy, while it could not be proven to be relevant for *MuRF1* induction during periods of fasting or starvation induced differentiation. Thus, it was tested if Tfeb might participate in *MuRF1* regulation during starvation. Because *MuRF1* is strongly unregulated during muscle differentiation and myotube formation, it was analyzed if a lack in Tfeb content would affect *MuRF1* expression during differentiation. And indeed knockdown of Tfeb inhibited the differentiation process. Supported by the findings of Settembre *et al.* and others who published starvation induced gene activation upon translocation of Tfeb into the nucleus, it was speculated if Tfeb binding to the *MuRF1* promoter would increase in C2C12 myoblasts after serum starvation (Settembre et al., 2012b). Since ChIP experiments showed an enriched binding of endogenous Tfeb of over 20 fold to the proximal promoter sequence of *MuRF1*, the obtained results prove that Tfeb does play a central role in the regulation of *MuRF1* in serum starvation induced muscle cell differentiation.

Due to embryonic lethality of Tfeb knock-out mice and the fact that the targeted muscle specific knock-out mice could not be generated, it was not possible to investigate loss-of-function studies *in-vivo*. To investigate the function of Tfeb *in-vivo* it would be important to generate muscle specific gain- and loss-of-function animal models.

4.5 ClassIIa HDAC 4 and 5 repress Tfeb mediated *MuRF1* induction

As introduced, the ClassIIa HDAC family members were shown to be potent negative regulators of cardiac and skeletal muscle atrophy (Matthew J. Potthoff et al., 2007). Interaction of ClassIIa HDACs was shown for many other DNA-binding transcription factors, transcriptional co-repressors, protein kinases as well as G-protein coupled receptors (Martin et al., 2007). Highly interesting for the studies investigations was the finding that class IIa HDACs interact with MEF2 transcription factor family members and by that negatively regulate *MuRF1* expression. Based on these findings it was hypothesized that Tfeb induced *MuRF1* expression could also be negatively regulated by class IIa HDACs. And indeed HDAC4 and 5 showed strongest inhibitory effects of the Tfeb induced Hs_*MuRF1*-luc construct induction. Supported by Co-IP based interaction studies as well as co-localization analysis in C2C12 myoblasts it was shown that Tfeb mediated *MuRF1* induction is strongly regulated by class IIa HDAC5 and HDAC4, respectively. However, binding between HDAC5 and Tfeb was stronger compared to HDAC4 and Tfeb. Previously it was shown by others that the two HDAC 4 and 5 both regulate skeletal muscle atrophy and compensate each other (Viviana Moresi et al., 2010b). No interaction or co-localization was found between TFEB and HDAC7 and 9, respectively, suggesting that their inhibition of Tfeb mediated *MuRF1* induction was indirect.

Other interaction partners of the class IIa HDACs are: CAMTA2 (K Song Cell), a DNA-anchoring transcriptional factor, which stimulates cardiac growth; and the NF-kB inhibitory transcriptional repressor IκBα, which is part of the NF-kB pathway, that also influences *MuRF1* expression (Martin et al., 2007). Since plenty of the indentified HDAC interaction partners participate in the regulation of muscle maintenance and structural homeostasis as well as skeletal and heart muscle atrophy, the interaction analysis of the newly indentified *MuRF1* regulator Tfeb and the ClassIIa HDACs became secondary aim of this study.

In summary, the decision for the following detailed interactional and functional mapping between Tfeb and HDAC5 was based first on their physical interaction, second on their co-localization, and third on functional assays with the Hs_*MuRF1*-luc construct.

4.6 HDAC5 interaction with full length Tfeb and is mediated by HDAC5s N-terminal amino acids 51-100

The functional mapping of HDAC5 deletion mutants with full length Tfeb was performed using Co-IP and luciferase assays. Since HDAC5 mutant 1-664 showed no inhibitory effect in luciferase assays but stable interaction with full length Tfeb in Co-IP, it was assumed that the HDAC domain, which was missing in this mutant, does play a central role in the repression of the Tfeb mediated *MuRF1* regulation. For future investigations, it would be of interest to see if Tfeb is also regulated via histone acetyl transferase (HAT) acetylation and possibly de-acetylated by HDAC5 and its HDAC domain. Current literature does suggest that the balance of acetylation and de-acetylation has strong influences on protein stability and thereby affects muscle wasting (Alamdari et al., 2013). Acetylation or de-acetylation based regulation has not been reported for Tfeb so far.

The interaction between full length Tfeb and HDAC5 was mediated by the N-terminal amino acids 51 to 100 of HDAC5. In addition to the decreasing interaction, the inhibitory effect observed for full length HDAC5 on the Tfeb mediated *MuRF1* induction declined, when compared with the two deletion clones 51-C and 100-C of HDAC5. However, the deletion clone 100-C showed a lower, but significant reduction of the Tfeb mediated *MuRF1* induction. No interaction was detectable with full length Tfeb in Co-IP analysis. The author assumed that this effect could be indirect, possibly mediated via another transcription factor associated with Tfeb, e.g. MEF2 since its binding site in HDAC5 sequence is adjacent (Matthew J. Potthoff et al., 2007). It would be valuable to investigate this suggestion via a triple Co-IP approach and an expansion of the functional luciferase assay shown in the appendix with an additional insertion of HDAC5. Further deletion of the following N-terminal amino acids of HDAC5 (HDAC5 175-C) resulted in a complete loss of the negative regulatory influence of the Tfeb mediated *MuRF1* induction. In addition, no interaction could be observed with full length Tfeb. Although the loading for the deletion mutants of HDAC5 of the represented experiment in figure 22 B is to a certain extent unequal, longer exposures of the eluate Western blots showed no interaction signal at all. Repeatedly performed experiments indicated identical results.

In summary, the obtained results lead to the conclusion that the amino acids 51-100 of HDAC5 are critical for interaction with full length Tfeb and that the HDAC domain is necessary for the negative regulation of the Tfeb mediated *MuRF1* induction.

4.7 Tfeb binds to HDAC5 via its N-terminal amino acids and requires its own bHLH domain to induce *MuRF1* expression

Since, in luciferase assays, the observed Tfeb mediated *MuRF1* induction was stronger than every other transcription factor that has been linked to the regulation *MuRF1* expression so far (Baskin & Taegtmeyer, 2011b; Cai et al., 2004b; Viviana Moresi et al., 2010b; Waddell et al., 2008b), the protein regions and bHLH domain in Tfeb were analyzed for their involvement in *MuRF1* promoter induction as well as inhibition via interaction with HDAC5. Deletion clone design was performed according to the formerly known structural data, extracted from OMIM and NCBI database. Presented results are in agreement with previous publications showing that the DNA binding of Tfeb was mediated by its bHLH domain. Deletion of this bHLH domain abolished induction of the Hs_*MuRF1*-luc construct and MuRF1 protein induction in C2C12 over-expression analysis, but did not reduce physical interaction with full length HDAC5. So it was concluded that the bHLH domain of Tfeb is relevant for DNA binding and subsequent induction of target genes, such as *MuRF1,* but not for HDAC5 interaction.

In contrast, HDAC5 interaction could be connected to the N-terminal amino acids in Tfeb protein, shown by the complete loss of interaction when Tfeb deletion mutant 128-C was applied in Co-IP assay with full length HDAC5. This deletion mutant was missing the glycine-rich region, which has not been linked to any regulatory or any other function so far. Looking at the distribution of the N-terminal deletion clone Tfeb 128-C in C2C12 myoblasts, the study's results confirmed the findings of Roczniak-Ferguson *et al.* who reported that human TFEB lacking the first 30 amino acids was mainly localized in the nucleus (Roczniak-Ferguson et al., 2012). As no NLS, NES or regulatory phosphorylation site has been published for this region, this observation cannot be explained until know and needs to be further investigated in the future. Even though this deletion clone did mainly localize to the nucleus, it showed reduced ability in Hs_*MuRF1*-luc induction. Probably because of reduced dimerisation capacity, which needs to be tested in prospective analysis.

For the internal Tfeb mutant missing amino acids 129-237, very similar Hs_*MuRF1*-luc induction results were observed as for the N-terminal Tfeb deletion mutant 128-C. This internal section of Tfeb contained multiple phosphorylation sites, which were analyzed in human TFEB protein by other groups. It was shown that phosphorylation of these sites produced 14-3-3 binding and maintained the complex inside the cytoplasm (Roczniak-Ferguson et al., 2012; Settembre et al., 2012b). Therefore the results are in agreement with these observations, showing that this mutant is mainly localized in the nucleus. The author suggests the following

explanation for the decline in Hs_*MuRF1*-luc induction: it could be reduced dimerisation ability due to deletion of the internal amino acids and a potential change in three-dimensional conformation. Tfeb deletion mutant Δ129-237 showed no sensitivity in luciferase assay analysis to full length HDAC5 inhibition. In addition, it can be assumed that HDAC5 binding with Tfeb is mostly mediated by the N-terminal amino acids of Tfeb and additionally by a partial internal region. To analyze this assumption in more detail, deletion mutants of Tfeb spanning smaller regions, e.g. 20-40 amino acids, need to be generated for future experiments. Additional Tfeb mutants would also be useful to characterize the dimerisation of Tfeb being necessary for *MuRF1* induction, and could be used in Co-IP, ChIP and luciferase analysis to improve the understanding of *MuRF1* regulation in more detail.

As the internal deletion clone Tfeb Δ129-237 showed no significant changes in subcellular localization compared to the wild type Tfeb, it is most likely that the previously mentioned phosphorylated serine residues, described to be regulatory, are not as important for Tfeb regulation in skeletal muscle cells as in HeLa cells, which were used by Settembre et al. and others (Roczniak-Ferguson et al., 2012; Sardiello et al., 2009b; Settembre et al., 2012b).

In summary, data show that the inhibitory influence of HDAC5 on Tfeb is mainly mediated via the N-terminal part of Tfeb and that the amino acids encoding for the bHLH domain of Tfeb are necessary for induction of *MuRF1* expression.

4.8 Upstream regulatory influences of PKD1 and 2 on HDAC5 inhibit Tfeb induction of *MuRF1*

Several publications indicated regulation of HDAC5 activity by PKD family members. More specifically, PKD1 was shown to phosphorylate HDAC5 (Huynh & McKinsey, 2006; Matthews et al., 2006). And indeed, the experiments presented here showed a direct interaction of PKD1 and PKD2 but not PKD3 with HDAC5. In addition, it was shown by Harrison *et al.* that the PKD1-HDAC5 axis plays a role in cardiac stress signaling (Harrison et al., 2006). The authors drew a regulatory network from PKC-dependent PKD1 activation over HDAC5, which itself negatively regulates MEF2 transcription factors that activate genes necessary for cardiac hypertrophy growth. As introduced, MEF2 was reported to regulate *MuRF1* expression as well (Baskin & Taegtmeyer, 2011b). On the basis of these findings the influence of the described PKD/HDAC axis on Tfeb was investigated using interaction analysis and luciferase assays.

As shown in this study, the Tfeb mediated *MuRF1* induction was strongly inhibited by HDAC5. But constitutive active isoforms of PKD1 or PKD2 reversed HDAC5 mediated inhibitory effects on Hs_*MuRF1*-luc construct indicating that PKD1 and 2 act in HDAC5 regulation. This was supported by Co-IP based interaction analysis, which showed that PKD1 and PKD2 but not PKD3 interact with HDAC5. Interaction mapping analysis between PKD1 and HDAC5 were performed by other members of the Fielitz Lab and are included in the manuscript in preparation.

These findings can be explained by previous reports from Liu *et al.* and Xu *et al.*, who showed that PKD1 mediates nuclear export of HDAC5 (Liu, Contreras, Shen, Randall, & Schneider, 2009; Xu et al., 2007). The analysis published by Xu *et al.* in 2007 showed that AngII rapidly increases HDAC5 phosphorylation and leads to its nuclear export in vascular smooth muscle cells. In this experiment AngII treatment induced MEF2 activity only moderately (~2 fold), as measured by a 3xMEF2-luciferase reporter construct. In addition, also FoxO transcription factors are not responsible for the AngII induced *MuRF1* expression and subsequently induced atrophy in skeletal muscles (T. Yoshida, Semprun-Prieto, Sukhanov, & Delafontaine, 2010b). The arising knowledge gap from these findings, concerning the AngII induced atrophy regulation working via *MuRF1* induction, could not be explained by the *MuRF1* regulating transcription factors identified so far.

4.9 Tfeb knock-down in C2C12 myotubes blocks AngII induced atrophy

Knowing that Tfeb is a very potent inducer of *MuRF1* expression and that AngII increases *MuRF1* expression, it was hypothesized that AngII induced atrophy was mediated by Tfeb. The experimental prove was performed using siRNA mediated Tfeb knock-down followed by AngII treatment in differentiated C2C12 myotubes. AngII induced atrophy of myotubes was inhibited in the absence of Tfeb.

This can be explained by the reduction of basal MuRF1 protein content when Tfeb levels are reduced in advance and the missing induction of *MuRF1* expression as a result from Tfeb deficiency. In addition, ChIP analysis in C2C12 myoblasts showed an enhanced binding of Tfeb to the *MuRF1* promoter, supporting the assumption of Tfeb being responsible for the transcriptional activation of *MuRF1* as a result of the atrophy stimulus AngII.

In summary, Tfeb mediates AngII induced atrophy in C2C12 myotubes. These results fill the knowledge gap described by Yoshida *et al.* in 2010, who described FoxO transcription factors

to regulate the AngII mediated *atrogin-1* induction and showed that *MuRF1* is regulated independently of FoxO by an unknown transcription factor.

4.10 Potential cross-talk in lysosomal and proteasomal transcriptional gene regulation is mediated by Tfeb

Since *MuRF1* encodes for a muscle enriched RING-finger E3 ubiquitin ligase of the UPS, the finding that Tfeb induced *MuRF1* expression was partially surprising. Namely because Tfeb was previously identified as a major regulator of lysosomal biogenesis and homeostasis, and has thus been linked to lysosomal and autophagosomal formation (Palmieri et al., 2011; Roczniak-Ferguson et al., 2012; Sardiello et al., 2009b; Settembre et al., 2012b). So far, the involvement of Tfeb to any other UPS related gene has not been described.

Data presented in this study (Appendix Figure3) showed that Tfeb is expressed in different skeletal muscles and various parts of the heart, which is in agreement with data described previously by Kuiper et al. (Kuiper et al., 2004, Appendix Figure 3). In addition, parallel increased expression of *MuRF1* and *Tfeb* upon starvation could be detected in the gastrocnemius muscle (GP) (Appendix Figure 2). This could be explained in part by own findings since Tfeb mediates *MuRF1* regulation upon starvation, as well as findings of others showing a starvation induced translocation of Tfeb into the nucleus (Settembre et al., 2012b).

Coming back to the lysosomal association of Tfeb and the newly discovered link to UPS gene regulation presented in this study, it is noteworthy that both processes, the lysosomal degradation and UPS mediated protein degradation, were shown to participate in skeletal muscle atrophy. It is of interest that the mTOR pathway, which has been shown to regulate TFEB and the classical autophagy pathway in mammalian cells, is not the major factor that controls autophagy in muscle cells (Fanzani, Conraads, Penna, & Martinet, 2012b). Rapamycin mediated inhibition of the mTOR pathway only barely (~10 %) increases protein breakdown in differentiated myotubes (Zhao et al., 2007b). This important publication connected lysosomal and proteasomal proteolysis to the IGF-1/AKT/FoxO3 pathway. Surprisingly, the authors did not show any *MuRF1* regulation and addressed the complete proteasomal degradation to atrogin-1. This is critical due to the previously introduced findings that atrogin-1 does not mediate the degradation of structural myofibrillar proteins, whereas MuRF1 does.

Summing up, the newly identified *MuRF1* regulator Tfeb could have similar connective functions in lysosomal and UPS regulation as FoxO3. Tfeb was reported to be an mTOR target

and that it activates various lysosomal genes, if this particular lysosomal activation is important for muscle atrophy, it needs to be further studied in the future. As lysosomal gene regulation or lysosomal biogenesis and autophagy were not analyzed in this present study, it is difficult to discuss, which particular influences Tfeb might have had on these highly balanced mechanisms. Anyway, the received data constrain large evidence that Tfeb has to be considered as a key transcriptional regulator of the lysosomal as well as the atrophy marker gene *MuRF1*.

4.11 Postulated pathway

The data obtained by this study are summarized in a working model (Figure 27). In an untreated condition, Tfeb binds to the conserved E-box elements in the genomic *MuRF1* promoter sequence, but HDAC5 (maybe also HDAC4) inhibits *MuRF1* expression. In presence of AngII, PKD1 (maybe PKD2) is activated via the angiotensin II type 1 receptor (AT1R) via PKC. Activated PKD1 now translocates to the nucleus, where it binds to and phosphorylates HDAC5, which than binds to the 14-3-3 chaperon protein that mediates nuclear export of HDAC5 (maybe also HDAC4) in a CRM-1 mediated mechanism. This relieves repression of Tfeb, which now activates *MuRF1* gene expression. It can be assumed that Tfeb activates *MuRF1* expression, most likely via binding to the E-box positions 1 and 3 in the MuRF1 promoter.

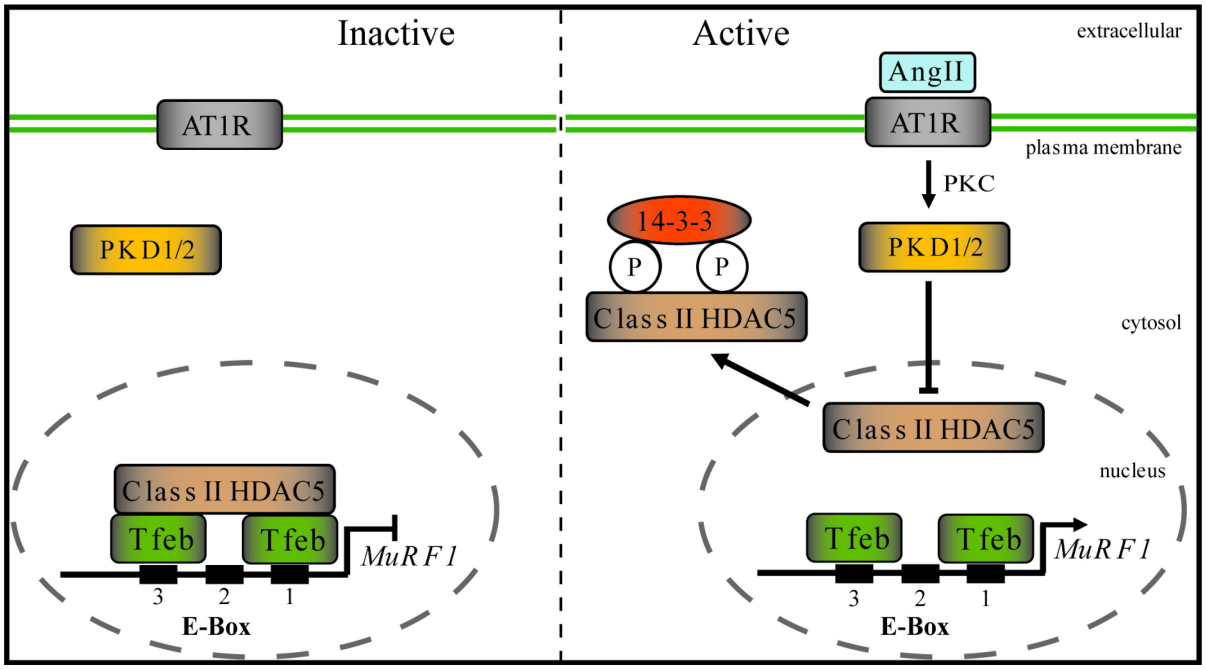

Figure 27: Schematic illustration of the postulated working model of AngII triggered *MuRF1* induction

Left side shows the inactive state, where ClassIIa HDAC5 binds to Tfeb and blocks *MuRF1* induction. In the right panel AngII binds to its plasma membrane bound receptor (AT1R), activates PKD1 via PKCε, which in turn initiates phosphorylation dependent 14-3-3 nuclear export of ClassIIa HDAC5 and enables Tfeb to activate *MuRF1* expression.

5 Summary

Skeletal muscle mass is permanently balanced as a result of fine tuned protein synthesis and degradation mechanisms. When overall protein synthesis exceeds degradation rates the result is muscle hypertrophy (increase in CSA of muscle fiber diameter). In contrast, skeletal muscle atrophy occurs when protein degradation exceeds protein synthesis, which happens in a variety of conditions, such as aging, starvation, cancer, cachexia or denervation. Degradation of muscle mass can sometimes be useful, e.g. as source for lipids, amino acids and glucose in case of critical malnutrition as well as several other physiological conditions. But a solid composition and thereby functional maintenance of muscles is necessary for healthy individuals as well as individuals suffering from atrophy releasing diseases as to retain their mobility and to preserve full heart functions. Since degradation of structural proteins in muscle tissue has been addressed mainly to the ubiquitin-proteasome-system, the regulation of the participating components needs to be understood in detail to develop constructive treatments and therapies for atrophy prevention. One of the key enzymes in skeletal and heart muscle atrophy is the E3 ubiquitin ligase MuRF1. Its expression levels and protein content was found to be elevated in almost every know atrophy model. MuRF1 is very critical for the muscles composition and thus their functional integrity, as it marks and initiates degradation of structural and contractile proteins via the UPS. Since MuRF1 plays a prominent role in muscle atrophy, its transcriptional regulation needs to be well understood to develop effective therapies for all the different atrophy models MuRF1 has been linked to. Several transcription factors (NF-κB, FoxO, myogenin and Mef2) have been identified to regulate *MuRF1* at different ratios and in diverse atrophy models. Importantly, they do not explain all *MuRF1* inducing events observed. To fill some of the remaining knowledge gaps, the studies primary aim was to find new transcriptional regulators for *MuRF1* and the second aim was to analyze potential involvements of the obtained candidates in pathways affecting skeletal muscle atrophy.

In summary, the major aim of this study was achieved. Tfeb was identified as a novel *MuRF1* regulator. In addition, evidence that Tfeb participates in AngII mediated atrophy were received, at least in C2C12 myotubes. Furthermore it could be demonstrated that Tfeb is necessary for C2C12 myoblasts to myotube differentiation. The significance of Tfeb for atrophy regulation became clear, since Tfeb is directly influenced by the *MuRF1* regulating PKD/HDAC axis. Therefore, this study presents a new and parallel working mechanism regulating *MuRF1* expression.

6 Appendix

Score	Expect	Method	Identities	Positives	Gaps
758 bits(1956)	0.0	Compositional matrix adjust.	449/483(93%)	459/483(95%)	1/483(0%)

Gln-rich

```
mmIsoA 53   EPEPTAAMASRIGLRMQLMREQAQQEEQRERMQQQAVMHYMQQQQQQQQQQ-LGGPPTPAI  111
            EP P A MASRIGLRMQLMREQAQQEEQRERMQQQAVMHYMQQQQQQQQQQ LGGPPTPAI
hsIso2 8    EPAPAATMASRIGLRMQLMREQAQQEEQRERMQQQAVMHYMQQQQQQQQQQQLGGPPTPAI   67

mmIsoA 112  NTPVHFQSPPPVPGEVLKVQSYLENPTSYHLQQSQHQKVREYLSETYGNKFAAHVSPAQG  171
            NTPVHFQSPPPVPGEVLKVQSYLENPTSYHLQQSQHQKVREYLSETYGNKFAAH+SPAQG
hsIso2 68   NTPVHFQSPPPVPGEVLKVQSYLENPTSYHLQQSQHQKVREYLSETYGNKFAAHISPAQG  127

mmIsoA 172  SPKPAPAASPGVRAGHVLSTSAGNSAPNSPMAMLHISSNPEKEFDDVIDNIMRLDSVLGY  231
            SPKP PAASPGVRAGHVLS+SAGNSAPNSPMAMLHI SNPE+E DDVIDNIMRLD VLGY
hsIso2 128  SPKPPPAASPGVRAGHVLSSSAGNSAPNSPMAMLHIGSNPERELDDVIDNIMRLDDVLGY  187

mmIsoA 232  INPEMQMPNTLPLSSSHLNVYSGDPQVTASMVGVTSSSCPADLTQKRELTDAESRALAKE  291
            INPEMQMPNTLPLSSSHLNVYS DPQVTAS+VGVTSSSCPADLTQKRELTDAESRALAKE
hsIso2 188  INPEMQMPNTLPLSSSHLNVYSSDPQVTASLVGVTSSSCPADLTQKRELTDAESRALAKE  247
```

bHLH

```
mmIsoA 292  RQKKDNHNLIERRRRFNINDRIKELGMLIPKANDLDVRWNKGTILKASVDYIRRMQKDLQ  351
            RQKKDNHNLIERRRRFNINDRIKELGMLIPKANDLDVRWNKGTILKASVDYIRRMQKDLQ
hsIso2 248  RQKKDNHNLIERRRRFNINDRIKELGMLIPKANDLDVRWNKGTILKASVDYIRRMQKDLQ  307
```

Leucine Zipper DUF3371

```
mmIsoA 352  KSRELENHSRRLEMTNKQLWLRIQELEMQARVHGLPTTSPSGVNMAELAQQVVKQELPSE  411
            KSRELENHSRRLEMTNKQLWLRIQELEMQARVHGLPTTSPSG+NMAELAQQVVKQELPSE
hsIso2 308  KSRELENHSRRLEMTNKQLWLRIQELEMQARVHGLPTTSPSGMNMAELAQQVVKQELPSE  367

mmIsoA 412  DGPGEALMLGPEVPEPEQMPALPPQAPLPSAAQPQSPFHHLDFSHGLSFGGGGDEGPTGY  471
            +GPGEALMLG EVP+PE +PALPPQAPLP   QP SPFHHLDFSH LSFGG  DEGP GY
hsIso2 368  EGPGEALMLGAEVPDPEPLPALPPQAPLPLPTQPPSPFHHLDFSHSLSFGGREDEGPPGY  427

mmIsoA 472  PDTLGTEHGSPFPNLSKKDLDLMLLDDSLLPLASDPLFSTMSPEASKASSRRSSFSMEEG  531
            P+ L   HGSPFP+LSKKDLDLMLLDDSLLPLASDPL STMSPEASKASSRRSSFSMEEG
hsIso2 428  PEPLAPGHGSPFPSLSKKDLDLMLLDDSLLPLASDPLLSTMSPEASKASSRRSSFSMEEG  487

mmIsoA 532  DVL  534
            DVL
hsIso2 488  DVL  490
```

Appendix Figure 1: Alignment of human and mouse TFEB protein sequences

Graph shows protein sequence alignment of the longest mouse Tfeb isoform A and the longest human TFEB Isoform 2. Amino acids encoding annotated Glycine rich domain are marked in violet, basic helix-loop-helix (bHLH) domain in blue, leucine zipper domain in green and DUF3371 domain in red (DUF3371 domain has not been associated to any function so far). Annotated sequences refer to UniProt human TFEB Entry: P19484; mouse Tfeb Entry: Q6P203. Alignment was performed using NCBI BLAST_P.

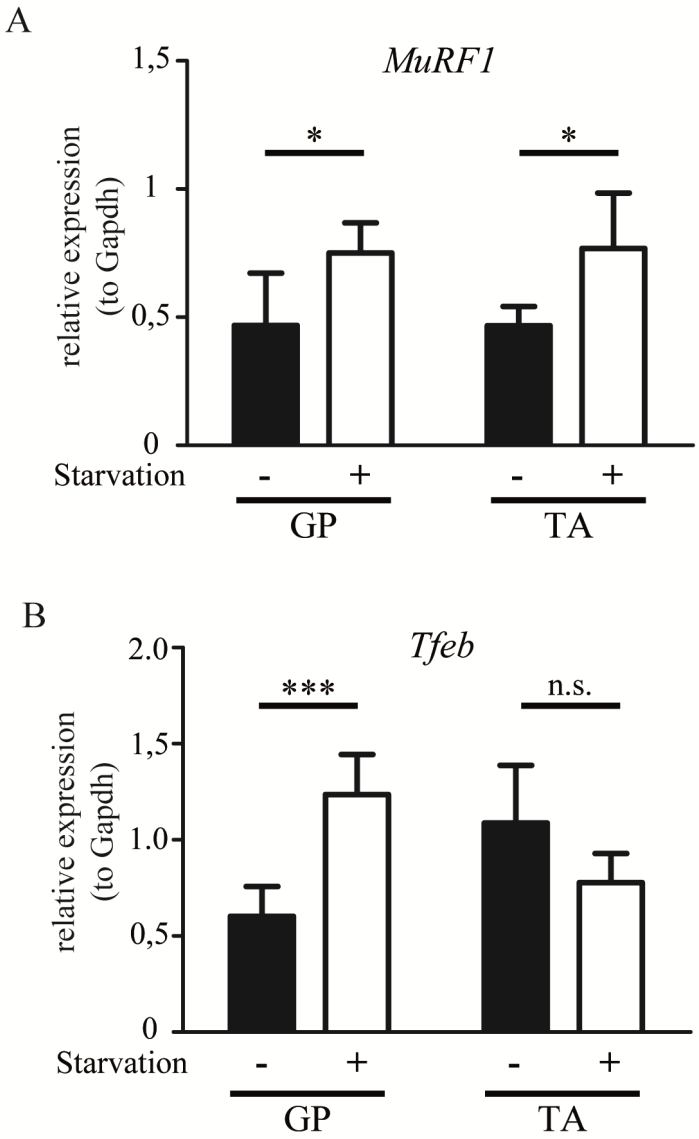

Appendix Figure 2: Starvation induced relative *in-vivo* expression of *MuRF1* and *Tfeb*

(**A**, **B**) Graphs show Real-Time expression analysis of mouse gastrocnemius (GP) and tibialis anterior (TA) muscle tissue. (**A**) *MuRF1* and (**B**) *Tfeb* expression relative to *Gapdh*, of control mice (n=4) and 24 h starved mice (n=6). Error bars represent SD. Student's t-test *p<.05; ***p<.001.

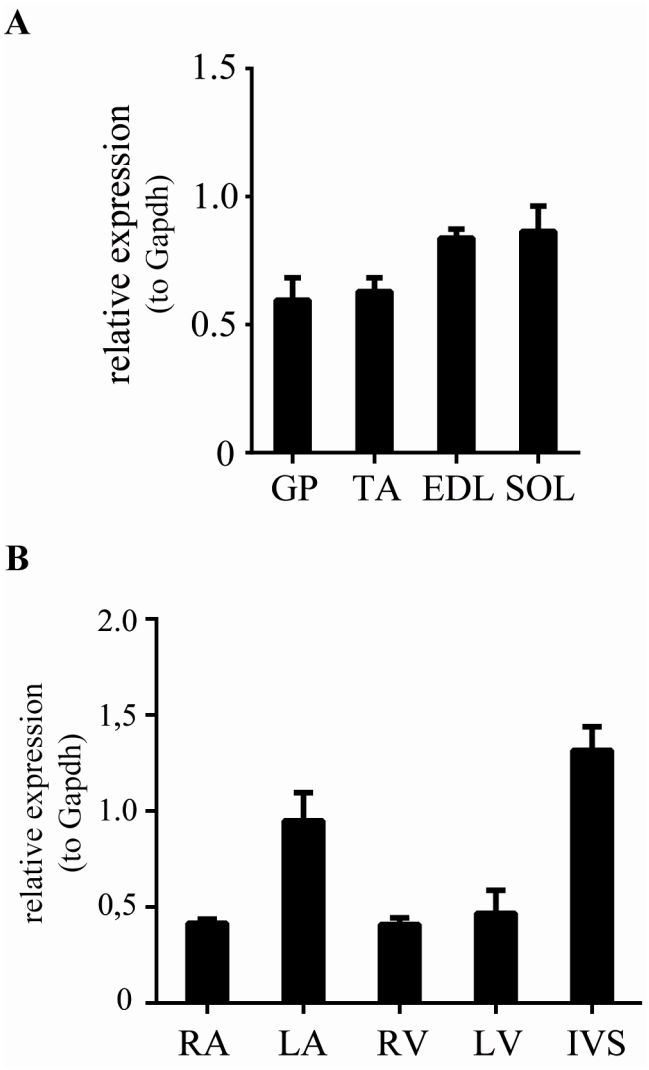

Appendix Figure 3: Relative expression of *Tfeb* in diverse muscle tissues

Real-Time analysis of *Tfeb* expression (relative to *Gapdh*) of (**A**) mouse skeletal muscle tissue. GP, gastrocnemius; TA, tibialis anterior; EDL, extensor digitorum longus; SOL, soleus. And of (**B**) mouse heart muscle tissue to 6. LA, left atrium; RA, right atrium; RV, right ventricle; LV, left ventricle; IVS, inter ventricular septum. Tissue was isolated from Bl6 WT mice, N=4.

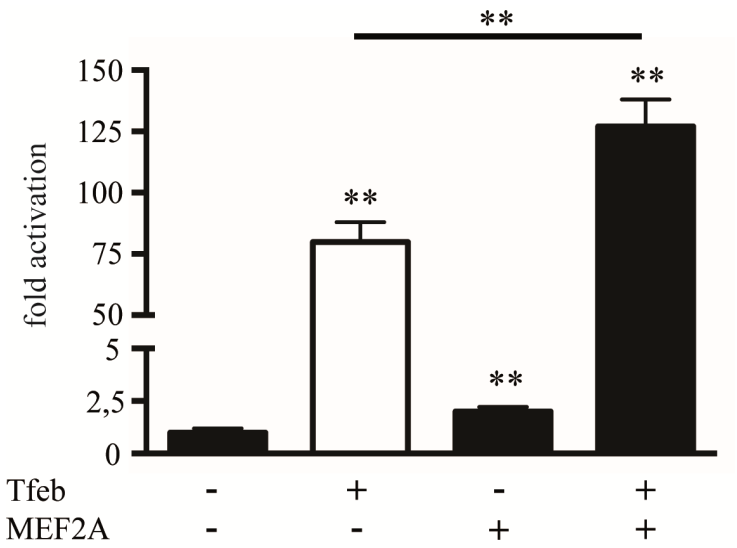

Appendix Figure 4: Co-induction of *M1P* construct by Tfeb and MEF2A overexpression

(**A**) HEK293 cells were transfected with expression plasmids encoding full length Tfeb and MEF2A together with the *M1P* reporter construct (size -543 bp), as indicated. Values were normalized to pCMV-*LacZ* transfection control vector expression and calculated as fold-activation in luciferase to β-Gal ratio compared to the reporter alone. Graph shows representative experiment in triplicates. Experiment has been repeated three times. Error bars represent SD. Students T-Test; ** $p < 0.005$.

7 Literature

Alamdari, N., Aversa, Z., Castillero, E., & Hasselgren, P.-O. (2013). Acetylation and deacetylation—novel factors in muscle wasting. *Metabolism*, *62*(1), 1–11. doi:10.1016/j.metabol.2012.03.019

Amitani, M., Asakawa, A., Amitani, H., & Inui, A. (2013). Control of food intake and muscle wasting in cachexia. *The International Journal of Biochemistry & Cell Biology*, *45*(10), 2179–2185. doi:10.1016/j.biocel.2013.07.016

Andrés, V., Cervera, M., & Mahdavi, V. (1995). Determination of the consensus binding site for MEF2 expressed in muscle and brain reveals tissue-specific sequence constraints. *Journal of Biological Chemistry*, *270*(40), 23246–23249.

Anker, S. D., Negassa, A., Coats, A. J., Afzal, R., Poole-Wilson, P. A., Cohn, J. N., & Yusuf, S. (2003). Prognostic importance of weight loss in chronic heart failure and the effect of treatment with angiotensin-converting-enzyme inhibitors: an observational study. *The Lancet*, *361*(9363), 1077–1083. doi:10.1016/S0140-6736(03)12892-9

Argilés, J. M., & López-Soriano, F. J. (1999). The role of cytokines in cancer cachexia. *Medicinal Research Reviews*, *19*(3), 223–248. doi:10.1002/(SICI)1098-1128(199905)19:3<223::AID-MED3>3.0.CO;2-N

Baskin, K. K., & Taegtmeyer, H. (2011). AMP-Activated Protein Kinase Regulates E3 Ligases in Rodent Heart. *Circulation Research*, *109*(10), 1153–1161. doi:10.1161/CIRCRESAHA.111.252742

Bechet, D., Tassa, A., Taillandier, D., Combaret, L., & Attaix, D. (2005). Lysosomal proteolysis in skeletal muscle. *The International Journal of Biochemistry & Cell Biology*, *37*(10), 2098–2114. doi:10.1016/j.biocel.2005.02.029

Bentzinger, C. F., Lin, S., Romanino, K., Castets, P., Guridi, M., Summermatter, S., … Rüegg, M. A. (2013). Differential response of skeletal muscles to mTORC1 signaling during atrophy and hypertrophy. *Skeletal Muscle*, *3*(1), 6.

Bentzinger, C. F., Romanino, K., Cloëtta, D., Lin, S., Mascarenhas, J. B., Oliveri, F., … Rüegg, M. A. (2008). Skeletal Muscle-Specific Ablation of raptor, but Not of rictor, Causes Metabolic Changes and Results in Muscle Dystrophy. *Cell Metabolism*, *8*(5), 411–424. doi:10.1016/j.cmet.2008.10.002

Bodine, S. C., Latres, E., Baumhueter, S., Lai, V. K.-M., Nunez, L., Clarke, B. A., … Glass, D. J. (2001). Identification of Ubiquitin Ligases Required for Skeletal Muscle Atrophy. *Science*, *294*(5547), 1704–1708. doi:10.1126/science.1065874

Bodine, S. C., Stitt, T. N., Gonzalez, M., Kline, W. O., Stover, G. L., Bauerlein, R., … Glass, D. J. (2001). Akt/mTOR pathway is a crucial regulator of skeletal muscle hypertrophy and can prevent muscle atrophy in vivo. *Nature Cell Biology*, *3*(11), 1014–1019.

Bonaldo, P., & Sandri, M. (2012). Cellular and molecular mechanisms of muscle atrophy. *Disease Models & Mechanisms*, *6*(1), 25–39. doi:10.1242/dmm.010389

Bricceno, K. V., Sampognaro, P. J., Meerbeke, J. P. V., Sumner, C. J., Fischbeck, K. H., & Burnett, B. G. (2012). Histone deacetylase inhibition suppresses myogenin-dependent atrogene activation in spinal muscular atrophy mice. *Human Molecular Genetics*, *21*(20), 4448–4459. doi:10.1093/hmg/dds286

Brink, M., Price, S. R., Chrast, J., Bailey, J. L., Anwar, A., Mitch, W. E., & Delafontaine, P. (2001). Angiotensin II induces skeletal muscle wasting through enhanced protein degradation and down-regulates autocrine insulin-like growth factor I. *Endocrinology*, *142*(4), 1489–1496.

Brink, M., Wellen, J., & Delafontaine, P. (1996). Angiotensin II causes weight loss and decreases circulating insulin-like growth factor I in rats through a pressor-independent mechanism. *Journal of Clinical Investigation*, *97*(11), 2509–2516. doi:10.1172/JCI118698

Brown, E. J., Albers, M. W., Bum Shin, T., Ichikawa, K., Keith, C. T., Lane, W. S., & Schreiber, S. L. (1994). A mammalian protein targeted by G1-arresting rapamycin–receptor complex. *Nature*, *369*(6483), 756–758. doi:10.1038/369756a0

Cai, D., Frantz, J. D., Tawa Jr., N. E., Melendez, P. A., Oh, B.-C., Lidov, H. G. W., … Shoelson, S. E. (2004). IKKβ/NF-κB Activation Causes Severe Muscle Wasting in Mice. *Cell*, *119*(2), 285–298. doi:10.1016/j.cell.2004.09.027

Camparo, P., Vasiliu, V., Molinie, V., Couturier, J., Dykema, K. J., Petillo, D., … Vieillefond, A. (2008). Renal Translocation Carcinomas: Clinicopathologic, Immunohistochemical, and Gene Expression Profiling Analysis of 31 Cases With a Review of the Literature. *Journal of Surgical Pathology May 2008*, *32*(5), 656–670. doi:10.1097/PAS.0b013e3181609914

Carr, C. S., & Sharp, P. A. (1990). A helix-loop-helix protein related to the immunoglobulin E box-binding proteins. *Molecular and Cellular Biology*, *10*(8), 4384–4388.

Centner, T., Yano, J., Kimura, E., McElhinny, A. S., Pelin, K., Witt, C. C., … Labeit, S. (2001). Identification of muscle specific ring finger proteins as potential regulators of the titin kinase domain. *Journal of Molecular Biology*, *306*(4), 717–726. doi:10.1006/jmbi.2001.4448

Chang, S., McKinsey, T. A., Zhang, C. L., Richardson, J. A., Hill, J. A., & Olson, E. N. (2004). Histone Deacetylases 5 and 9 Govern Responsiveness of the Heart to a Subset of Stress Signals and Play Redundant Roles in Heart Development. *Molecular and Cellular Biology*, *24*(19), 8467–8476. doi:10.1128/MCB.24.19.8467-8476.2004

Chang, S., Young, B. D., Li, S., Qi, X., Richardson, J. A., & Olson, E. N. (2006). Histone Deacetylase 7 Maintains Vascular Integrity by Repressing Matrix Metalloproteinase 10. *Cell*, *126*(2), 321–334. doi:10.1016/j.cell.2006.05.040

Clarke, B. A., Drujan, D., Willis, M. S., Murphy, L. O., Corpina, R. A., Burova, E., … Glass, D. J. (2007). The E3 Ligase MuRF1 Degrades Myosin Heavy Chain Protein in Dexamethasone-Treated Skeletal Muscle. *Cell Metabolism*, *6*(5), 376–385. doi:10.1016/j.cmet.2007.09.009

Cohen, S., Brault, J. J., Gygi, S. P., Glass, D. J., Valenzuela, D. M., Gartner, C., … Goldberg, A. L. (2009). During muscle atrophy, thick, but not thin, filament components are degraded by MuRF1-dependent ubiquitylation. *The Journal of Cell Biology*, *185*(6), 1083–1095. doi:10.1083/jcb.200901052

Costelli, P., Muscaritoli, M., Bossola, M., Penna, F., Reffo, P., Bonetto, A., … Fanelli, F. R. (2006). IGF-1 is downregulated in experimental cancer cachexia. *American Journal of Physiology - Regulatory, Integrative and Comparative Physiology*, *291*(3), R674–R683. doi:10.1152/ajpregu.00104.2006

Crespo, J. L., & Hall, M. N. (2002). Elucidating TOR Signaling and Rapamycin Action: Lessons from Saccharomyces cerevisiae. *Microbiology and Molecular Biology Reviews*, *66*(4), 579–591. doi:10.1128/MMBR.66.4.579-591.2002

Csibi, A., Cornille, K., Leibovitch, M.-P., Poupon, A., Tintignac, L. A., Sanchez, A. M. J., & Leibovitch, S. A. (2010). The Translation Regulatory Subunit eIF3f Controls the Kinase-Dependent mTOR Signaling Required for Muscle Differentiation and Hypertrophy in Mouse. *PLoS ONE*, *5*(2). doi:10.1371/journal.pone.0008994

Davis, I. J., Hsi, B.-L., Arroyo, J. D., Vargas, S. O., Yeh, Y. A., Motyckova, G., … Ladanyi, M. (2003). Cloning of an Alpha-TFEB fusion in renal tumors harboring the t (6; 11)(p21;

q13) chromosome translocation. *Proceedings of the National Academy of Sciences*, *100*(10), 6051–6056.

Dos D. Sarbassov, Ali, S. M., Kim, D.-H., Guertin, D. A., Latek, R. R., Erdjument-Bromage, H., … Sabatini, D. M. (2004). Rictor, a Novel Binding Partner of mTOR, Defines a Rapamycin-Insensitive and Raptor-Independent Pathway that Regulates the Cytoskeleton. *Current Biology*, *14*(14), 1296–1302. doi:10.1016/j.cub.2004.06.054

Eiseler, T., Döppler, H., Yan, I. K., Kitatani, K., Mizuno, K., & Storz, P. (2009). Protein kinase D1 regulates cofilin-mediated F-actin reorganization and cell motility through slingshot. *Nature Cell Biology*, *11*(5), 545–556. doi:10.1038/ncb1861

Fanzani, A., Conraads, V. M., Penna, F., & Martinet, W. (2012). Molecular and cellular mechanisms of skeletal muscle atrophy: an update. *Journal of Cachexia, Sarcopenia and Muscle*, *3*(3), 163–179. doi:10.1007/s13539-012-0074-6

Ferron, M., Settembre, C., Shimazu, J., Lacombe, J., Kato, S., Rawlings, D. J., … Karsenty, G. (2013). A RANKL-PKC -TFEB signaling cascade is necessary for lysosomal biogenesis in osteoclasts. *Genes & Development*, *27*(8), 955–969. doi:10.1101/gad.213827.113

Fielitz, J., Kim, M.-S., Shelton, J. M., Latif, S., Spencer, J. A., Glass, D. J., … Olson, E. N. (2007). Myosin accumulation and striated muscle myopathy result from the loss of muscle RING finger 1 and 3. *Journal of Clinical Investigation*, *117*(9), 2486–2495. doi:10.1172/JCI32827

Fielitz, J., Kim, M.-S., Shelton, J. M., Qi, X., Hill, J. A., Richardson, J. A., … Olson, E. N. (2008). Requirement of protein kinase D1 for pathological cardiac remodeling. *Proceedings of the National Academy of Sciences of the United States of America*, *105*(8), 3059–3063. doi:10.1073/pnas.0712265105

Fielitz, J., van Rooij, E., Spencer, J. A., Shelton, J. M., Latif, S., van der Nagel, R., … Bassel-Duby, R. (2007). Loss of muscle-specific RING-finger 3 predisposes the heart to cardiac rupture after myocardial infarction. *Proceedings of the National Academy of Sciences*, *104*(11), 4377–4382.

Finley, D. (2009). Recognition and Processing of Ubiquitin-Protein Conjugates by the Proteasome. *Annual Review of Biochemistry*, *78*(1), 477–513. doi:10.1146/annurev.biochem.78.081507.101607

Fisher, D. E., Carr, C. S., Parent, L. A., & Sharp, P. A. (1991). TFEB has DNA-binding and oligomerization properties of a unique helix-loop-helix/leucine-zipper family. *Genes & Development*, *5*(12A), 2342–2352.

Foletta, V. C., White, L. J., Larsen, A. E., Léger, B., & Russell, A. P. (2011). The role and regulation of MAFbx/atrogin-1 and MuRF1 in skeletal muscle atrophy. *Pflügers Archiv: European Journal of Physiology*, *461*(3), 325–335. doi:10.1007/s00424-010-0919-9

Fu, Y., & Rubin, C. S. (2011). Protein kinase D: coupling extracellular stimuli to the regulation of cell physiology. *EMBO Reports*, *12*(8), 785–796. doi:10.1038/embor.2011.139

Gilmore, T. D. (2006). Introduction to NF-κB: players, pathways, perspectives. *Oncogene*, *25*(51), 6680–6684. doi:10.1038/sj.onc.1209954

Glass, D. J. (2005). Skeletal muscle hypertrophy and atrophy signaling pathways. *The International Journal of Biochemistry & Cell Biology*, *37*(10), 1974–1984. doi:10.1016/j.biocel.2005.04.018

Glickman, M. H., & Ciechanover, A. (2002). The ubiquitin-proteasome proteolytic pathway: destruction for the sake of construction. *Physiological Reviews*, *82*(2), 373–428.

Gomes, M. D., Lecker, S. H., Jagoe, R. T., Navon, A., & Goldberg, A. L. (2001). Atrogin-1, a muscle-specific F-box protein highly expressed during muscle atrophy. *Proceedings of the National Academy of Sciences of the United States of America*, *98*(25), 14440–14445. doi:10.1073/pnas.251541198

Greer, E. L., Dowlatshahi, D., Banko, M. R., Villen, J., Hoang, K., Blanchard, D., … Brunet, A. (2007). An AMPK-FOXO Pathway Mediates Longevity Induced by a Novel Method of Dietary Restriction in C. elegans. *Current Biology*, *17*(19), 1646–1656. doi:10.1016/j.cub.2007.08.047

Greer, E. L., Oskoui, P. R., Banko, M. R., Maniar, J. M., Gygi, M. P., Gygi, S. P., & Brunet, A. (2007). The energy sensor AMP-activated protein kinase directly regulates the mammalian FOXO3 transcription factor. *The Journal of Biological Chemistry*, *282*(41), 30107–30119. doi:10.1074/jbc.M705325200

Gundersen, K. (2011). Excitation-transcription coupling in skeletal muscle: the molecular pathways of exercise. *Biological Reviews*, *86*(3), 564–600. doi:10.1111/j.1469-185X.2010.00161.x

Hallsson, J. H., Haflidadottir, B. S., Stivers, C., Odenwald, W., Arnheiter, H., Pignoni, F., & Steingrimsson, E. (2004). The basic helix-loop-helix leucine zipper transcription factor Mitf is conserved in Drosophila and functions in eye development. *Genetics*, *167*(1), 233–241.

Haq, R., & Fisher, D. E. (2011). Biology and Clinical Relevance of the Micropthalmia Family of Transcription Factors in Human Cancer. *Journal of Clinical Oncology*, *29*(25), 3474–3482. doi:10.1200/JCO.2010.32.6223

Harrison, B. C., Kim, M.-S., van Rooij, E., Plato, C. F., Papst, P. J., Vega, R. B., … McKinsey, T. A. (2006). Regulation of Cardiac Stress Signaling by Protein Kinase D1. *Molecular and Cellular Biology*, *26*(10), 3875–3888. doi:10.1128/MCB.26.10.3875-3888.2006

Hasty, P., Bradley, A., Morris, J. H., Edmondson, D. G., Venuti, J. M., Olson, E. N., & Klein, W. H. (1993). Muscle deficiency and neonatal death in mice with a targeted mutation in the myogenin gene. *Nature*, *364*(6437), 501–506. doi:10.1038/364501a0

Hay, N., & Sonenberg, N. (2004). Upstream and downstream of mTOR. *Genes & Development*, *18*(16), 1926–1945. doi:10.1101/gad.1212704

Hayashi, A., Seki, N., Hattori, A., Kozuma, S., & Saito, T. (1999). PKCν, a new member of the protein kinase C family, composes a fourth subfamily with PKCμ. *Biochimica et Biophysica Acta (BBA)-Molecular Cell Research*, *1450*(1), 99–106.

Hunter, R. B., Stevenson, E. J., Koncarevic, A., Mitchell-Felton, H., Essig, D. A., & Kandarian, S. C. (2002). Activation of an alternative NF-κB pathway in skeletal muscle during disuse atrophy. *The FASEB Journal*, *16*(6), 529–538. doi:10.1096/fj.01-0866com

Huynh, Q. K., & McKinsey, T. A. (2006). Protein kinase D directly phosphorylates histone deacetylase 5 via a random sequential kinetic mechanism. *Archives of Biochemistry and Biophysics*, *450*(2), 141–148. doi:10.1016/j.abb.2006.02.014

Jackman, R. W., Cornwell, E. W., Wu, C.-L., & Kandarian, S. C. (2013). Nuclear factor-κB signalling and transcriptional regulation in skeletal muscle atrophy. *Experimental Physiology*, *98*(1), 19–24. doi:10.1113/expphysiol.2011.063321

Jin, D., Takai, S., Sakaguchi, M., Okamoto, Y., Muramatsu, M., & Miyazaki, M. (2004). An Antiarrhythmic Effect of a Chymase Inhibitor after Myocardial Infarction. *Journal of Pharmacology and Experimental Therapeutics*, *309*(2), 490–497. doi:10.1124/jpet.103.061465

Karam, M., Legay, C., Auclair, C., & Ricort, J.-M. (2012). Protein kinase D1 stimulates proliferation and enhances tumorigenesis of MCF-7 human breast cancer cells through a

MEK/ERK-dependent signaling pathway. *Experimental Cell Research*, *318*(5), 558–569. doi:10.1016/j.yexcr.2012.01.001

Kedar, V., McDonough, H., Arya, R., Li, H.-H., Rockman, H. A., & Patterson, C. (2004). Muscle-specific RING finger 1 is a bona fide ubiquitin ligase that degrades cardiac troponin I. *Proceedings of the National Academy of Sciences*, *101*(52), 18135–18140. doi:10.1073/pnas.0404341102

Kee, H. J., & Kook, H. (2011). Roles and Targets of Class I and IIa Histone Deacetylases in Cardiac Hypertrophy. *Journal of Biomedicine and Biotechnology*, *2011*, 1–10. doi:10.1155/2011/928326

Kim, M.-S., Fielitz, J., McAnally, J., Shelton, J. M., Lemon, D. D., McKinsey, T. A., … Olson, E. N. (2008). Protein Kinase D1 Stimulates MEF2 Activity in Skeletal Muscle and Enhances Muscle Performance. *Molecular and Cellular Biology*, *28*(11), 3600–3609. doi:10.1128/MCB.00189-08

Kuiper, R. P., Schepens, M., Thijssen, J., Schoenmakers, E. F. P. M., & van Kessel, A. G. (2004). Regulation of the MiTF/TFE bHLH-LZ transcription factors through restricted spatial expression and alternative splicing of functional domains. *Nucleic Acids Research*, *32*(8), 2315–2322. doi:10.1093/nar/gkh571

Ladner, K. J., Caligiuri, M. A., & Guttridge, D. C. (2003). Tumor Necrosis Factor-regulated Biphasic Activation of NF-κB Is Required for Cytokine-induced Loss of Skeletal Muscle Gene Products. *Journal of Biological Chemistry*, *278*(4), 2294–2303. doi:10.1074/jbc.M207129200

Lainscak, M., Filippatos, G. S., Gheorghiade, M., Fonarow, G. C., & Anker, S. D. (2008). Cachexia: Common, Deadly, With an Urgent Need for Precise Definition and New Therapies. *The American Journal of Cardiology*, *101*(11, Supplement), S8–S10. doi:10.1016/j.amjcard.2008.02.065

Langen, R. C. J., Gosker, H. R., Remels, A. H. V., & Schols, A. M. W. J. (2013). Triggers and mechanisms of skeletal muscle wasting in chronic obstructive pulmonary disease. *The International Journal of Biochemistry & Cell Biology*, *45*(10), 2245–2256. doi:10.1016/j.biocel.2013.06.015

Laplante, M., & Sabatini, D. M. (2012). mTOR Signaling in Growth Control and Disease. *Cell*, *149*(2), 274–293. doi:10.1016/j.cell.2012.03.017

Laplante, M., & Sabatini, D. M. (2013). Regulation of mTORC1 and its impact on gene expression at a glance. *Journal of Cell Science*, *126*(8), 1713–1719. doi:10.1242/jcs.125773

LaValle, C. R., George, K. M., Sharlow, E. R., Lazo, J. S., Wipf, P., & Wang, Q. J. (2010). Protein kinase D as a potential new target for cancer therapy. *Biochimica et Biophysica Acta (BBA) - Reviews on Cancer*, *1806*(2), 183–192. doi:10.1016/j.bbcan.2010.05.003

Lecker, S. H. (2003). Ubiquitin-protein ligases in muscle wasting: multiple parallel pathways?: *Current Opinion in Clinical Nutrition and Metabolic Care*, *6*(3), 271–275. doi:10.1097/01.mco.0000068963.34812.e5

Lecker, S. H. (2006). Protein Degradation by the Ubiquitin-Proteasome Pathway in Normal and Disease States. *Journal of the American Society of Nephrology*, *17*(7), 1807–1819. doi:10.1681/ASN.2006010083

Lecker, S. H., Solomon, V., Mitch, W. E., & Goldberg, A. L. (1999). Muscle Protein Breakdown and the Critical Role of the Ubiquitin-Proteasome Pathway in Normal and Disease States. *The Journal of Nutrition*, *129*(1), 227S–237S.

Li, H.-H., Kedar, V., Zhang, C., McDonough, H., Arya, R., Wang, D.-Z., & Patterson, C. (2004). Atrogin-1/muscle atrophy F-box inhibits calcineurin-dependent cardiac hypertrophy by participating in an SCF ubiquitin ligase complex. *Journal of Clinical Investigation*, *114*(8), 1058–1071. doi:10.1172/JCI200422220

Li, Y.-P., & Reid, M. B. (2000). NF-κB mediates the protein loss induced by TNF-α in differentiated skeletal muscle myotubes. *American Journal of Physiology - Regulatory, Integrative and Comparative Physiology*, *279*(4), R1165–R1170.

Liu, Y., Contreras, M., Shen, T., Randall, W. R., & Schneider, M. F. (2009). α-Adrenergic signalling activates protein kinase D and causes nuclear efflux of the transcriptional repressor HDAC5 in cultured adult mouse soleus skeletal muscle fibres. *The Journal of Physiology*, *587*(5), 1101–1115. doi:10.1113/jphysiol.2008.164566

Ma, X., Godar, R. J., Liu, H., & Diwan, A. (2012). Enhancing lysosome biogenesis attenuates BNIP3-induced cardiomyocyte death. *Autophagy*, *8*(3), 297–309.

Macpherson, P. C. D., Wang, X., & Goldman, D. (2011). Myogenin Regulates Denervation-Dependent Muscle Atrophy in Mouse Soleus Muscle. *Journal of Cellular Biochemistry*, *112*(8), 2149–2159. doi:10.1002/jcb.23136

Mammucari, C., Milan, G., Romanello, V., Masiero, E., Rudolf, R., Del Piccolo, P., … Sandri, M. (2007). FoxO3 Controls Autophagy in Skeletal Muscle In Vivo. *Cell Metabolism*, *6*(6), 458–471. doi:10.1016/j.cmet.2007.11.001

Martin, M., Kettmann, R., & Dequiedt, F. (2007). Class IIa histone deacetylases: regulating the regulators. *Oncogene*, *26*(37), 5450–5467. doi:10.1038/sj.onc.1210613

Matthews, S. A., Liu, P., Spitaler, M., Olson, E. N., McKinsey, T. A., Cantrell, D. A., & Scharenberg, A. M. (2006). Essential Role for Protein Kinase D Family Kinases in the Regulation of Class II Histone Deacetylases in B Lymphocytes. *Molecular and Cellular Biology*, *26*(4), 1569–1577. doi:10.1128/MCB.26.4.1569-1577.2006

McGee, S. L., & Hargreaves, M. (2010). AMPK-mediated regulation of transcription in skeletal muscle. *Clinical Science*, *118*(8), 507–518. doi:10.1042/CS20090533

McGee, S. L., & Hargreaves, M. (2010). Histone modifications and exercise adaptations. *Journal of Applied Physiology*, *110*(1), 258–263. doi:10.1152/japplphysiol.00979.2010

McKinsey, T. A., Zhang, C. L., & Olson, E. N. (2001). Control of muscle development by dueling HATs and HDACs. *Current Opinion in Genetics & Development*, *11*(5), 497–504.

McKinsey, T. A., Zhang, C. L., & Olson, E. N. (2001). Identification of a Signal-Responsive Nuclear Export Sequence in Class II Histone Deacetylases. *Molecular and Cellular Biology*, *21*(18), 6312–6321. doi:10.1128/MCB.21.18.6312-6321.2001

Miska, E. A., Karlsson, C., Langley, E., Nielsen, S. J., Pines, J., & Kouzarides, T. (1999). HDAC4 deacetylase associates with and represses the MEF2 transcription factor. *The EMBO Journal*, *18*(18), 5099–5107. doi:10.1093/emboj/18.18.5099

Mizushima, N., Levine, B., Cuervo, A. M., & Klionsky, D. J. (2008). Autophagy fights disease through cellular self-digestion. *Nature*, *451*(7182), 1069–1075. doi:10.1038/nature06639

Moresi, V., Carrer, M., Grueter, C. E., Rifki, O. F., Shelton, J. M., Richardson, J. A., … Olson, E. N. (2012). Histone deacetylases 1 and 2 regulate autophagy flux and skeletal muscle homeostasis in mice. *Proceedings of the National Academy of Sciences*, *109*(5), 1649–1654. doi:10.1073/pnas.1121159109

Moresi, V., Williams, A. H., Meadows, E., Flynn, J. M., Potthoff, M. J., McAnally, J., … Olson, E. N. (2010). Myogenin and Class II HDACs Control Neurogenic Muscle Atrophy by Inducing E3 Ubiquitin Ligases. *Cell*, *143*(1), 35–45. doi:10.1016/j.cell.2010.09.004

Murton, A. J., Constantin, D., & Greenhaff, P. L. (2008). The involvement of the ubiquitin proteasome system in human skeletal muscle remodelling and atrophy. *Biochimica et Biophysica Acta (BBA) - Molecular Basis of Disease*, *1782*(12), 730–743. doi:10.1016/j.bbadis.2008.10.011

Nabeshima, Y., Hanaoka, K., Hayasaka, M., Esuml, E., Li, S., Nonaka, I., & Nabeshima, Y. (1993). Myogenin gene disruption results in perinatal lethality because of severe muscle defect. *Nature*, *364*(6437), 532–535. doi:10.1038/364532a0

Nakashima, K., & Yakabe, Y. (2007). AMPK Activation Stimulates Myofibrillar Protein Degradation and Expression of Atrophy-Related Ubiquitin Ligases by Increasing FOXO Transcription Factors in C2C12 Myotubes. *Bioscience, Biotechnology, and Biochemistry*, *71*(7), 1650–1656.

Pagan, J., Seto, T., Pagano, M., & Cittadini, A. (2013). Role of the Ubiquitin Proteasome System in the Heart. *Circulation Research*, *112*(7), 1046–1058.

Palmieri, M., Impey, S., Kang, H., di Ronza, A., Pelz, C., Sardiello, M., & Ballabio, A. (2011). Characterization of the CLEAR network reveals an integrated control of cellular clearance pathways. *Human Molecular Genetics*, *20*(19), 3852–3866. doi:10.1093/hmg/ddr306

Penner, C. G., Gang, G., Wray, C., Fischer, J. E., & Hasselgren, P.-O. (2001). The Transcription Factors NF-κB and AP-1 Are Differentially Regulated in Skeletal Muscle during Sepsis. *Biochemical and Biophysical Research Communications*, *281*(5), 1331–1336. doi:10.1006/bbrc.2001.4497

Perkins, N. D. (2007). Integrating cell-signalling pathways with NF-κB and IKK function. *Nature Reviews Molecular Cell Biology*, *8*(1), 49–62. doi:10.1038/nrm2083

Peterson, J. M., Bakkar, N., & Guttridge, D. C. (2011). NF-κB Signaling in Skeletal Muscle Health and Disease. In *Current Topics in Developmental Biology* (Vol. 96, pp. 85–119). Elsevier. Retrieved from http://linkinghub.elsevier.com/retrieve/pii/B9780123859402000048

Petroski, M. D. (2008). The ubiquitin system, disease, and drug discovery. *BMC Biochemistry*, *9*(Suppl 1), S7. doi:10.1186/1471-2091-9-S1-S7

Pickart, C. M. (2000). Ubiquitin in chains. *Trends in Biochemical Sciences*, *25*(11), 544–548.

Potthoff, M. J., & Olson, E. N. (2007). MEF2: a central regulator of diverse developmental programs. *Development*, *134*(23), 4131–4140. doi:10.1242/dev.008367

Potthoff, M. J., Wu, H., Arnold, M. A., Shelton, J. M., Backs, J., McAnally, J., … Olson, E. N. (2007). Histone deacetylase degradation andMEF2 activation promote the formation of slow-twitch myofibers. *Journal of Clinical Investigation*, *117*(9), 2459–2467. doi:10.1172/JCI31960

Reed, S. A., Sandesara, P. B., Senf, S. M., & Judge, A. R. (2011). Inhibition of FoxO transcriptional activity prevents muscle fiber atrophy during cachexia and induces hypertrophy. *The FASEB Journal*, *26*(3), 987–1000. doi:10.1096/fj.11-189977

Roczniak-Ferguson, A., Petit, C. S., Froehlich, F., Qian, S., Ky, J., Angarola, B., … Ferguson, S. M. (2012). The Transcription Factor TFEB Links mTORC1 Signaling to Transcriptional Control of Lysosome Homeostasis. *Science Signaling*, *5*(228), ra42–ra42. doi:10.1126/scisignal.2002790

Roig, E., Perez-Villa, F., Morales, M., Jiménez, W., Orús, J., Heras, M., & Sanz, G. (2000). Clinical implications of increased plasma angiotensin II despite ACE inhibitor therapy in patients with congestive heart failure. *European Heart Journal*, *21*(1), 53–57. doi:10.1053/euhj.1999.1740

Rommel, C., Bodine, S. C., Clarke, B. A., Rossman, R., Nunez, L., Stitt, T. N., … Glass, D. J. (2001). Mediation of IGF-1-induced skeletal myotube hypertrophy by PI(3)K/Akt/mTOR and PI(3)K/Akt/GSK3 pathways. *Nature Cell Biology*, *3*(11), 1009–1013. doi:10.1038/ncb1101-1009

Rybin, V. O., Guo, J., Harleton, E., Zhang, F., & Steinberg, S. F. (2012). Regulatory Domain Determinants That Control PKD1 Activity. *Journal of Biological Chemistry*, *287*(27), 22609–22615. doi:10.1074/jbc.M112.379719

Sabatini, D. M., Erdjument-Bromage, H., Lui, M., Tempst, P., & Snyder, S. H. (1994). RAFT1: A mammalian protein that binds to FKBP12 in a rapamycin-dependent fashion and is homologous to yeast TORs. *Cell*, *78*(1), 35–43. doi:10.1016/0092-8674(94)90570-3

Sacheck, J. M., Ohtsuka, A., McLary, S. C., & Goldberg, A. L. (2004). IGF-I stimulates muscle growth by suppressing protein breakdown and expression of atrophy-related ubiquitin ligases, atrogin-1 and MuRF1. *American Journal of Physiology - Endocrinology and Metabolism*, *287*(4), E591–E601. doi:10.1152/ajpendo.00073.2004

Sanchez, A. M., Csibi, A., Raibon, A., Cornille, K., Gay, S., Bernardi, H., & Candau, R. (2012). AMPK promotes skeletal muscle autophagy through activation of forkhead FoxO3a

and interaction with Ulk1. *Journal of Cellular Biochemistry*, *113*(2), 695–710. doi:10.1002/jcb.23399

Sandri, M. (2008). Signaling in Muscle Atrophy and Hypertrophy. *Physiology*, *23*(3), 160–170. doi:10.1152/physiol.00041.2007

Sandri, M. (2010). Autophagy in health and disease. 3. Involvement of autophagy in muscle atrophy. *American Journal of Physiology - Cell Physiology*, *298*(6), C1291–C1297. doi:10.1152/ajpcell.00531.2009

Sarbassov, D. D., Ali, S. M., Sengupta, S., Sheen, J.-H., Hsu, P. P., Bagley, A. F., … Sabatini, D. M. (2006). Prolonged Rapamycin Treatment Inhibits mTORC2 Assembly and Akt/PKB. *Molecular Cell*, *22*(2), 159–168. doi:10.1016/j.molcel.2006.03.029

Sardiello, M., Palmieri, M., di Ronza, A., Medina, D. L., Valenza, M., Gennarino, V. A., … Polishchuk, R. S. (2009a). A gene network regulating lysosomal biogenesis and function. *Science Signalling*, *325*(5939), 473.

Sartorelli, V., & Fulco, M. (2004). Molecular and cellular determinants of skeletal muscle atrophy and hypertrophy. *Science Signaling*, *2004*(244), re11.

Schiaffino, S., Dyar, K. A., Ciciliot, S., Blaauw, B., & Sandri, M. (2013). Mechanisms regulating skeletal muscle growth and atrophy. *FEBS Journal*, n/a–n/a. doi:10.1111/febs.12253

Schmidt, M., & Finley, D. (2013). Regulation of proteasome activity in health and disease. *Biochimica et Biophysica Acta (BBA)-Molecular Cell Research*. Retrieved from http://www.sciencedirect.com/science/article/pii/S0167488913003108

Semprun-Prieto, L. C., Sukhanov, S., Yoshida, T., Rezk, B. M., Gonzalez-Villalobos, R. A., Vaughn, C., … Delafontaine, P. (2011). Angiotensin II induced catabolic effect and muscle atrophy are redox dependent. *Biochemical and Biophysical Research Communications*, *409*(2), 217–221. doi:10.1016/j.bbrc.2011.04.122

Senf, S. M., Dodd, S. L., & Judge, A. R. (2009). FOXO signaling is required for disuse muscle atrophy and is directly regulated by Hsp70. *AJP: Cell Physiology*, *298*(1), C38–C45. doi:10.1152/ajpcell.00315.2009

Settembre, C., Zoncu, R., Medina, D. L., Vetrini, F., Erdin, S., Erdin, S., … Vellard, M. C. (2012a). A lysosome-to-nucleus signalling mechanism senses and regulates the lysosome via mTOR and TFEB. *The EMBO Journal*, *31*(5), 1095–1108.

Sohns, W., van Veen, T. A. B., & van der Heyden, M. A. G. (2010). Regulatory roles of the ubiquitin-proteasome system in cardiomyocyte apoptosis. *Current Molecular Medicine*, *10*(1), 1–13.

Song, K., Backs, J., McAnally, J., Qi, X., Gerard, R. D., Richardson, J. A., … Olson, E. N. (2006). The Transcriptional Coactivator CAMTA2 Stimulates Cardiac Growth by Opposing Class II Histone Deacetylases. *Cell*, *125*(3), 453–466. doi:10.1016/j.cell.2006.02.048

Song, Y.-H., Li, Y., Du, J., Mitch, W. E., Rosenthal, N., & Delafontaine, P. (2005). Muscle-specific expression of IGF-1 blocks angiotensin II–induced skeletal muscle wasting. *Journal of Clinical Investigation*, *115*(2), 451–458. doi:10.1172/JCI200522324

Steingrímsson, E., Copeland, N. G., & Jenkins, N. A. (2004). Melanocytes and the Microphthalmia Transcription Factor Network. *Annual Review of Genetics*, *38*(1), 365–411. doi:10.1146/annurev.genet.38.072902.092717

Steingrímsson, E., Tessarollo, L., Reid, S. W., Jenkins, N. A., & Copeland, N. G. (1998). The bHLH-Zip transcription factor Tfeb is essential for placental vascularization. *Development*, *125*(23), 4607–4616.

Stitt, T. N., Drujan, D., Clarke, B. A., Panaro, F., Timofeyva, Y., Kline, W. O., … Glass, D. J. (2004). The IGF-1/PI3K/Akt pathway prevents expression of muscle atrophy-induced ubiquitin ligases by inhibiting FOXO transcription factors. *Molecular Cell*, *14*(3), 395–403.

Sturany, S. (2000). Molecular Cloning and Characterization of the Human Protein Kinase D2. A NOVEL MEMBER OF THE PROTEIN KINASE D FAMILY OF SERINE THREONINE KINASES. *Journal of Biological Chemistry*, *276*(5), 3310–3318. doi:10.1074/jbc.M008719200

Tan, M., Xu, X., Ohba, M., Ogawa, W., & Cui, M.-Z. (2003). Thrombin Rapidly Induces Protein Kinase D Phosphorylation, and Protein Kinase C δ Mediates the Activation. *Journal of Biological Chemistry*, *278*(5), 2824–2828. doi:10.1074/jbc.M211523200

Tawa, N. E., Odessey, R., & Goldberg, A. L. (1997). Inhibitors of the proteasome reduce the accelerated proteolysis in atrophying rat skeletal muscles. *Journal of Clinical Investigation*, *100*(1), 197–203.

Thomas, D. R. (2007). Loss of skeletal muscle mass in aging: Examining the relationship of starvation, sarcopenia and cachexia. *Clinical Nutrition*, *26*(4), 389–399. doi:10.1016/j.clnu.2007.03.008

Tiffin, N., Adi, S., Stokoe, D., Wu, N.-Y., & Rosenthal, S. M. (2004). Akt Phosphorylation Is Not Sufficient for Insulin-Like Growth Factor-Stimulated Myogenin Expression but Must Be Accompanied by Down-Regulation of Mitogen-Activated Protein Kinase/Extracellular Signal-Regulated Kinase Phosphorylation. *Endocrinology*, *145*(11), 4991–4996. doi:10.1210/en.2004-0101

Tintignac, L. A., Lagirand, J., Batonnet, S., Sirri, V., Leibovitch, M. P., & Leibovitch, S. A. (2005). Degradation of MyoD Mediated by the SCF (MAFbx) Ubiquitin Ligase. *Journal of Biological Chemistry*, *280*(4), 2847–2856. doi:10.1074/jbc.M411346200

Tisdale, M. J. (1997). Biology of Cachexia. *Journal of the National Cancer Institute*, *89*(23), 1763–1773. doi:10.1093/jnci/89.23.1763

Valverde, A. M., Sinnett-Smith, J., Van Lint, J., & Rozengurt, E. (1994). Molecular cloning and characterization of protein kinase D: a target for diacylglycerol and phorbol esters with a distinctive catalytic domain. *Proceedings of the National Academy of Sciences*, *91*(18), 8572–8576.

Vega, R. B., Harrison, B. C., Meadows, E., Roberts, C. R., Papst, P. J., Olson, E. N., & McKinsey, T. A. (2004). Protein Kinases C and D Mediate Agonist-Dependent Cardiac Hypertrophy through Nuclear Export of Histone Deacetylase 5. *Molecular and Cellular Biology*, *24*(19), 8374–8385. doi:10.1128/MCB.24.19.8374-8385.2004

Vega, R. B., Matsuda, K., Oh, J., Barbosa, A. C., Yang, X., Meadows, E., … Richardson, J. A. (2004). Histone deacetylase 4 controls chondrocyte hypertrophy during skeletogenesis. *Cell*, *119*(4), 555–566.

Waddell, D. S., Baehr, L. M., van den Brandt, J., Johnsen, S. A., Reichardt, H. M., Furlow, J. D., & Bodine, S. C. (2008a). The glucocorticoid receptor and FOXO1 synergistically activate the skeletal muscle atrophy-associated MuRF1 gene. *American Journal of Physiology - Endocrinology and Metabolism*, *295*(4), E785–E797. doi:10.1152/ajpendo.00646.2007

Wan, M., Wu, X., Guan, K.-L., Han, M., Zhuang, Y., & Xu, T. (2006). Muscle atrophy in transgenic mice expressing a human TSC1 transgene. *FEBS Letters*, *580*(24), 5621–5627. doi:10.1016/j.febslet.2006.09.008

Wang, Q. J. (2006). PKD at the crossroads of DAG and PKC signaling. *Trends in Pharmacological Sciences*, *27*(6), 317–323. doi:10.1016/j.tips.2006.04.003

Wang, Y., & Pessin, J. E. (2013). Mechanisms for fiber-type specificity of skeletal muscle atrophy: *Current Opinion in Clinical Nutrition and Metabolic Care*, *16*(3), 243–250. doi:10.1097/MCO.0b013e328360272d

Weissman, A. M. (2001). Themes and variations on ubiquitylation. *Nat Rev Mol Cell Biol*, *2*(3), 169–178. doi:10.1038/35056563

Wilkinson, K. D. (2000). Ubiquitination and deubiquitination: Targeting of proteins for degradation by the proteasome. *Seminars in Cell & Developmental Biology*, *11*(3), 141–148. doi:10.1006/scdb.2000.0164

Wullschleger, S., Loewith, R., & Hall, M. N. (2006). TOR Signaling in Growth and Metabolism. *Cell*, *124*(3), 471–484. doi:10.1016/j.cell.2006.01.016

Xu, X., Ha, C.-H., Wong, C., Wang, W., Hausser, A., Pfizenmaier, K., … Jin, Z.-G. (2007). Angiotensin II Stimulates Protein Kinase D-Dependent Histone Deacetylase 5 Phosphorylation and Nuclear Export Leading to Vascular Smooth Muscle Cell Hypertrophy. *Arteriosclerosis, Thrombosis, and Vascular Biology*, *27*(11), 2355–2362. doi:10.1161/ATVBAHA.107.151704

Yoshida, T., Semprun-Prieto, L., Sukhanov, S., & Delafontaine, P. (2010a). IGF-1 prevents ANG II-induced skeletal muscle atrophy via Akt- and Foxo-dependent inhibition of the ubiquitin ligase atrogin-1 expression. *AJP: Heart and Circulatory Physiology*, *298*(5), H1565–H1570. doi:10.1152/ajpheart.00146.2010

Yoshida, T., Tabony, A. M., Galvez, S., Mitch, W. E., Higashi, Y., Sukhanov, S., & Delafontaine, P. (2013a). Molecular mechanisms and signaling pathways of angiotensin II-induced muscle wasting: Potential therapeutic targets for cardiac cachexia. *The International Journal of Biochemistry & Cell Biology*. doi:10.1016/j.biocel.2013.05.035

Yoshida, T., Tabony, A. M., Galvez, S., Mitch, W. E., Higashi, Y., Sukhanov, S., & Delafontaine, P. (2013b). Molecular mechanisms and signaling pathways of angiotensin II-induced muscle wasting: Potential therapeutic targets for cardiac cachexia. *The International Journal of Biochemistry & Cell Biology*. doi:10.1016/j.biocel.2013.05.035

Yuan, J., Bae, D., Cantrell, D., Nel, A. E., & Rozengurt, E. (2002). Protein Kinase D Is a Downstream Target of Protein Kinase Cθ. *Biochemical and Biophysical Research Communications*, *291*(3), 444–452. doi:10.1006/bbrc.2002.6469

Zhao, J., Brault, J. J., Schild, A., Cao, P., Sandri, M., Schiaffino, S., … Goldberg, A. L. (2007a). FoxO3 Coordinately Activates Protein Degradation by the Autophagic/Lysosomal

and Proteasomal Pathways in Atrophying Muscle Cells. *Cell Metabolism*, *6*(6), 472–483. doi:10.1016/j.cmet.2007.11.004

Zugaza, J. L., Sinnett-Smith, J., Van Lint, J., & Rozengurt, E. (1996). Protein kinase D (PKD) activation in intact cells through a protein kinase C-dependent signal transduction pathway. *The EMBO Journal*, *15*(22), 6220.

Danksagung

Zu allererst möchte ich Herrn PD Dr. med. Jens Fielitz für die Möglichkeit danken, diese Arbeit unter seiner Betreuung und in seinem Labor durchgeführt haben zu können. Jens, danke dir für das Interessante Projekt, die gute Betreuung und die wissenschaftliche Freiheit die du mir in den Jahren gewährt hast. Zudem möchte ich dir für die Chance danken, die Entwicklung des jungen Labors, den Mitarbeitern/innen und den Projekten mit begleitet und gestaltet haben zu können.

Des Weiteren möchte ich Herrn Prof. Dr. Thomas Sommer für die Betreuung meiner Doktorarbeit als Universitätsprofessor danken. Thomas, danke dass deine Tür stets offen Stand und ich mit allen Problemen bei dir immer ein offenes Ohr gefunden habe.

Natürlich möchte ich mich auch herzlich bei meinen ehemaligen Laborkollegen/innen bedanken. Die gemeinsame jahrelange Arbeit war zwar nicht immer leicht, aber wir haben es gemeinsam geschafft, wir haben uns gegenseitig motiviert und unterstützt wenn es nötig wurde. Ohne eure Hilfe wäre dieses Projekt nicht zu einem solchen Abschluss gekommen, vielen Danke dafür.

Jida, dir danke ich speziell für dein stets offenes Ohr, auch wenn du nicht immer hören wolltest was ich zu sagen hatte, du hast meist hilfreich an meiner „linken“ Seite gesessen, und mir manchmal bei einem Bier oder anderem Genussmittel Ratschläge gegeben die mich des Öfteren weiter gebracht haben. Dörte, du bist mir mit deiner ruhigen und diplomatischen Art zu meiner „rechten“ Seite hilfreich gewesen. Du gehörst mit Jida zu den „alten Hasen“ des Labors und warst zum richtigen Zeitpunkt offen aber auch kritisch mir und meinen Daten gegenüber, danke dir dafür. Danke sage ich auch zu unserer Neuen „alten“ Melanie, danke dir für deinen Einsatz und deine Unterstützung. Dein Rat war an der einen oder anderen Stelle äußerst hilfreich und lehrreich und ich habe von dir so einiges lernen können.

Ein besonderer Dank geht an die technischen Assistentinnen der AG Fielitz. Ihr habt für mich und das Projekt viele helfende Hände gehabt und habt mir ab und an den Rücken frei gehalten, somit seid ihr ein Rückhalt in stressigen Zeiten für mich gewesen, danke euch vielmals dafür. Sibylle, dir danke ich ganz besonders für die schönen Gespräche und deine offene und herzliche Art, du warst immer (m)eine Motivation am „frühen Morgen“ für mich. Janine, du hast mit deiner guten Laune auch mich mitgerissen und warst dem Labor eine liebevolle und treue Seele. Es hat immer Spaß gemacht mit dir zusammen zu arbeiten. Franziska, danke dir für die „Bestätigung“ meiner Daten, du bist eine tolle Nachfolgerin gewesen. Und bei Xiaoxi

muss ich mich für die vielen guten Diskussionen bedanken, durch dich ist mein Englisch nicht komplett eingerostet und es war eigentlich immer spaßig mit dir zu „streiten“.

Weiterhin möchte ich „Danke“ an meine Praktikanten Michael und Marcel sagen. Ich hoffe ich konnte euch, im Gegenzug zu eurer tatkräftigen Unterstützung, etwas beibringen und euch motivieren weiter in der Wissenschaft erfolgreich zu forschen. Es gibt viele weitere Kollegen und Kolleginnen am ECRC, dem MDC und anderen Institutionen, denen ich nicht namentlich Danken kann, die ich aber sicherlich nicht vergessen habe und werde.

Ein besonderer Dank geht auch an Sahar, du hast mir bei der Korrektur meiner Arbeit geholfen und bist bei unseren Treffen zu einer Freundin der Familie geworden.

Einen riesigen Dank möchte ich natürlich auch meiner Mutter aussprechen, sie hat mir mein wissenschaftliches Studium ermöglicht und mir somit den Weg geebnet um ihr nun auf diesem Wege und mit diesem Abschluss zu danken. Ich weiß wie schwer das Leben es einem manchmal macht, umso mehr bin ich froh, dass du weiterhin an meiner Seite stehst.

Doch den größten Dank muss ich abschließend meiner Frau Ilona aussprechen. Sie hat mir über die Jahre treu zur Seite gestanden und mich motiviert weiter zu machen, auch wenn es mal schwierig war. Du hast mir den Rücken frei gehalten, gerade zum Ende hin während der Schreibphase und dass obwohl du selbst an deiner eigenen Doktorarbeit hättest schrieben wollen und wir lernen mussten, gemeinsam mit unseren kleinen Louis den neuen Alltag zu meistern. Dafür kann ich dir nicht genug danken.